Biomedical & Life Sciences | Lancaster University

INVESTAGING THE ROLE OF KIFC1 AND CENTROSOME AMPLIFICATION IN PRIMARY AND METASTATIC UVEAL MELANOMA

TOWARDS BUILDING A PROTAC TO TARGET KIFC1

Umar Patel

Biomedical Science MSc by Research

Supervised by Dr Morgan Gadd and Dr Andrew Fielding

Biomedical and Life Sciences

Faculty of Health and Medicine

Lancaster University

October 2019

I, Umar Patel, confirm that the work presented in this thesis is my own and has not been submitted in substantially the same form for the award of a higher degree elsewhere. Where information has been derived from other sources, I confirm this has been indicated in the thesis.

Abstract

Uveal melanoma is melanoma of the uveal tract, which develops into liver metastasis in approximately 50% of patients. Lack of therapeutic targets means that survival from metastatic uveal melanoma remains at 8% after two years, a survival rate that had not improved since 1973 (Singh et al., 2011). Recent in silico genomics research has revealed uveal melanoma to express genes associated with centrosome amplification (de Almeida et al., 2019). Although centrosome amplification causes cancer (Levine et al., 2017), it has been described as an "Achilles' heel" for cancer cells as they require mechanisms to cluster their centrosomes to avoid multipolar mitosis, aneuploidy and cell death (Kwon et al., 2008). KIFC1, a kinesin-14 motor protein, is essential for clustering centrosomes and avoiding multipolar mitosis (Kwon et al., 2008). Frequently found to be overexpressed in cancers with centrosome amplification, KIFC1 overexpression has been shown to increase proliferation, survival and invasiveness (Pannu et al., 2015b), but seems to be dispensable in normal somatic cells (Watts et al., 2013). Small molecule KIFC1 inhibitors do exist, but current options display off target effects and require high doses to generate an effect (Yukawa et al., 2018).

In this project, metastatic uveal melanoma cell lines have been shown to display centrosome amplification for the first time. Furthermore, KIFC1 depletion in primary and uveal melanoma cell lines reduces proliferation, clonogenicity and survival while increasing the frequency of apoptosis and multipolar mitosis. The addiction to KIFC1 observed in primary uveal melanoma cells, which have insignificant levels of centrosome amplification, implies that KIFC1 has centrosome clustering-independent oncogenic activity in primary uveal melanoma and may be a novel therapeutic target.

A novel therapeutic alternative to small molecule inhibitors is the use of small-molecule PROTACs, which are bifunctional chimeras that hijack the ubiquitin-proteasome system to induce degradation of disease-causing target proteins, while also working at lower concentrations and with better specificity than the small molecule inhibitors that they are derived from (Buhimschi et al., 2018). In this project, analogues of the KIFC1 inhibitor CW069 were synthesised as the first step towards producing KIFC1-targetting PROTACs.

Contents

I would like to express my gratitude to Dr Morgan Gadd and Dr Andrew Fielding for their expert guidance and patience throughout my research and writing. This undertaking would not have been possible without their supervision and I am tremendously fortunate to have been a part of their research groups.

I would also like to express my appreciation for Marine Aublette (Gadd group), Kim Fabian-Kolpanowicz and April Yue Hu (Fielding group) for their help throughout this dissertation. Thanks also to the Allinson-Copeland-Gadd and Fielding-Lindsay-Taylor groups for the chance to develop my skills, and for the cakes.

Lastly, thanks to my parents, family and friends for their enthusiastic support and encouragement this past year.

1. Introduction

1.1. Uveal Melanoma

Around 5% of all melanomas occur in the eye (Chang et al., 1998), and approximately 85% of these occur in the uveal tract, comprising the choroid, iris and ciliary body, and are referred to as uveal melanoma. Although rare, it is still the most common ocular cancer and predominantly affects the elderly, with median age of diagnosis being 62 years, while the peak age range of diagnosis remains between 70–79 years (Reviewed by Krantz et al., 2017). Its incidence is approximately five per million in the USA, with a 30% greater incidence in males than females. Furthermore, it affects non-Hispanic Caucasians (6.02 per million) at a much higher rate than other races, such as Hispanics (1.67 per million), Asians (0.31 per million) and African Americans (0.39 per million) (Reviewed by Krantz et al., 2017). Incidence also increases with latitude, ranging from two per million in Spain and Italy to eight per million in Norway and Denmark (Virgili et al., 2007).

Although originating in melanocytes, uveal melanoma shares few similarities with cutaneous melanoma. They do both disproportionately affect those with fair skin, blue eyes and red or blonde hair (Weis et al., 2006), but uveal melanoma has a far lower mutational burden than cutaneous melanoma and unlike cutaneous melanoma, uveal melanoma has a very defined mutational landscape (Krauthammer et al., 2012). Gene expression profile classification stratified uveal melanoma cases into two molecular classes with significant differences in prognosis. Furthermore, class 1 was split between class 1A, with 2% risk of metastasis and 1B, with 21% risk of metastasis. Meanwhile, class 2 has a 72% risk for metastasis (Reviewed by Helgadottir and Hoiom, 2016). Despite effective local control of the tumour, around half of all uveal melanoma patients develop metastasis, mainly to the liver, leaving a mere 8% survival rate within two years upon metastasis (Reviewed by Krantz et al., 2017).

Uveal melanoma has a very distinct mutational landscape. Around 92.5% of patients harbour mutations in *GNAQ* and *GNA11*, both alpha subunits of G-proteins. Furthermore, tumours without these mutations instead gained mutations in *CYSLTR2*, a G-Protein-Coupled Receptor, or *PLCB4*, a downstream effector of *GNAQ*, accounting for 4% and 2.5% of patients in total, all of which activated the oncogenic YAP (Feng et al., 2014), MAPK and Akt/PKB pathways (Van Raamsdonk et al., 2010). Interestingly, these mutations occur in a mutually exclusive pattern and no difference was found in overall survival or metastasis between them. Furthermore, the fact that such mutations occur very early in tumorigenesis, led to the theory

that mutations in uveal melanoma are two-layered. The first layer initiates tumours via a common pathway in a nearly mutually exclusive manner, while the second layer progresses tumours to confer different prognoses (Figure 1.1) (Reviewed by Bakhoum and Esmaeli, 2019).

BAP1, located on chromosome 3p21.1, is one such gene in which mutations affect prognostic outcome. Although present in up to 33% of uveal melanoma tumours (Bakhoum and Esmaeli, 2019), inactivating mutations were present in 84% of metastatic uveal melanoma tumours (Harbour et al., 2010). Furthermore, all samples with *BAP1* mutations also exhibited loss of chromosome 3, while 83.3% of all uveal melanoma samples with chromosome 3 monosomy also showed additional mutations in *BAP1* (Robertson et al., 2017), indicating a 'two-hit' model of inactivation. BAP1 is a tumour suppressive deubiquitinase, stabilising IP3R3 to modulate calcium influx and induce apoptosis (Bononi et al., 2017). Furthermore, BAP1 interacts with and stabilises BRCA1 (Nishikawa et al., 2009) and contributes to DNA double strand break repair (Ismail et al., 2014). With regards to metastasis, *BAP1* depletion doubled the rate of transmigration compared to control uveal melanoma cells (Onken et al., 2018).

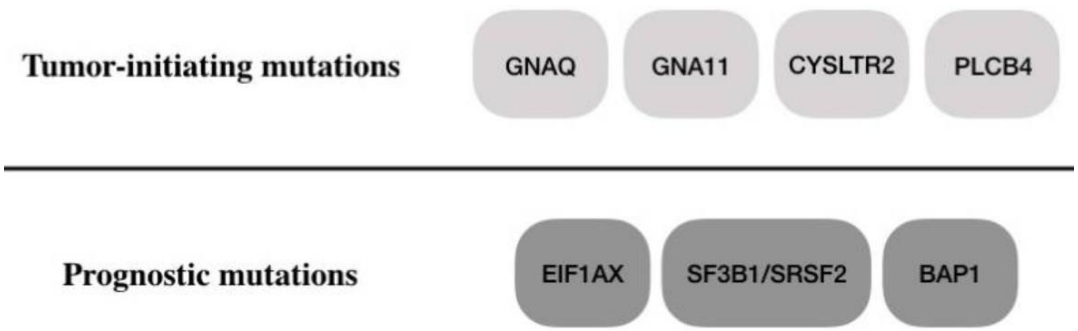

Figure 1.1. The two layers of mutation associated with uveal melanoma. *Mutations in genes associated with proliferative G-protein signalling initiate tumorigenesis and occur in 98% of uveal melanoma tumours in a mutually exclusive fashion from each other. Prognostic mutations are thought to progress the tumour via different pathways and can occur either by monosomy 3 and BAP1 inactivation or disomy 3 and a combination of SF3B1 or SRSF2 mutation with or without EIF1AX mutations (Bakhoum and Esmaeli, 2019).*

EIF1AX mutations are seen in approximately 14-20% of uveal melanomas. They are associated with class 1 tumours, good prognosis and are inversely associated with metastasis (Reviewed by Helgadottir and Hoiom, 2016), but this may be because they are almost only ever seen in disomy 3 tumours and are mutually exclusive to *BAP1* loss (Martin et al., 2013). Although its mechanism is unknown, the role of *EIF1AX* as an initiator of translation and its mutation

profile has led to the theory that it may alter how certain tumour suppressors are expressed by alternative start codon recognition (Martin et al., 2013).

Mutations in *SF3B1* and *SRSF2* occur in 23% and 4% of uveal melanomas respectively, with somatic copy number alteration profiles associated with each mutation implying a common molecular pathway for the two (Helgadottir and Hoiom, 2016). Although mutations to these genes are associated with good prognosis and low risk for metastasis, possibly due to rare association with BAP1 loss and monosomy 3, they do also indicate a risk of late-onset metastasis (Yavuzyigitoglu et al., 2016).

The strategy for treating uveal melanoma can be split into either removing the eye, known as enucleation, or preserving the eye by treating it with surgery, radiation or laser therapy. A randomised trial found that, after 12 years there is no difference in mortality between enucleation and ^{125}Iodine brachytherapy. These therapies are excellent in controlling the local tumour, however, they do not reduce the chance of developing long-term metastasis, which stands at 50% after 15 years. Amazingly, uveal melanoma cells have been found to be circulating in the blood before the initial tumours are even clinically detectable (Reviewed by Krantz et al., 2017). Furthermore, circulating primary uveal melanoma cells have been identified as a prognostic factor for distant metastasis and survival (Schuster et al., 2007).

The long-term survival for patients of metastatic uveal melanoma is poor as it cannot be treated with the same methods used to treat the primary tumours. Positivity was taken from the successes of targeted and immunotherapy in cutaneous melanoma, but the mutations in uveal melanoma are quite different; for example, *BRAF* mutations in uveal melanoma are very rare (Rimoldi et al., 2003). Furthermore, the successes of immunotherapy in cutaneous melanoma metastasis has been credited to the high frequency of coding mutations which give rise to neoantigens (Van Allen et al., 2015), but in contrast uveal melanoma has a low mutational burden (Krauthammer et al., 2012). Furthermore, *IDO1* and *TIGIT*, two immune checkpoint inhibitors which limit T-cell activity upon cancer cells, are among the most highly expressed mRNAs in monosomy-3 metastatic uveal melanoma, and likely reduce efficacy of anti-CTLA-4 or anti PD-1 inhibitors (Robertson et al., 2017).

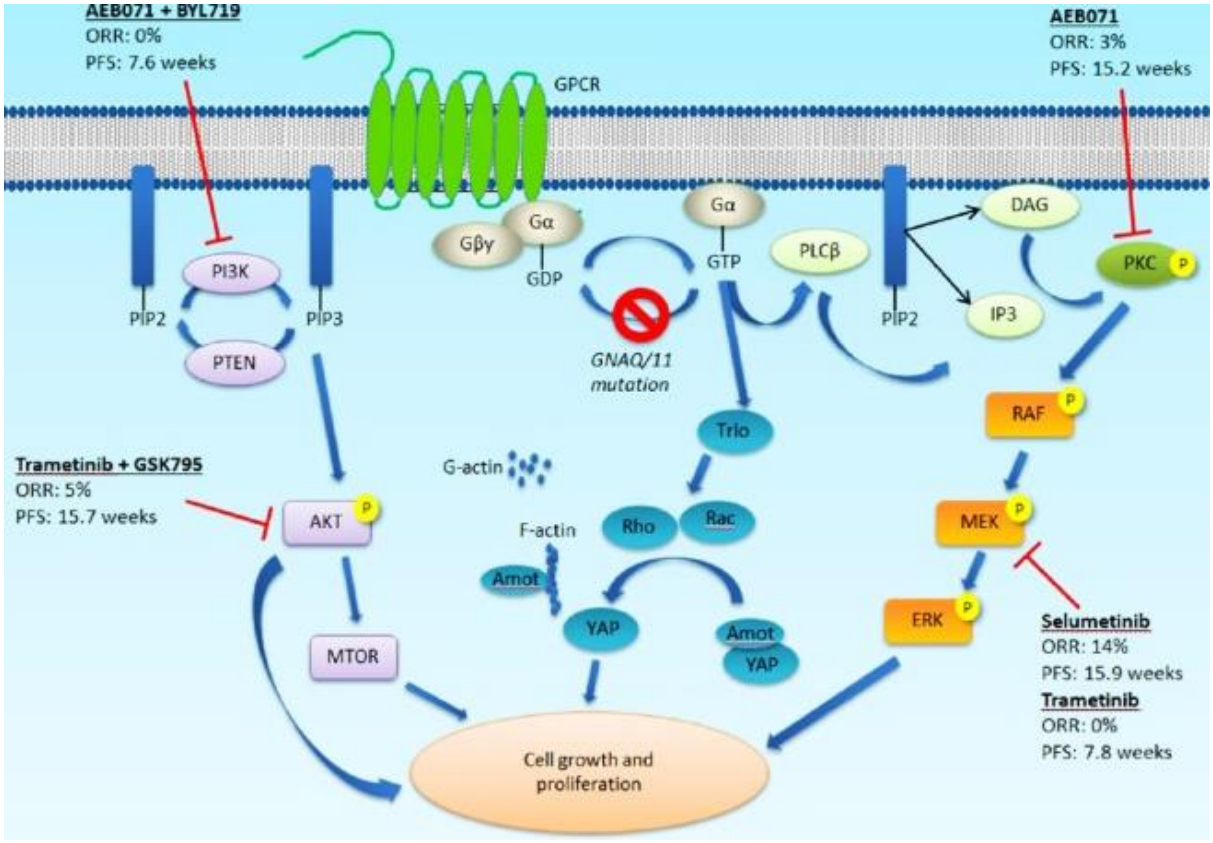

Figure 1.2. The Gα signalling pathway in uveal melanoma and the various attempts at inhibition of downstream effectors. *G-Protein Coupled Receptor signalling is mediated through a heterotrimer made up of Gα and Gβγ. Activating GNAQ/GNA11 mutations cause constitutive activation of Gα, which activates phospholipase C, the PI3K pathway, the YAP pathway and the MAPK pathway to induce proliferation. Therapies targeting downstream effectors of GNAQ and GNA11 have so far had limited success. PFS – Progression Free Survival. ORR – Overall Response Rate (Yang et al., 2018).*

Surgery is generally the gold standard to treat uveal melanoma metastasis. However, only 10% of liver metastases are resectable and often present as multiple tumours in both hepatic lobes. In non-resectable metastases, chemotherapy is used (Violanti et al., 2019). Various chemotherapeutic agents adopted from cutaneous melanoma treatment are used on their own or in combination therapy, but response rates range from 0% to 15%, and none have been shown to increase survival rates (Yang et al., 2018). Furthermore, various targeted therapies have been attempted, such as inhibition of the MAPK, PKC and PI3K pathways, which are downstream of *GNAQ*/*GNA11*. Although response rates remain poor (Figure 1.2) (Reviewed by Yang et al., 2018), direct inhibition of *GNAQ*/*GNA11* has yielded an effective pre-clinical inhibitor (Onken et al., 2018).

All in all, despite the many medical treatments available, no systemic therapy to suppress metastasis has improved overall survival or reduced the risk of metastasis (Violanti et al., 2019) and frankly, there has been no significant change in overall survival of uveal melanoma patients between 1973 and 2008 (Singh et al., 2011). New therapeutic targets common to primary and metastatic uveal melanoma, but dispensable in healthy cells, need to be identified and exploited. Fortunately, the fact that centrosome amplification occurs in uveal melanoma (de Almeida et al., 2019) may provide the perfect target.

1.2. Centrosome Amplification

Centrosomes are intracellular organelles made of a pair of orthogonally arranged centrioles enveloped inside pericentriolar material that act as the main microtubule organising centres in cells (Reviewed by Nigg and Raff, 2009). The centrosome replicates once during S-phase under tight regulation to ensure that the cell only has two centrosomes during mitosis, ensuring a bipolar spindle forms to accurately divide the genome in two during anaphase. Beyond this, the centrosome is the dominant organelle in terms of nucleating and organising microtubules during interphase, taking part in various functions including determining cell polarity, assembling cilia and tasks specific to differentiated cells (Reviewed by Nigg and Raff, 2009).

The number of centrosomes in a cell can sometimes be found to be increased, termed centrosome amplification. Such an increase in number arises from a variety of aberrant processes including cytokinesis failure and cell-cell fusion where centrosome number and genome number doubles. Centrosome amplification can also arise from *de novo* centriole formation (Khodjakov et al., 2002), overduplication of centrioles (Denu et al., 2018) or even through fragmentation of over-elongated centrioles (Marteil et al., 2018).

Centrosome Amplification Induces Tumorigenesis

Centrosome amplification is seen in a wide variety of cancers (de Almeida et al., 2019), and is thought to translate to a greater risk for poor prognosis (Chan, 2011). As early as 1914, Theodor Boveri hypothesised that extra centrosomes caused cancer (Boveri, 2008). Around 100 years later, evidence for this claim has begun to stack up. Initially, the consequences of centrosome amplification were unclear, especially as in most cell types, extra centrosomes were seen to be clustered into pseudo-bipolar spindles, allowing the cell to avoid a multipolar mitosis and the high levels of aneuploidy that followed (Quintyne et al., 2005). Nevertheless, it was still known that centrosome amplification drove chromosomal instability (Lingle et al., 2002).

Overexpression of Plk4 in *Drosophila* produced cells in which 60% had centrosome amplification (Basto et al., 2008). Although these flies showed developmental delay,

transformed adult flies were viable and fertile stocks were maintained for over 2 years, as the extra centrosomes were clustered into pseudo-bipoles by the action of Ncd (*Drosophila* homologue of human KIFC1). Although these flies showed no obvious tumour growth in themselves, partly since very little cell division occurs in adult flies and few mutations cause cancer in *Drosophila*, transplantation assays into adult flies formed tumours, and several injected hosts formed multiple tumours originating from the primary transplanted cells. On the contrary, wild type cell transplantation was not associated with any tumour formation. Interestingly, when using neural progenitor cells, centrosome amplification interfered with asymmetric division during development, causing genomic instability (Basto et al., 2008). However, similar transplantation experiments using wing tissue with centrosome amplification also caused tumorigenesis, which is important as wing tissue does not contain asymmetrically dividing cells (Sabino et al., 2015).

On the other hand, centrosome amplification in mammalian embryonic neural progenitor cells resulted in microcephaly due to aneuploidy-mediated cell death but did not cause tumorigenesis. However, this was attributed to inefficient clustering mechanisms and p53-mediated apoptosis (Marthiens et al., 2013). Furthermore, centrosome amplification in the skin of mice did not induce tumorigenesis, even with p53 inactivation (Vitre et al., 2015). However, doxycycline-inducible Plk4 overexpression-mediated centrosome amplification did induce tumorigenesis in mice but did not affect progression (Levine et al., 2017). Interestingly, although centrosome amplification did induce aneuploidy, it did not increase DNA damage or tetraploidisation above levels observed in wild type cells. Truncation of one APC tumour suppressor allele coupled with Plk4 overexpression accelerated intestinal tumour development in mice, produced larger and more numerous tumours and increased the likelihood of inactivation of the remaining APC allele (Levine et al., 2017). Similarly, $Plk4^{Dox}$ mice which were fed doxycycline (doxy) developed spontaneous tumours sooner than wild type mice, and when the p53 status was analysed, it was found that tumours with centrosome amplification showed a wide range of p53 inactivation and downstream p53 signalling pathway downregulation (Levine et al., 2017).

This experiment further proved the theory that centrosome amplification caused aneuploidy, and, in time, that aneuploidy would inactivate p53 pathways, allowing tumorigenesis. This is a reasonable theory, as it has been found that centrosome amplification arises as early as the

premalignant condition, but expansion of centrosome amplification and acceleration of progression relies on p53 repression (Lopes et al., 2018). Lending further credence to this is the demonstration that centrosome amplification induces low level chromosomal instability capable of pushing cancer cell evolution (Ganem et al., 2009), (Silkworth et al., 2009).

Centrosome Amplification Induces Chromosomal Instability

Initially, it was thought that centrosome amplification drove tumour evolution through aneuploidy arising from multipolar mitosis (Reviewed by Nigg and Raff, 2009). However, it was demonstrated that this theory had not considered that multipolar mitosis compromises cell fitness. Of the squamous cell carcinoma cells analysed that attempted multipolar mitosis, only 20% successfully completed division, with the rest dying in mitosis, interphase or undergoing cell cycle arrest (Ganem et al., 2009). Of the few that successfully divided, none managed to divide again, with most dying in interphase. In comparison, cells of the same cell line which underwent bipolar mitosis successfully divided 94% of the time in the first round and 90% of the time in the second round. Furthermore, the frequency of multipolar mitoses did not match the observed rates of chromosomal instability observed in other cell lines. This meant that multipolar mitosis could not account for the chromosomal instability seen due to centrosome amplification, as it occurred too infrequently and left no viable progeny (Ganem et al., 2009).

The alternative mechanism put forward was that during mitosis, cells with centrosome amplification form “transient multipolar intermediates” before clustering centrosomes, and that intermediate arrangement predisposes such cells to form attachments where two or more centrosomes attach to the same chromatid, called merotelic attachments (Ganem et al., 2009), which are known to cause lagging chromosomes and chromosomal instability (Thompson and Compton, 2008). Observation of such cells showed that they did spend a long part of mitosis in a transient multipolar configuration, and high-resolution microscopy showed that they also formed many merotelic attachments. Furthermore, the increased rate of lagging chromosomes, the result of merotely, drastically increased in multipolar cells, implying that merotelic attachments are enriched in cells that take a multipolar shape (Ganem et al., 2009).

Merely a month later, it was published that colorectal cancer cells which rarely underwent multipolar anaphase but did form multipolar intermediates earlier in mitosis also had merotelic enrichment (Silkworth et al., 2009). Furthermore, the presence of extra centrosomes correlated with up to a ten-fold increase in lagging chromosomes during bipolar anaphase. Artificial centrosome amplification in normal, chromosomally stable cells also increased the frequency of lagging chromosomes and missegregation up to eight-fold, while subsequent restoration of normal centrosome number then reduced the frequency of lagging chromosomes to wild type levels (Ganem et al., 2009). An alternative source of chromosomal instability in cells with centrosome amplification also observed was that a single chromosome would make proper kinetochore attachments and bi-orient between two centrosomes, which would then cluster to the same pole upon anaphase. However, these represented a tiny fraction of the merotely-induced lagging chromosomes (Ganem et al., 2009). Collectively, these findings suggested that centrosome amplification was capable of inducing chromosome instability.

Centrosome Amplification Contributes to Poor Cancer Outcomes

Aside from initiating cancer, the ongoing chromosomal instability associated with centrosome amplification has been linked with poor disease prognosis. For example, centrosome amplification is associated with poor overall and recurrence free survival. It is also associated with high risk cancer subtypes, along with higher grade and stage (Chan, 2011). Furthermore, induction of centrosome amplification by doxy-inducible Plk4 caused de-differentiation and stem cell-like marker expression (Denu et al., 2016).

Centrosome amplification has also been linked with metastatic disease in patient samples. This was supported by migration assays in which cells with amplified centrosomes had a higher displacement and migration velocity. Similar results were observed in wound healing and Boyden chamber assays by both genetic and chemical induction of centrosome amplification, upon which vimentin was found to have increased (Pannu et al., 2015a).

A mechanism to explain the invasiveness of cancers with centrosome amplification may be that cancer cells with Plk4-mediated centrosome amplification are observed to form protrusions that invade the surrounding matrix (Godinho et al., 2014). Furthermore, an assay

for fibroblast-lead migration showed that almost every single cell found to be invasive contained extra centrosomes. Cells with centrosome amplification were also shown to be invasive in 3D cultures as opposed to control cells. (Godinho et al., 2014) Strikingly, the collective nature of invasion where an initial protrusion provided a track for many subsequent cells into the extracellular matrix resembled invasiveness *in vivo*. The fact that invasive cells with centrosome amplification retained E-cadherin indicated that the invasiveness was not due to epithelial to mesenchymal transition (EMT) which, along with the collective invasion phenotype, resembled ErbB2 oncogene-mediated invasiveness (Godinho et al., 2014). Furthermore, cells with centrosome amplification produced defective cell-cell junctions, allowing them to scatter after mitosis instead of forming cell-cell contacts like cells with normal centrosome number. Such an invasive phenotype associated with centrosome amplification was found to be due to overactivation of Rac1, an invasive and metastatic oncogene, independent of EGF signalling. Furthermore, a Rac1 antagonist, RhoA, was found to be under activated. Reversal of invasive phenotypes by Rac1 inhibition compounded that Rac1 activity was a key driver of centrosome amplification induced cellular invasion (Godinho et al., 2014).

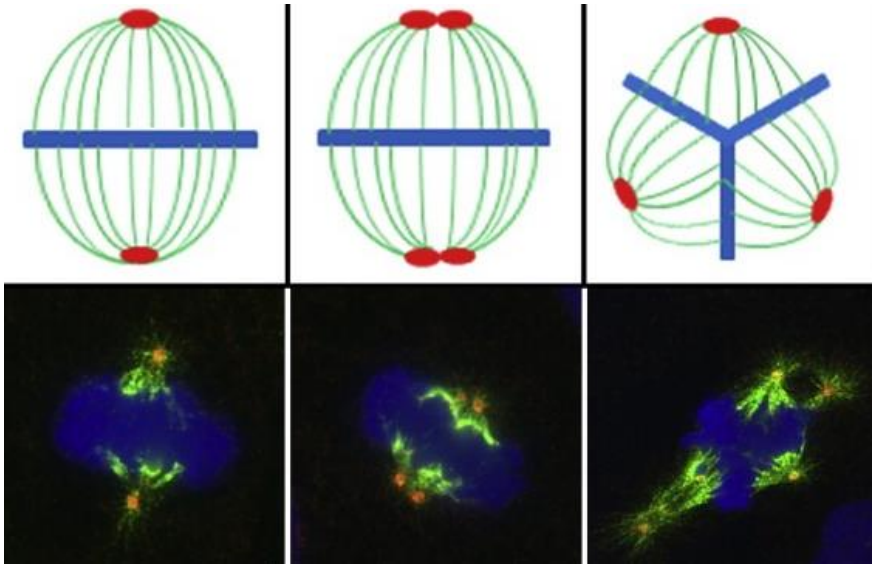

Figure 1.3. Coping with Amplified Centrosomes. *A cell with normal numbers of centrosomes will undergo bipolar mitosis, where a 4N genome is split equally into two daughter cells (left). A cell with centrosome amplification and the ability to cluster its centrosomes will do so to undergo pseudo-bipolar mitosis, where a 4N genome will be split between two daughter cells (centre). A cell with centrosome amplification without the ability to cluster the centrosomes will undergo multipolar anaphase, where a 4N genome is split 3 or more ways, causing massive aneuploidy and cell death (Kramer et al., 2011).*

Although centrosome amplification provides cancer cells with a wealth of mechanisms for evolution and adaptation, the presence of more than two centrosomes can lead to the possibility of multipolar mitosis, anaphase and cell division. The result would be that a 4N genome is spit 3 or more ways into 3 or more daughter cells which would therefore have huge aneuploidy and are likely to die (Ganem et al., 2009). Cancer cells displaying centrosome amplification therefore require a mechanism to regulate their amplified centrosomes during mitosis. Centrosome clustering is the most common and well-studied of these mechanisms, whereby cells gather their supernumerary centrosomes into just two poles, allowing for the formation of a pseudo-bipolar mitotic spindle for the cell to divide in two (Figure 1.3).

The mechanism for clustering of centrosomes is multifaceted, and spans regulation by the spindle assembly checkpoint (SAC), cooperation between actin and microtubule forces and associations between mitotic microtubules and motor proteins (Reviewed Kramer et al., 2011 and Ogden et al., 2012). Generally, centrosome clustering describes how multiple microtubule organising centres (MTOCs) are clustered together during prometaphase, such that come metaphase, a pseudo-bipolar spindle has formed. The first genome wide screen to identify proteins required for centrosome clustering carried out in *Drosophila* found that the "top hit" was Ncd, a kinesin-14 motor protein homologous to the human kinesin-14 KIFC1 (Kwon et al., 2008).

1.3. KIFC1

Kinesin-14 family member C1, widely known as KIFC1 but also known as hsKIFC1 or HSET in *Homo sapiens*, Ncd in *Drosophila melanogaster* and XCTK2 in *Xenopus laevis*, is a member of the Kinesin-14 microtubule motor protein family and is among the most widely studied kinesins (She and Yang, 2017).

In cells with no centrosomes, such as oocytes, KIFC1 is known to be essential for ensuring pseudo-bipolar mitosis (Mountain et al., 1999). Furthermore, KIFC1 is functionally expressed in sperm cells (Xiao et al., 2017). However, its function in normal cells is not known. In somatic cells with normal numbers of centrosomes, KIFC1 seems relatively dispensable, as KIFC1 depleted cells produced shorter and less focused poles, likely due to loss of outward forces, but did not affect mitosis or chromosomal segregation (Cai et al., 2009).

Like all kinesin-14s, KIFC1 has 3 functional domains; an N-terminal tail, a central coiled coil stalk and a C-terminal motor domain (Figure 1.4). The motor domain contains the ATPase catalytic core and microtubule-binding sites. Adjacent to the catalytic core, the conserved neck region acts as a transducer to transfer energy from ATP hydrolysis into movement and regulates lever rotations and step size (Hallen et al., 2011).

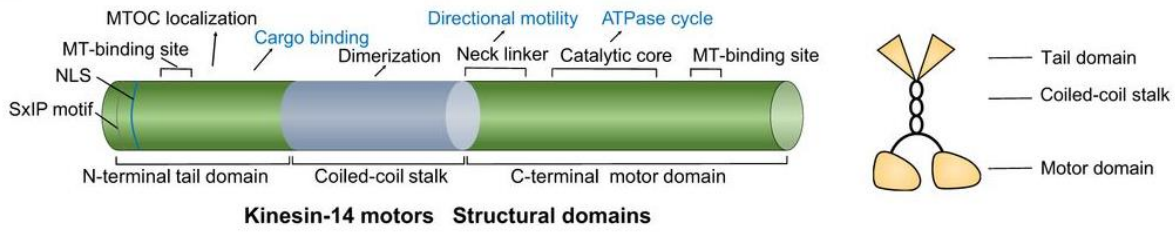

Figure 1.4. Schematic Representation of KIFC1 Structural Domains. *KIFC1 has 3 domains. The C-terminal motor domain contains a microtubule binding site which is manipulated by the neck linker, which is powered by the ATPase catalytic core. The coiled coil stalk allows dimerization while the N-terminal tail domain diversifies function and localises KIFC1 to the nucleus, the microtubule organising complexes and uniquely, allows KIFC1 to bind positive ends of microtubules (She and Yang, 2017).*

The N-terminal tail end of KIFC1 is crucial in diversifying kinesin function. For example, positively-charged residues in the tail region of Ncd were shown to act as an "electrostatic tether" to microtubules (Furuta and Toyoshima, 2008), while mouse KIFC1 was found to have

a 19-residue sequence that targets the tail to membrane-bound organelles (Goshima et al., 2005). Furthermore, a study involving 26 different KIFC1 tail, stalk and neck-motor chimeras found that although distinct functions exist between interspecies KIFC1 homologues, function was regulated by the tail domain. Interestingly, it was found that human KIFC1 shared functional overlap with other KIFC1s and was interchangeable with the *S. pombe* homologue (Simeonov et al., 2009).

An interesting feature of the tail domain unique to KIFC1 is that it has been shown to be able to associate with the positive ends of microtubules by interaction with EB1, mediated between the evolutionary conserved Serine-X-Isoleucine-Proline (SxIP) motif of KIFC1, and the EB homology domain of EB1. This means that KIFC1 can bind two antiparallel microtubules at opposite ends (Braun et al., 2013). Although the underlying function of this is not known, it has been hypothesised that positive-end binding is required for search and capture of kinetochore microtubules, thus allowing their transport to the spindle pole (Goshima et al., 2005). Importantly, it is this function that is thought to allow KIFC1 to cluster extra centrosomes into bipolar spindles, thus playing a role in avoiding aneuploidy in certain cancer cells (Reviewed by Xiao and Yang, 2016).

1.4. The Role of KIFC1 in Cancer

KIFC1 Provides A Selective Advantage to Cancer Cells with Extra Centrosomes

The link between KIFC1 and cancer was first reported in a genome-wide RNAi screen in near-tetraploid *Drosophila* cells with amplified centrosomes showing a reliance on Ncd (KIFC1 homologue) to efficiently suppress multipolar mitosis and subsequent aneuploidy-induced apoptosis (Kwon et al., 2008). Secondary analysis showed that KIFC1 knockdown increased the frequency of multipolar mitosis and depleted cell viability by >90% in N1E-115 neuroblastoma cancer cells, a cell line where nearly 100% of cells harbour amplified centrosomes. Most of the cells underwent apoptosis, while most of the remaining cells entered senescence (Kwon et al., 2008). Similar results were seen in three human breast cancer cell lines, with the extent of cell death proportional to the extent of centrosome amplification. The importance of these findings was underscored by the fact that cells with normal centrosome numbers were barely affected by KIFC1 knockdown (Kwon et al., 2008).

KIFC1 clusters amplified centrosomes by two mechanisms related to spindle-pole focusing. Firstly, KIFC1 contains a microtubule binding site at its N-terminus, as well as its C-terminal motor domain (Braun et al., 2013). This allows it to cross-link neighbouring microtubules. Coupled to its minus-end directed activity, this leads to the focusing of spindle pole minus ends and hence clustering of neighbouring microtubules and their attached centrosomes (Figure 1.5). Secondly, in conjunction with CEP215, KIFC1 acts as a tether between microtubule minus ends and centrosomes (Chavali et al., 2016), again allowing for centrosomes to be clustered as microtubule minus ends are focused at spindle poles.

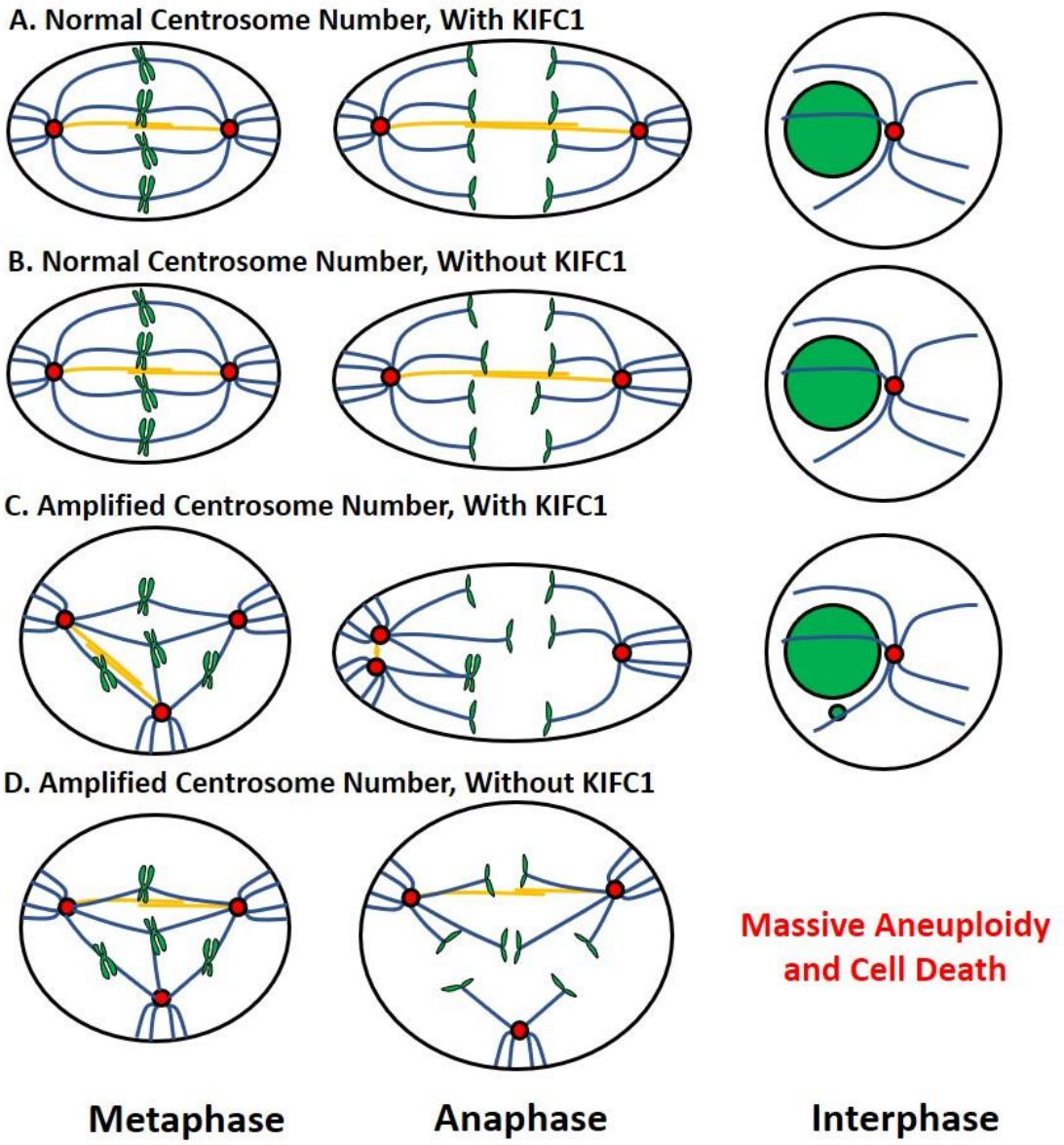

Figure 1.5. The Context Dependent Reliance Upon KIFC1. *A) In normal cells with normal centrosome (red) number, KIFC1 is involved with assembling a focused microtubule spindle (blue) and provides outwards pushing force antagonistic to the inward pulling force of Eg5. This produces a focused spindle amid chromosomal (green) stability. B) In normal cells with KIFC1 ablation, the lack of KIFC1-mediated outward forces produces a broad, shortened and less focused spindle, but mitosis will still occur amid chromosomal stability. C) Cells with centrosome amplification will form a "transient multipolar intermediate" before anaphase, allowing merotelic attachments to form. An anaphase delay would allow KIFC1 to pull centrosomes towards each other by interpolar microtubules (yellow) to form a pseudo-bipolar spindle. In the process, merotelic attachments would cause low level aneuploidy, lagging chromosomes and micronuclei. In this case, cells are still viable but have background aneuploidy, which could be considered beneficial for cancer cells. D) Cells with amplified centrosomes and KIFC1 depletion will also form "transient multipolar intermediates" but will not be able to cluster their centrosomes before anaphase, and so the genome would be sheared into more than two parts, causing massive aneuploidy, cell cycle arrest and cell death.*

KIFC1 may also contribute to centrosome clustering by non-direct mechanisms. For example, a functional SAC, allowing for a delay in anaphase if chromosomes are not aligned, is thought to be critical during centrosome clustering (Kwon et al., 2008). An anaphase delay would likely give KIFC1 the required time to cluster the multipolar intermediate to a pseudo-bipolar spindle. Such an anaphase delay would be mediated by deregulation of the SAC upon KIFC1 knockdown (Pannu et al., 2015b). Upon mitotic exit, KIFC1 is needed no more and thus is degraded by ubiquitination, possibly by binding to APC/C via its D-box before degradation by the 26s proteasome (Min et al., 2014). By such centrosome clustering, KIFC1 rescues cancer cells from large scale aneuploidy and cell death (Kwon et al., 2008), while allowing them to maintain a consistent source of genomic instability (Ganem et al., 2009).

KIFC1 is Overexpressed in Many Cancers

Following on from these findings, it is no surprise that KIFC1 has been shown to be overexpressed at the mRNA and protein levels in a wide variety of cancers by a wide variety of methods. For example, analysis of single-channel microarray data from the Gene Expression Omnibus database found a more than five-fold increase in KIFC1 expression in breast cancer over normal tissue matched to the same patients, and three-fold increases in glioblastoma and colon cancer patients (Pannu et al., 2015b). An exhaustive, in-depth search of the available literature showed that KIFC1 overexpression has been demonstrated in multiple stages of a whole host of cancers when compared to matched and unmatched normal tissue and cell lines of the same organs, outlined in Table 1.

Table 1.1. *An exhaustive list of reports of KIFC1 overexpression sorted by cancer type, including the technique(s) used to verify overexpression and the papers in which this was reported. IHC -Immunohistochemistry. qPCR – quantitative Polymerase Chain Reaction. FISH – Fluorescence In Situ Hybridisation.*

Cancer Type	Technique	Reference
Meningioma	Microarray	(Jungwirth et al., 2019)
Prostate Cancer	qPCR Western Blotting qPCR IHC	(Sekino et al., 2019) (Sekino et al., 2017)
Hepatocellular Carcinoma	Database analysis (TCGA), Western Blotting, qPCR	(Teng et al., 2019)

	Database analysis (TGCA) qPCR Database analysis (TGCA) IHC Database analysis (GEPIA) Database analysis (TGCA)	(Shi et al., 2018) (Han et al., 2019) (Fu et al., 2018) (Chen et al., 2017)
Breast Cancer (TNBC) Breast Cancer	Microarray Database analysis (COSMIC, Membranome, Druggable Genome, Secretome, CAN genes, Kinome) qPCR Western Blotting Database Analysis (GEO) FISH Western Blotting	(Patel et al., 2018) (Li et al., 2015) (Pannu et al., 2015b)
Renal Cell Carcinoma	IHC qPCR Western Blotting	(Li et al., 2018)
Testicular Cancer (Seminoma)	qPCR Western Blotting IHC	(Xiao et al., 2017)
Oesophageal Squamous Cell Carcinoma	IHC	(Imai et al., 2017)
Lung Cancer (Non-Small Cell Lung Carcinoma) Lung Cancer	Database analysis (Oncomine) qPCR IHC Western Blot Database Analysis (GEO)	(Liu et al., 2016) (Pannu et al., 2015b)
Gastric Cancer	Microarray qPCR	(Oue et al., 2016) (Zhang et al., 2016a)
Ovarian Cancer	Microarray IHC Database Analysis (GEO, TGCA)	(Mittal et al., 2016) (Pawar et al., 2014)
Glioblastoma	Database Analysis (GEO)	(Pannu et al., 2015b)
Colon Cancer	Database Analysis (GEO)	(Pannu et al., 2015b)
Cervical Cancer	Database Analysis (GEO)	(Pannu et al., 2015b)

One mechanism of KIFC1 transcriptional deregulation could lie with gene amplification. Analysis of a TNBC breast cancer cohort and database data showed correlation between increased KIFC1 expression and copy number (Patel et al., 2018). Furthermore, FISH of two bacterial artificial chromosome probes, one to the KIFC1 gene locus and the other to the nearby centromere of chromosome 6 showed KIFC1 copy number increases relative to centromere copy number in three of four breast tumours sampled. Meanwhile, matched paracancerous tissue displayed no amplification whatsoever. Only 5% KIFC1 copy number increases were due to chromosome 6 polyploidy, defined as more than two copies of each locus at a 1:1 ratio, while 38% of cells counted harboured three or more copies of KIFC1 relative to one or two copies of the centromere. Such gene amplifications also correlated with KIFC1 protein expression increases shown by Western blotting (Pannu et al., 2015b).

Aside from gene amplification, KIFC1 overexpression could also occur by increased induction of the *KIFC1* gene. Evidence exists that KIFC1 is a downstream target of the oestrogen signalling system. KIFC1 overexpression in serous ovarian adenocarcinomas was found to correlate with high expression of E2F1, E2F2 and E2F3 transcription factors (Mittal et al., 2016), while E2F8 expression correlates with KIFC1 overexpression in TNBCs. Incidentally, an E2F8 binding site was found upstream of the KIFC1 gene (Patel et al., 2018).

In oestrogen-receptor positive breast cancer cells, stimulation with E2 (oestrogen 17- β oestradiol) was shown to induce a seven-fold increase in KIFC1 expression, along with varying up and downregulations in 37 other kinesins (Zou et al., 2014). More specifically, it seemed that KIFC1 was acted upon by AAA Nuclear Coregulator Cancer-Associated (ANCCA). ANCCA is an AAA+ ATPase in the oestrogen signalling system, ectopic treatment of which induced strong KIFC1 upregulation, even in the absence of E2. Conversely, suppression of KIFC1 expression was seen in ANCCA-suppressed cells, even after E2 treatment (Zou et al., 2014). Chromatin immunoprecipitation (ChIP) demonstrated that ANCCA occupied kinesin promoters in the absence of E2 but showed a marked increase in occupancy upon E2 treatment, indicating both oestrogen dependent and independent activation of kinesin expression. ANCCA was also required for E2-dependent recruitment of E2F1 and MLL1, a H3K4 histone methylase, to the kinesin promoters (Zou et al., 2014). This is important as trimethylation of H3K4 to H3K4me3 is important for assembly of the RNA polymerase II pre-initiation complex (Zou et al., 2014).

KIFC1 is also a downstream transcriptional target of p110CUX1, revealed by ChIP in breast cancer and HeLa cells and elegantly verified in three complementary experiments (Sansregret et al., 2011). p110CUX1 was shown to be able to bind the KIFC1 promoter, and KIFC1 expression increased 2.3-fold after p110CUX1 overexpression. KIFC1 expression then fell when p110CUX1 was suppressed by a doxy-inducible shRNA. Upon reduction of shRNA expression by removal of doxycycline, KIFC1 expression showed a greater than nine-fold increase (Sansregret et al., 2011).

p110CUX1 requires E2F factors to exert transcriptional effects (Truscott et al., 2008). This was first indicated by the observation that p110CUX1 binding sites on DNA also held E2F binding sites close by, and that mutants keeping wild-type E2F from binding DNA significantly reduced p110CUX1-mediated transcription, using POLA1 as the reporter gene. Furthermore, affinity chromatography and coimmunoprecipitation showed that p110CUX1 weakly interacted with E2F1 and E2F2, while ChIP showed drastic increases in E2F1 and E2F2 binding to DNA upon overexpression of p110CUX1 (Truscott et al., 2008).

Taken together, it is likely that upon E2 induction, more ANCCA binds to the KIFC1 promoter thus increasing recruitment of MLL1 and E2F1. This increases p110CUX1 binding, which in turn increases MLL1 and E2F1 binding. MLL1-mediated methylation allows the assembly of the RNA polymerase II pre-initiation complex, thus inducing KIFC1 transcription. More research is required to elucidate further details of this pathway. Nevertheless, it is important to note that E2Fs (Reviewed by Kent and Leone, 2019), p110CUX1 (Reviewed by Sansregret et al., 2011) and ANCCA (Zou et al., 2014) are all overexpressed in cancer.

KIFC1 Expression Negatively Affects Patient Prognosis

As KIFC1 is often found to be overexpressed in cancer, it is logical to suspect that its expression may affect clinical outcome. Incidentally, out of the 15 published studies (at the time of writing) to address the relationship between KIFC1 and cancer prognosis, only two found no significant association. In breast cancer, KIFC1 expression was shown to exhibit no association between extent of cancer spread to nodes and extent of metastasis (Li et al., 2015), while observation of 132 squamous cell carcinomas (SCCs) showed KIFC1 expression was not associated with survival, even though 75% of samples showed KIFC1 overexpression (Imai et

al., 2017). This implies that KIFC1 may simply be involved in pathogenesis but not progression of SCC.

On the contrary, a large body of evidence across various cancers shows an inverse correlation between KIFC1 levels and prognosis (Table 2). For example, higher KIFC1 expression has been associated with lower progression free survival, disease free survival, recurrence free survival, relapse free survival, distant metastasis free survival and overall survival. Patients overexpressing KIFC1 are also more two times less likely to survive in renal cell carcinoma (Li et al., 2018), or three times less likely to survive in TNBC (Ogden et al., 2017). Furthermore, increased KIFC1 expression is also associated with increased likelihood of relapse (Sekino et al., 2017), higher grade (Table 2) and shorter time for recurrence (Fu et al., 2018). Incidentally, this raises the possibility of KIFC1 expression to be used as a prognostic biomarker. Out of a panel of 21 TNBC biomarkers, KIFC1 expression significantly correlated with only Ki67 expression in Caucasian patients, and showed no correlation in African American patients, suggesting that KIFC1 isn't simply a surrogate biomarker (Ogden et al., 2017). Furthermore, KIFC1 has been proposed as a prognostic biomarker in various other cancer types (Table 2).

Table 1.2. *An exhaustive list of reports of negative prognostic measurements associated with KIFC1 overexpression and the papers in which this was reported. References with an asterisk (*) recognise KIFC1 as a potential prognostic biomarker.*

Cancer Type	**Prognostic Measurement**	**Reference**
Meningioma	Higher Grade	(Jungwirth et al., 2019)
Hepatocellular Carcinoma	Reduced Overall Survival, Disease Free Survival	(Teng et al., 2019)*
	Reduced Overall Survival	(Shi et al., 2018)
	Reduced Overall Survival, Disease Free Survival	(Han et al., 2019)
	Reduced Overall Survival, Disease Free Survival	(Fu et al., 2018)*
	Reduced Overall Survival, Higher Grade	(Chen et al., 2017)*
Renal Cell Carcinoma	Overall Survival, Disease Free Survival, Higher Grade, Increased Recurrence	(Li et al., 2018)*
Breast Cancer (TNBC)	Reduced Overall Survival, Progression Free Survival,	(Ogden et al., 2017)*
	Distant Metastasis Free Survival	(Pannu et al., 2015b)*
	Reduced Overall Survival, Progression Free Survival	

Breast Cancer	Higher Grade	(Pannu et al., 2015b)*
Prostate Cancer	Reduced Relapse Free Survival	(Sekino et al., 2017)
Lung Cancer (Non-Small Cell Lung Carcinoma)	Reduced Overall Survival, Progression Free Survival	(Liu et al., 2016)*
Ovarian Cancer	Reduced Overall Survival, Higher Grade Reduced Overall Survival, Higher Grade	(Mittal et al., 2016)* (Pawar et al., 2014)*

KIFC1 Enhances Proliferation in Cancer Cells

Although clustering amplified centrosomes to avoid multipolar mitosis is clearly an important evolutionary advantage to cancer cells, the fact that KIFC1 overexpression was the second highest predictive factor of lung cancer metastasis to the brain, second only to N-Cadherin (Grinberg-Rashi et al., 2009), and the supposed role of KIFC1 in docetaxel resistance (De et al., 2009) suggests multiple likely roles for KIFC1 in cancer which were not initially appreciated. The link between KIFC1 and altered proliferation and cell cycle regulation was first uncovered by analysis of KIFC1 expression networks in ovarian adenocarcinomas to produce a protein interactome. KIFC1 was predicted to interact directly with a variety of proteins involved in progressing the cell cycle and mitosis, including PRC1 (cytokinesis), CDC20 (activates APC/C), CDK1 (cell cycle progression), PLK1 (cell cycle progression), TPX2 (spindle microtubule assembly), NUSAP1 (spindle microtubule assembly) and MAD2L1 (spindle assembly checkpoint), along with a variety of mitotic kinesins (Pawar et al., 2014). A similar suite of genes was also associated with KIFC1 overexpression in a study in 2016 (Mittal et al., 2016).

Further exploration by overexpression of KIFC1 with transfection of active GFP-KIFC1 into HeLa cells resulted in increased proliferation with a cell doubling time of 11h compared to 16h in control cells. Furthermore, cells overexpressing KIFC1 were more able to form viable colonies compared to control cells, and even more so when compared to cells with KIFC1 knockdown (Pannu et al., 2015b). Although no further KIFC1 overexpression studies have been reported, a variety of KIFC1 knockdown studies have shown decreases in cell viability in breast cancer (Li et al., 2015), Non-small cell lung carcinoma (NSCLC) (Liu et al., 2016),

prostate cancer (Sekino et al., 2017), testicular cancer (Xiao et al., 2017) and hepatocellular carcinoma (HCC) (Fu et al., 2018).

This data was supported by the observation that higher levels of KIFC1 induced higher expression of Ki67, cyclins A and D, Aurora B kinase (Pannu et al., 2015b), Aurora A kinase, cyclin E, centrin-2 (Li et al., 2018), PCNA and cyclin B1 (Chen et al., 2017), as well as higher BrdU incorporation into the DNA, indicating a higher proportion of cells going through S-phase. Higher phosphorylated CDK1 and phosphorylated Histone-H3 expression was also observed, indicating a higher proportion of cells also entered M-phase (Pannu et al., 2015b).

The role of KIFC1 in cancer cell proliferation was further illustrated by *in vivo* studies in mice in which renal cell carcinoma (RCC) cells transfected with either control or KIFC1 siRNA were subcutaneously injected into mice (Li et al., 2018). After 35 days, tumour tissues isolated from mice injected with cells with KIFC1 knockdown had a significantly reduced volume and weight when compared to cells expressing normal levels of KIFC1, showing that KIFC1 had a positive effect on tumour growth *in vivo*. Interestingly, PI3K and p-AKT expression was much lower in tumour tissue with KIFC1 knockdown, indicating that KIFC1 may regulate tumour growth by the PI3K/AKT pathway (Li et al., 2018). This was supported by the fact that KIFC1 knockdown in HCC cells also decreases levels of activated p-AKT and p-PI3K (Fu et al., 2018).

Interestingly the upregulation of Aurora B kinase and HIF1α observed upon KIFC1 overexpression, but no decrease upon KIFC1 knockdown, prompted Pannu *et al.* (2015a) to posit that KIFC1 forms an "oncogenic axis" with Aurora B kinase and HIF1α, which are both classical oncogenes. The fact that KIFC1 knockdown did not decrease Aurora B kinase and HIF1α implied that KIFC1 was not normally a regulator of such proliferative pathways, rather it had gained oncogenic function in cancer cells (Pannu et al., 2015b).

KIFC1 Alters Cell Cycle Kinetics in Cancer Cells

To investigate the possible proliferation-enhancing role of KIFC1, cell cycle dynamics were assessed. HeLa cells with artificial KIFC1 overexpression showed a marked decrease in the time taken to complete the cell cycle compared to control cells, 10.5h vs 13h respectively, which arose from the shortening of G2/M. This was supported by the fact that cyclin B1

expression, which induces the G2/M transition, peaked at 8 hrs in KIFC1 overexpressing cells and 10 hrs in control cells. Cells with KIFC1 knockdown took 14 hrs to complete the cell cycle, mediated by a longer G2/M phase (Pannu et al., 2015b). This was mirrored in fibroblasts by the fact that KIFC1 knockdown delayed by 2 hrs the degradation of Cyclin A (Kim and Song, 2013), which is degraded throughout the G2/M and is completely degraded at mitotic exit (Yam et al., 2002). Incidentally, overexpression of KIFC1 in HeLa cells did not change the proportion of cells transitioning between G1 and S-phase (Pannu et al., 2015b).

The role of KIFC1 in the cell cycle was further validated in RCC cell lines (Li et al., 2018) and NSCLC cell lines where knockdown of KIFC1 arrested those cells in G2/M phase. This was explained by the fact that KIFC1 knockdown reduced CDK1 expression and increased p21 expression (Liu et al., 2016). This is important as CDK1 complexes with cyclin B1 to form Maturation Promotion Factor (MPF), which induces transition between G2 and M phases, while p21 inhibits the kinase activity of MPF (Abbas and Dutta, 2009). Interestingly, MPF stabilises KIFC1 concentrations in the cell by phosphorylating it at Ser6, protecting KIFC1 from degradation by APC/C (Singh et al., 2014), possibly indicating a positive feedback loop between KIFC1 stabilisation and MPF expression. This would make sense as KIFC1 is stabilised by MPF-mediated phosphorylation, while it is destabilised upon MPF inhibition (Reviewed by Xiao and Yang, 2016). In contrast to NSCLC and RCC cells, however, HCC cells overexpressing KIFC1 were reported to show no discernible change in cell cycle distribution upon KIFC1 knockdown (Fu et al., 2018).

Nevertheless, faster progression through G2/M upon KIFC1 overexpression, and the opposite upon knockdown, raised the possibility that the G2/M checkpoint and Spindle Assembly Checkpoint (SAC) may become compromised upon KIFC1 overexpression. One critical component of the SAC is the Mad1-Mad2 axis, imbalances in which result in effects ranging from mitotic arrest to mitotic acceleration (Schuyler et al., 2012). For example, Mad1 overexpression with no corresponding increase in Mad2 in *Xenopus* extracts removed SAC function altogether (Chung and Chen, 2002). In HeLa cells, KIFC1 overexpression caused a significant increase in Mad1 expression, while leaving Mad2 levels unaffected (Pannu et al., 2015b). The accelerated progression into anaphase, even in the presence of spindle fibres not under tension, likely causes low-level aneuploidy, all mediated by an impaired SAC. This is very interesting because Mad1 is a downstream transcriptional target of p110CUX1 (Harada

et al., 2008), a transcriptional activator of KIFC1 (Sansregret et al., 2011). Although the possibility exists that KIFC1 and Mad1 are coincidentally both downstream targets of a classical oncogene, the observed increase in Mad1 upon artificial KIFC1 overexpression (Pannu et al., 2015b) indicates a degree of positive feedback.

KIFC1 Inhibits Apoptosis and Increases Survival Signalling in Cancer Cells

Tumour growth relies on both maximising proliferative activity while also minimising apoptosis. Having shown that KIFC1 overexpression enhances cell proliferation, while knockdown hinders it, it was also noticed that KIFC1 overexpression in HeLa cells significantly enhanced survival by increasing survivin and Bcl-2 expression (Pannu et al., 2015b), both of which are anti-apoptotic proteins. However, KIFC1 knockdown did not decrease the levels of survivin and p-survivin, with levels remaining comparable to those observed in control cells. This prompted the authors to suggest that KIFC1 overexpression "thrusts survival signalling into an 'overdrive' mode", supported by the fact that IHC staining of clinical samples showed nuclear KIFC1 Weighted Index (WI) correlated strongly with survivin WI and Ki67 WI (Pannu et al., 2015b). However, increased Bax expression (pro-apoptotic) and decreased Bcl-2 expression was observed upon KIFC1 knockdown in gastric cancer cells (Zhang et al., 2016a). The same was observed in HCC cells and prostate cancer cells, where KIFC1 knockdown prompted decreased Bcl-2 expression while increasing the proapoptotic Bax, p53 (Fu et al., 2018), c-PARP and cleaved caspase-3 expression (Sekino et al., 2019). Experiments in HCC cells also mirrored the trend that KIFC1 expression positively affected a cell's survival, as flow cytometry data showed marked increases in the rate of apoptosis upon KIFC1 knockdown (Fu et al., 2018)

Such KIFC1-mediated increases in survival expression were shown to translate to physiological effects in breast cancer cells exposed to UV-C radiation, as cells with KIFC1 knockdown showed much higher levels of cleaved caspase-3, a marker for apoptosis, when compared to control cells. Furthermore, cells overexpressing KIFC1 showed reduced levels of caspase-3, indicating that KIFC1 mediates promotion of cancer cell survival. This was correlated by cell viability assays after UV-C radiation, where cells overexpressing KIFC1 showed greater growth than those with KIFC1 knockdown (Pannu et al., 2015b).

The increased survivin expression upon KIFC1 overexpression indicated a possible interaction between KIFC1 and survivin (Pannu et al., 2015b). Co-immunoprecipitation of whole cell lysates in cells that either overexpressed KIFC1, had KIFC1 knockdown or expressed wild-type levels of KIFC1 showed that anti-KIFC1 antibody co-precipitated survivin in all three conditions, while anti-survivin antibody co-precipitated KIFC1. The levels of survivin were drastically increased in cells overexpressing KIFC1, while KIFC1 knockdown had little effect compared to control cells. This suggested that KIFC1 interacts in a complex with survivin (Pannu et al., 2015b).

Since the effect of survivin is regulated by ubiquitination and degradation in a cell-cycle dependent manner, peaking between G2/M and declining at G1 (Zhao et al., 2000), the significance of the KIFC1-survivin interaction was compounded by immunoblotting when reduced polyubiquitin signals at the survivin band were observed in lysates of cells overexpressing KIFC1, despite the increased survivin expression. Furthermore, increased polyubiquitin signal was observed in cells with KIFC1 knockdown when compared to control cells, even though survivin levels were the same. This implied a novel role of KIFC1 in possibly protecting survivin from ubiquitination (Pannu et al., 2015b). However, it is worth noting that the nature of the polyubiquitin signals were not characterised, and so it cannot be said with certainty that the reduced polyubiquitin signal reduced survivin degradation.

KIFC1 Promotes Invasiveness and Metastasis

The link between KIFC1 and cancer was first alluded to upon discovery that KIFC1 was a positive indicator of NSCLC metastasis to the brain (Grinberg-Rashi et al., 2009). Furthermore, it was proposed as a marker for metastatic onset in ovarian cancer (Pawar et al., 2014). Since then, KIFC1 expression in clinical samples has been associated with metastasis in TNBC (Ogden et al., 2017), RCC (Li et al., 2018) and HCC (Fu et al., 2018). This is supported by the fact that KIFC1 knockdown reduced the expression of a host of pro-metastatic proteins including MMP-2, MMP-9, VEGF in RCC (Li et al., 2018), and N-Cadherin, MMP-2, β-catenin, Slug and ZEB1 in HCC (Fu et al., 2018) and HIF1α in breast cancer cells (Pannu et al., 2015b). Meanwhile, KIFC1 overexpression increased expression of various EMT markers, including N-Cadherin, Vimentin, TWIST1 and p-AKT, while inhibiting expression of E-Cadherin, validated

by immunoblotting and IF microscopy. Furthermore, it was observed that cells with KIFC1 overexpression displayed a spindle shape, indicating mesenchymal morphology, while cells with KIFC1 knockdown showed a cobblestone appearance, characteristic of epithelial morphology (Han et al., 2019).

Such KIFC1-mediated differential expression of metastasis-involved proteins upon KIFC1 knockdown resulted in a more than twofold decrease in migration and invasiveness in HCC (Fu et al., 2018) and RCC cells (Li et al., 2018). Furthermore, invasiveness and migratory capacity increased upon overexpression of KIFC1 in HCC cell lines. These effects were translated *in vivo*, where mice injected with HCC cells overexpressing KIFC1 had larger and more numerous lung metastases than mice injected with control HCC cells. As expected, lung metastasis was inhibited in mice injected with HCC cells with KIFC1 knockdown compared to control groups. Such data was corroborated by Haematoxylin and Eosin staining of mouse lung tissue (Han et al., 2019).

To identify the key molecules involved in KIFC1-mediated EMT in HCC, suspected transcription factors were screened by RT-PCR, with TWIST1 observed to be up or downregulated at the mRNA level upon KIFC1 overexpression or knockdown (Han et al., 2019). TWIST1 induces EMT through a variety of pathways including AKT, MAPK and STAT3 (Reviewed by Khan et al., 2013), but only AKT expression was found to change upon KIFC1 overexpression or knockdown (Han et al., 2019). One protein which takes part in HCC metastatic development through the AKT/TWIST1 EMT pathway is gankyrin (Fu et al., 2011), and it was found that gankyrin expression also increased or decreased as KIFC1 was over or underexpressed. Furthermore, gankyrin overexpression negated the effects of KIFC1 deficiency and vice versa, with cells increasing invasiveness and migratory capacity, and increasing the number and size of metastatic nodules in mice. This was further validated by the fact that a positive association was found between KIFC1 and gankyrin expression in clinical HCC samples (Han et al., 2019). This collection of data showed that KIFC1 mediates EMT transition, at least in HCC cells, through gankyrin, which acts as a downstream effector of EMT. This could possibly be because TWIST1 is a downstream transcriptional target of HIF1α (Yang and Wu, 2008), which is overexpressed by overexpression of KIFC1.

KIFC1 Induces Drug Resistance in Cancer Cells

One way of treating certain cancers is by using taxanes such as docetaxel and paclitaxel. These molecules bind to β-tubulin and inhibit the exchange of free tubulin in microtubules, disrupting the spindle formation and mitosis and eventually causing cell death. Although half of all patients treated with docetaxel display clinical responses, tumours often show resistance (Wang et al., 2014). In core biopsies taken from breast tumours resistant to docetaxel, it was found that KIFC1 was slightly overexpressed compared to sensitive cells. Furthermore, overexpression of KIFC1 more than doubled the proportion of surviving cells upon treatment with 4 nmol/L of docetaxel. It was found that KIFC1 achieves this effect by reversing the stabilisation of microtubules by docetaxel, evidenced by the increased amounts of free tubulin in cells in cells overexpressing KIFC1 (De et al., 2009). Similar dependence upon KIFC1 expression for docetaxel resistance was also seen in castration-resistant prostate cancer, in which almost every patient treated with docetaxel became refractory (Sekino et al., 2017). Furthermore, a follow up to the prostate cancer study found that KIFC1 expression was increased eightfold in docetaxel resistant cells compared to sensitive parental cells of the same cell line. In these cell lines, KIFC1 depletion and KIFC1 inhibition both suppressed docetaxel-resistant cell growth, while combination treatment with KIFC1 inhibitor and docetaxel reduced viability in both docetaxel resistant and sensitive cells (Sekino et al., 2019).

KIFC1 Function is Dispensable in Most Normal Cells

Unlike many other cancer targets, KIFC1 function seems dispensable in most non-cancerous cells. KIFC1 knockdown in cells with normal centrosomes caused no negative effect in mitosis, but did cause negative effects in oocytes, which are acentrosomal, implying that centrosomes 'masked' the role of KIFC1 in somatic cells (Mountain et al., 1999). Kwon *et al.* found that upon KIFC1 knockdown, the higher the degree of centrosome amplification in cancer cells, the higher the degree of multipolar mitosis, large scale aneuploidy and subsequent apoptosis or senescence, reducing cell viability by more than 90% after six days. Meanwhile, diploid

control cells were left unaffected by KIFC1 knockdown (Kwon et al., 2008). In support of this, small molecule inhibition of KIFC1 in cancer cells with centrosome amplification increased multipolar mitosis from 30% in control cells to 98% in treated cells. Interestingly, KIFC1 inhibition did not affect normal fibroblasts or affect the clonogenicity of primary human bone marrow cells (Watts et al., 2013), which is important as inhibition of many other targets in cancer cause long term effects such as bone marrow injury and myelosuppression (Reviewed by Wang et al., 2006).

However, potential inhibition of KIFC1 may not necessarily be side effect free. Evidence exists for a context-specific requirement for KIFC1. As mentioned, KIFC1 generates the force required for meiosis in oocytes without centrosomes (Mountain et al., 1999). Furthermore, KIFC1 is also required for spermiogenesis. It has been found to be expressed in human testis and localised in unique patterns, gathering at the pole of the nuclei of immature spermatids (Xiao et al., 2017) allowing it to perform two major functions of spermiogenesis, acrosome biogenesis and nuclear deformation, both occurring due to KIFC1's ability for vesicular trafficking by transportation along the microtubule (Reviewed by Xiao and Yang, 2016). The fact that KIFC1 takes part in central functions during oocyte and sperm cell development alongside embryo gestation may mean that treatment with KIFC1 inhibitors could negatively affect pregnant patients or even cause infertility.

Initially, the addiction of cancer cells with centrosome amplification to KIFC1 had been well established, and the selectivity that KIFC1 seemed to provide against cancer cells with centrosome amplification warranted the development of KIFC1 inhibitors. However, work published in recent years outlining the alternative roles of KIFC1 has shown that therapeutic targeting of KIFC1 may be a suitable option in cancers both with and without centrosomes amplification (Figure 1.6)

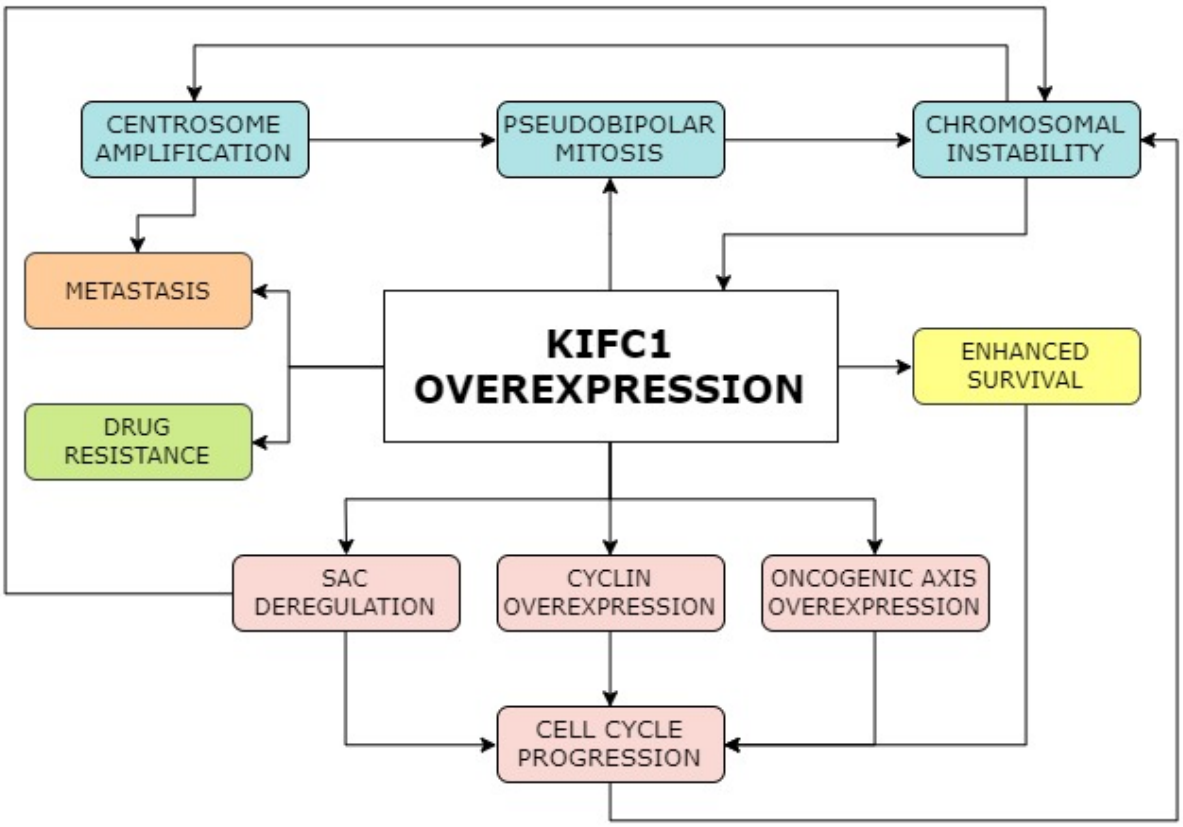

Figure 1.6. The Many Roles of KIFC1 in Driving Cancer Progression. *Although it is not known whether KIFC1 is overexpressed before centrosome amplification, KIFC1 expression allows cells with centrosome amplification to undergo pseudo-bipolar mitosis, avoiding massive aneuploidy and inducing low level chromosomal instability, a hallmark of cancer. This would allow further evolution of cancer cells, including the possibility of further KIFC1 overexpression. Furthermore, KIFC1 induces expression of certain cyclins, Mad1 and the "oncogenic axis", which drive aberrant cell proliferation. Mad1 overexpression deregulates the Spindle Assembly Complex (SAC), which allows an anaphase delay for pseudo-bipolar mitosis. Furthermore, both centrosome amplification and KIFC1 overexpression induce metastatic phenotypes, while KIFC1 induces taxanes resistance and causes overexpression of survivin and Bcl-2, both of which allow evasion of apoptosis.*

1.5. KIFC1 Inhibitors

Inhibitors do exist against KIFC1 and as expected, they induce multipolar mitosis in cancer cells with amplified centrosomes. Furthermore, they are all thought to bind KIFC1 in different manners.

CW069

CW069 was discovered through a chemogenomic approach based on Eg5 kinesin inhibitors on the principle that similar proteins bind similar ligands. Upon testing on N1E-115 neuroblastoma cells, treatment with CW069 increased the frequency of multipolar mitosis from 30% to over 90% of cells but did not induce multipolar mitosis in normal fibroblasts (Watts et al., 2013). Furthermore, treatment of N1E-115 cells with both CW069 and KIFC1 siRNA did not increase the frequency of multipolar mitosis above cells treated with only KIFC1 siRNA, which indicates that the inhibitor recapitulated the effect of KIFC1 knockdown. Differential scanning fluorimetry confirmed that CW069 binds allosterically to destabilise KIFC1 without denaturing it, while also showing that the CW069 binding is site specific, confirming *in silico* predictions. However, the dosages used to induce multipolar mitosis ranged between 100 and 200 μM (Watts et al., 2013), which is relatively high compared to alternative KIFC1 inhibitors

AZ82

High-throughput screening of 800,000 molecules followed by multiple cycles of medicinal chemistry yielded AZ82, a small molecule which binds the KIFC1/microtubule complex to inhibit the release of ADP and binding of ATP by KIFC1 (Wu et al., 2013). This was found by fluorescent nucleotide exchange experiments in which AZ82 reduced the fluorescent ADP/ATP exchange of KIFC1/microtubule complexes to basal levels of just KIFC1 alone, which is considered a negative control. AZ82 was shown to bind the KIFC1/microtubule complex by dialysis of 1 μM of AZ82 against buffer, KIFC1, microtubules and KIFC1 together with microtubules. Although free AZ82 was dispersed evenly among all sections, mass spectrometry showed that AZ82 was significantly enriched in the KIFC1/microtubule complex (Wu et al., 2013). Importantly, AZ82 had no activity on a panel of nine other similar kinesins. Treatment with just 1.2 μM of AZ82 increased frequency of multipolar mitosis in BT549 breast cancer cell line cells from 12% to approximately 30%, while 48% of mitotic divisions ended in

mitotic catastrophe, as opposed to 8% with control treatment. However, it was also reported that nonspecific killing of cells was observed above 4 μM (Wu et al., 2013).

SR31527

A high-throughput KIFC1 ATPase assay of over 30,000 compounds yielded SR31527 as a potent KIFC1 inhibitor. Biolayer interferometry showed that SR31527 binds KIFC1 directly without involving microtubules, while molecular modelling indicated that it binds allosterically at a novel site. In multiple breast cancer cell lines with centrosome amplification, 50 μM of SR31527 increased the frequency of multipolar mitosis, including an eight-fold increase in the case of BT549. Furthermore, treatment with SR31527 decreased viability and clonogenicity. At 50 μM, SR31527 killed up to 83% of TNBCs, while in normal human lung fibroblast cells, SR31527 had no effect. However, SR31527 killed almost all normal human lung fibroblast cells at 100 μM, indicating that the drug does display some off target cytotoxic effects (Zhang et al., 2016b).

In fission yeast, overexpression of human KIFC1 without a corresponding overexpression of Cut7 induces monopolar spindles and cell death, which means inhibition of KIFC1 would decrease cell death. This allowed evaluation of KIFC1 inhibitors because in wild type yeast, a specific inhibitor would cause no detriment, but in KIFC1-overexpressing yeast, the inhibitor would reduce monopolar spindle formation and thus reduce the loss of KIFC1-mediated viability. Conversely, changes in the growth of wild type fission yeast by inhibitors would indicate that the inhibitor has off target effects, and the extent of any reduced viability loss would depend on whether the inhibitor inhibited KIFC1 more than it interfered with yeast mitosis (Yukawa et al., 2018).

Interestingly, all three inhibitors reduced viability in non-KIFC1-overexpressing fission yeast whose drug resistance mechanisms had been removed (control), indicating that the inhibitors had off-target effects (Yukawa et al., 2018). These “off-targets” would have been likely to include proteins that were not alternative kinesin-14s, as deletion of pkl1 and klp2 kinesin-14 proteins is still viable (Troxell et al., 2001). Nevertheless, AZ82 reduced KIFC1-mediated viability loss, indicating that it is an effective KIFC1 inhibitor. On the other hand, treatment with CW069 in KIFC1-overexpressing yeast increased cell death, indicating that its KIFC1

inhibitory properties were outweighed by its off-target toxicity. Furthermore, SR31527 did not affect viability loss in KIFC1-overexpressing cells, indicating that its KIFC1-inhibitory effects were neutralised by the off-target toxicity it causes. It is worth noting that the off-target toxic effect was relatively modest in the first place, indicating that its KIFC1-inhbitory effect is also modest (Yukawa et al., 2018).

Although KIFC1 inhibitors do exist, none are at the clinical testing stage, possibly because they seem to suffer from off-target toxicological effects, and in the case of CW069, weak biochemical activity.

1.6. PROTACS

Proteolysis-targeting chimeras, also known as PROTACs are hetero-bifunctional molecules made up of an E3 ubiquitin ligase-binding ligand and a target binding ligand linked by a linker region. This means that PROTACs can bind a target protein and E3 ubiquitin ligase simultaneously to form a ternary complex. The proximity of the target protein and E3 ubiquitin ligase means that ubiquitin molecule(s) activated by an E1 ubiquitin-activating enzyme can be transferred from an E2 ubiquitin-conjugating enzyme to the target protein via the E3 ubiquitin ligase, thus marking the target protein for degradation by the proteasome (Schneekloth et al., 2008) (Figure 1.7). This means that PROTACs can degrade oncogenic proteins by "hijacking" the ubiquitin proteasome system.

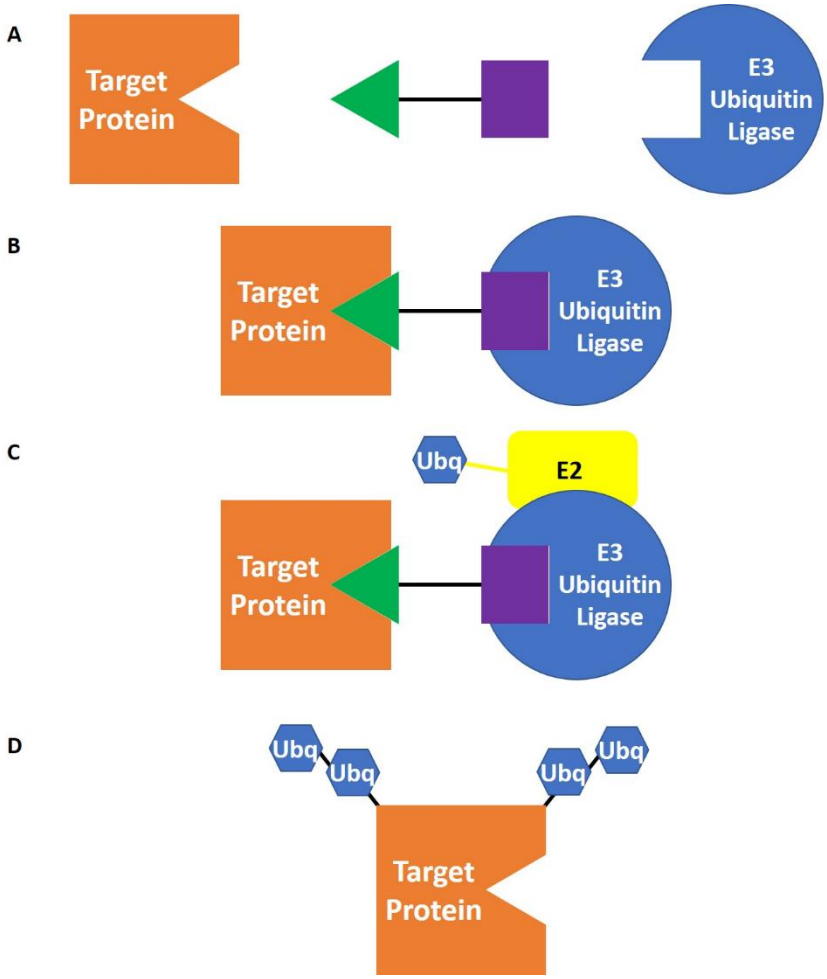

Figure 1.7. A Crude Representation of PROTAC Action. *A) PROTACs are bifunctional and so incorporate recruiters for both the target protein and an E3 ubiquitin ligase. B) By binding both the target protein and the E3 ubiquitin ligase to form a ternary complex, the PROTAC brings the two proteins in proximity to each other. The intermolecular protein interactions between the two proteins stabilises the interaction. C) An E2 ubiquitin-conjugating enzyme binds to the E3 ubiquitin ligase and delivers activated ubiquitin molecules. D) The target protein is now polyubiquitinated and ready for degradation by the 26S proteasome.*

PROTACs can be constructed using small molecule ligands as recruiters for both target protein and E3 ubiquitin ligase. An early such example is the SARM-nutlin PROTAC, which recruited the MDM2 E3 ubiquitin ligase to the androgen receptor and significantly reduced levels of androgen receptor. Furthermore, the role of the proteasome was confirmed by reduced effectiveness upon protease inhibition (Schneekloth et al., 2008). PROTAC-mediated degradation effects have been shown to be quite rapid and sustained for long periods of time. For example, degradation of RIPK2 with a PROTAC was observed as early as 1h after treatment and protein levels only recovered after 24h (Bondeson et al., 2015). Furthermore, PROTACs show broad tissue distribution and can reduce target protein levels by over 90% *in vivo* using only nanomolar concentrations, producing results comparable to RNA interference (Bondeson et al., 2015).

PROTACs provide a benefit over small molecules as they catalyse multiple rounds of protein degradation, which means less than stoichiometric levels are required (Bondeson et al., 2015), whereas small molecule inhibitors work by stoichiometric occupation of the active site or other allosteric sites on target proteins. This is important as 75% of the proteome doesn't have an active site, for example E3 ubiquitin ligases, which means many proteins are simply "undruggable". In the case of PROTACs, inhibition is not required by the recruiters, rather the targets simply need to be bound (Reviewed by An and Fu, 2018). Furthermore, mutations in oncoproteins have been known to mediate resistance to small molecules. However, PROTACs based on the same small molecules have been shown to degrade the same mutant oncoproteins. For example, a C481S mutation to BTK mediates resistance to ibrutinib in more than 80% of chronic lymphocytic leukaemia patients, however a PROTAC derived from ibrutinib reduced mutant BTK levels by more than 99% while improving specificity (Buhimschi et al., 2018). Ultimately, PROTACs provide the opportunity to target undruggable and mutant proteins, whilst also improving the specificity and reducing the dosages required compared to the inhibitors they are based upon.

As mentioned, PROTACs induce degradation of target proteins by effectively catalysing the interaction between the target protein and an E3 ubiquitin ligase, which executes the final step of attaching an activated ubiquitin molecule onto the target protein.

Ubiquitin itself is reversibly attached to lysine residues of a target protein either as a single molecule, called mono-ubiquitination, or as part of a chain, called poly-ubiquitination, by its N-terminal methionine residue or any of its seven lysine residues (K6, K11, K28, K33, K48 and K63) (Reviewed by Akutsu *et al.*, 2016). These chains can be homotypic, where the ubiquitin chain is comprised of molecules attached by the same residue, or heterotypic, where molecules can be branched. Furthermore, ubiquitin molecules themselves may be subject to further post-translational modification, providing an countless possibilities for diversity and specificity (Reviewed by Akutsu *et al.*, 2016).

One of the ways in which ubiquitin exerts effects is through the lysine it is attached by, with each type of linkage being associated with specific cellular functions.

K6 attachments are one of the least well-characterised ubiquitin linkages, although it is known that it is not associated with degradation as inhibition of the proteasome has been found to not increase its abundance (Kim *et al.*, 2011). However, they were found to be enriched upon UV stress (Elia *et al.*, 2015) and associated with the BRCA1-BARD1 DNA damage repair E3 ubiquitin ligase complex (Morris and Solomon, 2004). K6 linkages also increase upon mitochondrial depolarisation, indicating impairment and the need for mitophagy (Ordureau *et al.*, 2014), which is significantly delayed in cells expressing K6 mutant ubiquitin (Ordureau *et al.*, 2015).

K11 signals are established as a proteasomal signal used in cell cycle regulation. For example, APC/C uses the K11-specific E2 ubiquitin-activating enzyme to ubiquitinate substrates for degradation (Reviewed by Wickliffe *et al.*, 2012). Furthermore, knockdown of a K11-specific deubiquitinase called Cezanne causes increased K11 ubiquitination of HIF1α and HIF2α and their subsequent degradations, but not through the proteasome (Bremm *et al.*, 2014).

K27 attachments to chromatin upon DNA damage have been shown to propagate the DNA damage response, while cells unable to form such attachments have been shown to be unable to activate the DNA damage response (Gatti *et al.*, 2015). Furthermore, K27 attachments have been implicated in activating immune responses in response to bacterial DNA by acting as a scaffold for the recruitment of other immune proteins (Reviewed by Akutsu *et al.*, 2016).

K29 attachments have been shown to take part in the canonical Wnt signalling pathway. K29 ubiquitination of axin, a scaffold protein within the β-catenin destruction complex, disrupts

its interactions with Wnt co-receptors, subsequently attenuating Wnt/ β-catenin signalling (Fei *et al.*, 2013). Furthermore, the TRABID deubiquitinase, a positive regulator of the Wnt/ β-catenin pathway, exerts its effects by deubiquitinating K29 attachments (Licchesi *et al.*, 2011).

K33 attachments have been implicated in post-golgi membrane trafficking. The Cullin 3-KLHL20 E3 ubiquitin ligase complex was found to K33 ubiquitinate coronin 7, which was then transported to the trans golgi network (Yuan *et al.*, 2014).

K48 are the most common chains and target proteins for degradation, however, the previous dogma that K48 tetra-ubiquitin chains are required for proteasomal degradation has begun to be challenged, with proteins such as cyclin B being more efficiently degraded with multiple, short chains as opposed to single, longer chains, while two di-ubiquitin chains have been observed to be a better proteasomal substrate than one tetra-ubiquitin chain (Reviewed by Swatek and Komander, 2016).

K63 chains have been shown to have a wealth of functions in the cell, including in proteasomal degradation of dihydrofolate reductase (Hofmnan and Pickart, 1999) and lysosomal degradation of EGFR (Huang *et al.*, 2013). It also takes part in regulation of the Wnt signalling pathway (Tauriello and Maurice, 2010) and in transport of endocytosis and trafficking (Reviewed by Erpapazoglou *et al.*, 2014).

It is important to note that combinations of such linkages in various numbers of branched and straight chains with and without various protein modifications provide a vast diversity of signals in the cell. To perceive signals propagated by ubiquitin chains, cells recognise proteins with specific states of ubiquitination using a diverse set of ubiquitin binding proteins (Reviewed by Husnjak and Dikic, 2012).

1.7. Project Aims

Therapeutic options for prevention and treatment of metastatic uveal melanoma are poor in part due to a lack of therapeutic targets (Violanti et al., 2019). However, recent research has shown that centrosome amplification does exist in uveal melanoma, which may provide a therapeutic target (de Almeida et al., 2019). Although centrosome amplification causes cancer (Levine et al., 2017), it also poses as an "Achilles heel" for cancer cells as they rely on centrosome clustering to avoid multipolar mitosis, massive aneuploidy and cell death (Kwon et al., 2008). An integral part of the clustering process is KIFC1, and depletion of KIFC1 does cause multipolar mitosis and cell death in cells with centrosome amplification (Kwon et al., 2008). KIFC1 has also been shown to have oncogenic effects independent of centrosome clustering, including in cells with very low levels of centrosome amplification (Pannu et al., 2015b). Furthermore, KIFC1 function seems to be dispensable in normal somatic cells (Watts et al., 2013). Small molecule KIFC1 inhibitors do exist, but they suffer from off target effects (Yukawa et al., 2018) or have poor biochemical activity (Watts et al., 2013). A novel way to get around such problems may be the use of PROTACs, which work at lower concentrations and with better specificity than the small molecule inhibitors that they are derived from (Buhimschi et al., 2018).

The aims of this project, therefore, are twofold:

1) Explore centrosome amplification and the role of KIFC1 in primary uveal melanoma (Mel270) and liver metastatic uveal melanoma (Omm2.3 and Omm2.5) cell lines derived from the same patient.

   To our knowledge, centrosome amplification has previously never been assessed in uveal melanoma metastases. Furthermore, the role of KIFC1 has also never been assessed in primary or metastatic uveal melanoma.

2) Generate promising KIFC1 binders for the formation of PROTAC molecules.

   This will be done by first synthesising the CW069 inhibitor. For possible linker attachment locations, CW069 analogues with altered functional groups will be synthesised. To identify which functional groups are non-crucial for binding to KIFC1, and therefore suitable for attachment with a linker, a structure activity relationship

(SAR) assay will be performed using a recombinant KIFC1 motor protein domain. Dispensable functional groups will then be used to attach various linkers and E3 ubiquitin ligase recruiters to produce PROTACs, which will then be assessed for efficacy.

2. Methods and Materials

2.1. Methods

All reagents from Thermo-Fisher Scientific (Waltham, MA), unless otherwise stated.

Cell Culture

Cells were cultured in Full RPMI media (RPMI-1640-Glutamax, 10% FBS, 1% penicillin/streptomycin) and incubated at 37^{o}C in 5% CO_2. To passage cells, cells were trypsinised, resuspended and re-plated in fresh Full RPMI media.

Plates were aspirated and washed with trypsin. Trypsin was again added, and the plates incubated for 10 minutes at 37^{o}C in 5% CO_2. After trypsinisation, the plate was agitated, and cells resuspended in full media, pipetting up and down 25 times to obtain a single celled suspension. A portion of the single celled suspension would then be added to full RPMI in another plate.

siRNA Transfection

To knock down expression of certain genes, siRNA transfections were undertaken.

On day 0, passaging cells were trypsinised, re-plated in the relevant dishes and left for 24 hours to seed in Full RPMI. On day 1, the media was then aspirated and rinsed with PBS before being replaced with “no add” RPMI (RPMI-1640-Glutamax only). The relevant siRNA was mixed and incubated with optiMEM and RNAiMax for 20 minutes before being added to the media at a final concentration of 40 nM. 24 hours later, on day 2, the media was aspirated and replaced with full RPMI. 24 hours later, on day 3, the cells are ready to manipulate.

Clonogenic Assay

To evaluate the changes in cell survival and clonogenicity of cells with and without siRNA-mediated knockdown of certain genes, clonogenic assays were undertaken.

64,000 cells were plated into the wells of 12-well dishes in Full RPMI and left for 24 hours to seed. On day 1, the media was aspirated and rinsed with PBS before being replaced with “no add” RPMI. The relevant siRNA was mixed and incubated with optiMEM and RNAiMax for 20

minutes before being added to the media at a final concentration of 40 nM. 24 hours later, on day 2, the cells were trypsinised and 1000 cells (Omm2.3 & Omm2.5) or 10,000 cells (Mel270) were plated into the wells of 6-well dishes, making sure to use a single celled suspension.

14-21 days later, or once the "Mock" colonies had grown to comprise approximately 50 cells, the media was aspirated, and the cells were rinsed with 2 mL PBS. The cells were fixed with 2 mL 4% PFA in PBS (15 mins) and rinsed once more with 2 mL PBS. The cells were then stained with 1 mL 0.5% w/v Crystal Violet (30 mins, R.T). The cells were washed with 3 x 3 mL tap water, left to air dry for 1 hour and stored long term at room temperature.

MTT Assay

To evaluate the changes in viability and growth of cells with and without siRNA-mediated knockdown of certain genes, MTT assays were undertaken.

The relevant siRNA was mixed and incubated with RNAiMax and OptiMEM in the wells of 96-well dishes for 20 minutes and then seeded with 7500 cells in 100 µL of Full RPMI per well before being left for 24 hours. On day 1, the media was aspirated and replaced with 125 µL of Full RPMI. At hour 0, set arbitrarily on day 1, 10 µL of formazan was added to each well, mixed thoroughly and left to incubate for 4 hours at 37^{o}C. After this, 100 µL of isopropanol + 0.04 M HCl was added and mixed thoroughly to dissolve all crystals in the well. Absorbance was read at 500 nm on a Tecan Magellan plate reader.

Cell Lysis

To obtain cell lysates, hot lysis was performed with Laemmli buffer.

Plates were washed twice with PBS before being heated to 105^{o}C on a heat block. Heated Laemmli buffer was added and the plates scraped with a dry cell scraper. Lysates were transferred to screw-cap tubes and heated for 10 minutes, vortexing every 2 minutes.

BCA Assay

To determine protein concentrations of the lysates, BCA assays were undertaken.

10 µL of lysate was diluted 1 in 5 in milliQ water. 10 µL of diluted lysate was pipetted in triplicate in a 96-well plate along with 10 µL triplicates of BSA standards. A BCA reagent comprising 50:1 Solution A: Solution B was made up and 200 µL was mixed into each well. After incubation at 37^{o}C for 30 minutes, absorbance was read using the pre-set BCA assay protocol on the Perkin Elmer VICTOR plate reader.

SDS-Polyacrylamide Gel Electrophoresis (SDS-PAGE)

To separate proteins in cell lysates based on molecular weight, SDS-PAGE was carried out.

A 10% resolving gel mixture was made up and 4.5 mL poured between a short plate and backing plate clamped together in a Bio-rad Mini-PROTEAN Tetra Handcast cassette. 0.5 mL of Propan-2-ol was poured on top of the gel mixture to eliminate bubbles. Once set, the Propan-2-ol was poured off and ~1 mL of the stacking gel was poured on top with a comb inserted and left to set.

Once set, the plates, containing the gel, were transferred to a Bio-rad Mini-PROTEAN Tetra Handcast tank and submerged in SDS-PAGE running buffer. The comb was removed and protein lysates (containing 10% 10x SDS-PAGE Loading Buffer and boiled at 100^{o}C for 5 minutes) were loaded into the gel wells along with 2 µ of Amersham ECL Rainbow marker and run at 60 V for 20 minutes, followed by 150 V until the dye front reached the bottom of the gel.

Western Blot Protein Transfer

To preserve separated proteins for detection, the proteins were transferred from the gel to a nitrocellulose membrane.

A transfer stack was made of blotting tissue, nitrocellulose membrane, polyacrylamide gel and blotting tissue after soaking with 36 mL of transfer buffer (Bio-rad). Air bubbles were

rolled out between each layer and the proteins were transferred using the pre-set “mixed molecular weight Bio-rad protocol” on the Bio-rad Trans-blot Turbo transfer system.

Antibody Probing of Nitrocellulose Membranes

To detect specific proteins, the nitrocellulose blot was probed with antibodies.

The nitrocellulose blot was soaked in Ponceau S for 30 seconds to visualise protein bands, before the blot was trimmed to size and then washed with milliQ water. The Ponceau S was rinsed off in PBS on the rocker (3 mins, R.T) and then blocked in 5% milk powder in PBS on the rocker for (1 hour, R.T). The nitrocellulose blot was incubated in primary antibody diluted in 5% milk powder in PBS on the rocker (16 hours, 4^{o}C).

The nitrocellulose blot was then washed in PBS on the rocker (3 x 5 mins, R.T). The relevant secondary antibody diluted in 5% milk powder in PBS was applied and incubated on the rocker (1 hour, R.T), before the blot was washed in PBS-T (3 x 5 mins, R.T) and in PBS on the rocker (1 x 5 mins, R.T).

The membranes were then visualised on a LiCOR Odyssey Fc and images for figures exported from the Image-Studio software.

Paraformaldehyde (PFA) Fixed Immunofluorescent (IF) Staining

To visualise soluble proteins by IF in cells with and without siRNA knockdown of certain genes, PFA fixing and IF staining was undertaken.

A circular coverslip was placed into the bottom of each well in a 12-well dish. 140,000 cells were plated into each well, on top of the coverslips, and underwent siRNA knockdowns as outlined above. On day 3 of the siRNA transfection, the media was *very gently* aspirated and rinsed with 1 mL PBS. The cells were fixed in 1 mL 4% PFA in PBS (15 mins) before rinsing with 1 mL PBS. The coverslips were then removed from the well and placed face up onto parafilm in a large dish. Each coverslip was treated with 100 µL 0.2% Triton X-100 in PBS (10 mins) and then blocked in 5% goat serum in PBS (30 mins). Each coverslip was then treated with 100 µL primary antibody in 100 µL 5% goat serum in PBS (2 hours, R.T). The coverslips were then

washed with 200 µL PBS (3 x 5 mins) before being treated with 100 µL secondary immunofluorescent antibody in 5% goat serum in PBS (2 hours, R.T). The coverslips were again washed with 200 µL PBS (3 x 5 mins) and their edges dabbed dry with Kimwipe tissue paper. 15 µL of Moviol + DAPI was placed onto glass microscope slides and the coverslips were placed face down onto the slides, allowed to dry overnight and stored long term at 4^{o}C in the dark.

Methanol Fixed IF Staining

To visualise dense, insoluble proteins by IF in cells with and without siRNA knockdown of certain genes, methanol fixing and IF staining was undertaken.

A circular coverslip was placed into the bottom of each well in a 12-well dish. 140,000 cells were plated into each well, on top of the coverslips, and underwent siRNA knockdowns as outlined above. On day 3 of the siRNA transfection, the media was *very gently* aspirated and rinsed with 1 mL PBS. The cells were fixed in 500 µL -20^{o}C methanol (15 mins, -20^{o}C) before rinsing with 1 mL PBS. The coverslips were then removed from the well and placed face up onto parafilm in a large dish. Each coverslip was blocked in 100 µL 5% goat serum in PBS (30 mins). Each coverslip was then treated with 100 µL primary antibody in 5% goat serum in PBS (2 hours, R.T). The coverslips were then washed with 200 µL PBS (3 x 5 mins) before being treated with 100 µL secondary immunofluorescent antibody in 5% goat serum in PBS (2 hours, R.T). The coverslips were again washed with 200 µL PBS (3 x 5 mins) and their edges dabbed dry with Kimwipe tissue paper. 15 µL of Moviol + DAPI was placed onto glass microscope slides and the coverslips were placed face down onto the slides, allowed to dry overnight and stored long term at 4^{o}C in the dark.

Flow Cytometry

To examine cell cycle dynamics of cells with and without siRNA knockdown of certain genes, flow cytometry was undertaken.

250,000 cells were plated into 60mm dishes and underwent siRNA knockdowns as outlined above. On day 3 of the siRNA transfection, approximately 1 million cells were pelleted (1000rpm, 5 mins) and the supernatant discarded. The cells were resuspended in 1 mL PBS.

The process was repeated, and the cells were resuspended in 100 µL of PBS. The cells were vortexed at low speed and 900 µL of ethanol was added dropwise before leaving on ice for 30 minutes.

After ethanol fixation, the cells were pelleted (1000 rpm, 5 mins) and the supernatant discarded. The cells were resuspended in 500 µL PBS. The process was repeated, and the cells were resuspended in 50 µL RNase A solution and 450 µL PBS. The resuspended cells were transferred to flow cytometry tubes and 30 µL propidium iodide (1 mg/mL) was added. The tubes were capped and wrapped in foil for 15 minutes before analysing on a Beckman-Coulter Cytoflex flow cytometer.

Kinesin Assay

A phosphate standard curve was made up by incubating 0, 3, 5, 7, 10, 15 or 20 µL of phosphate standard with milliQ water up to a volume of 30 µL in a half volume 96-well plate. 70 µL of cytophos was added per well and scanned at 650 nm on the Tecan Magellan plate reader.

The assay was run according to the HTS kinesin endpoint assay (Cytoskeleton, Denver, CO).

CW069 Synthesis Pathway 1

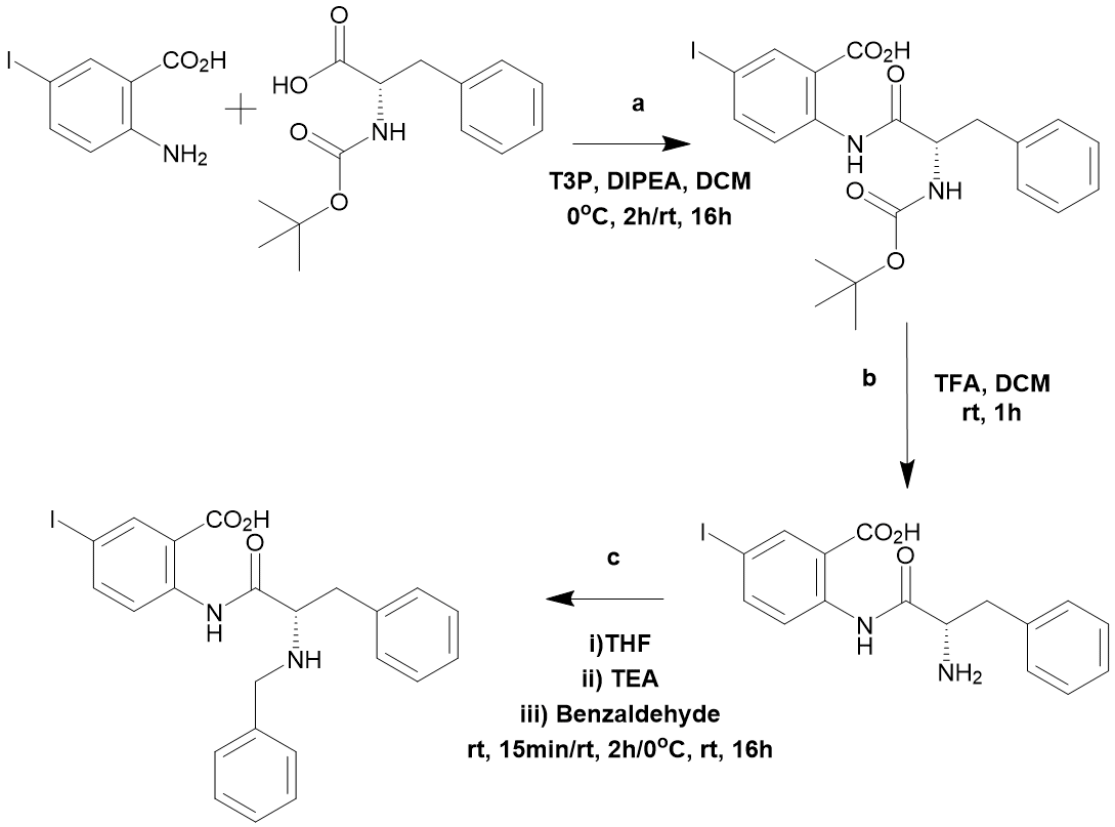

Reaction a. Amide Coupling

Attempt 1

N-Boc-phenylalanine (350 mg, 1.331 mmol, 1 eqv) and DIPEA (N,N-diisopropylethylamine) (1 mL, 7.740 mmol, 5.81 eqv) were dissolved in 30 mL of DCM (dichloromethane) and stirred. The mixture was cooled to 0°C, T3P (propanephosphonic acid anhydride) (1 g (50% w/w), 3.143 mmol, 2.36 eqv) was added and stirred at rt for 2 hrs. 2-amino-5-iodobenzoic acid (700 mg, 2.639 mmol, 1.98 eqv) was added dropwise over 10 mins and stirred at rt for 16 hrs.

The compound was extracted 3x with 30 mL DCM, washed 2x with 20 mL water, dried over Na_2SO_4 and filtered. The organic layer was evaporated by rotavapor and dried in vacuo to produce a brown oil.

The compound was separated by Flash Silica Chromatography using 20% Ethyl acetate in hexane. Pooled fractions were evaporated by rotavapor and dried *in vacuo* to produce a white powder.

Upon checking ^{1}H-NMR, non-equal integrations of peaks belonging to each compound indicated that although they eluted at the same point, they were not linked.

Attempt 2

N-Boc-phenylalanine (250 mg, 0.950 mmol, 1 eqv) and 2-amino-5-iodobenzoic acid (252 mg, 0.950 mmol, 1 eqv) were dissolved in 30 mL of DCM and stirred. DIPEA (340 µL, 1.98 mmol, 2 eqv) was added and the mixture cooled to 0^{o}C. T3P (680 µL (50% w/w), 1.14 mmol, 1.2 eqv) was added dropwise over 10 mins and stirred at rt for 16 hrs.

The compound was extracted 3x with 30 mL DCM, washed 2x with 20 mL water, dried over $MgSO_4$ and filtered. The organic layer was evaporated by rotavapor and dried in vacuo to produce a brown oil.

The compound was separated by Flash Silica Chromatography using 20% Ethyl acetate in hexane. Pooled fractions were evaporated by rotavapor and dried *in vacuo* to produce a white powder.

Upon checking ^{1}H-NMR, non-equal integrations of peaks belonging to each compound indicated that although they eluted at the same point, they were not linked.

Attempt 3. Because thin layer chromatography after the workup showed compound sticking to the silica, the possibility that the N-Boc-phenylalanine was being coupled but not further reacted was entertained. Therefore, HATU (hexafluorophosphate azabenzotriazole tetramethyl uronium) was used instead of T3P. The reaction was still a failure.

Attempts 4 and 5. The compound sticking to the silica after the workup might have been due to the possibility that the NH_2 group on the 2-amino-5-iodobenzoic acid was not electronegative enough to undertake a nucleophilic attack on the coupled N-Boc-Phenylalanine. Therefore, Ethyl-2-animo-5-iodobenzoate was used as the electron withdrawing property of the ethyl group would make the NH_2 group more electronegative, and therefore more amenable to nucleophilic attack. However, the reaction still failed.

Experiment Number	**Starting Material 1**	**Coupling Agent**
UPXP1, UPXP2	2-amino-5-iodobenzoic acid	T3P
UPXP3	2-amino-5-iodobenzoic acid	HATU
UPXP4	Ethyl-2-amino-5-iodobezoate	T3P
UPXP5	Ethyl-2-amino-5-iodobezoate	HATU

At this point, the decision was made to pursue the “optimised pathway” (Watts et al., 2013), named such because although it had more steps, it was published to have produced better yields.

CW069 Synthesis Pathway 2

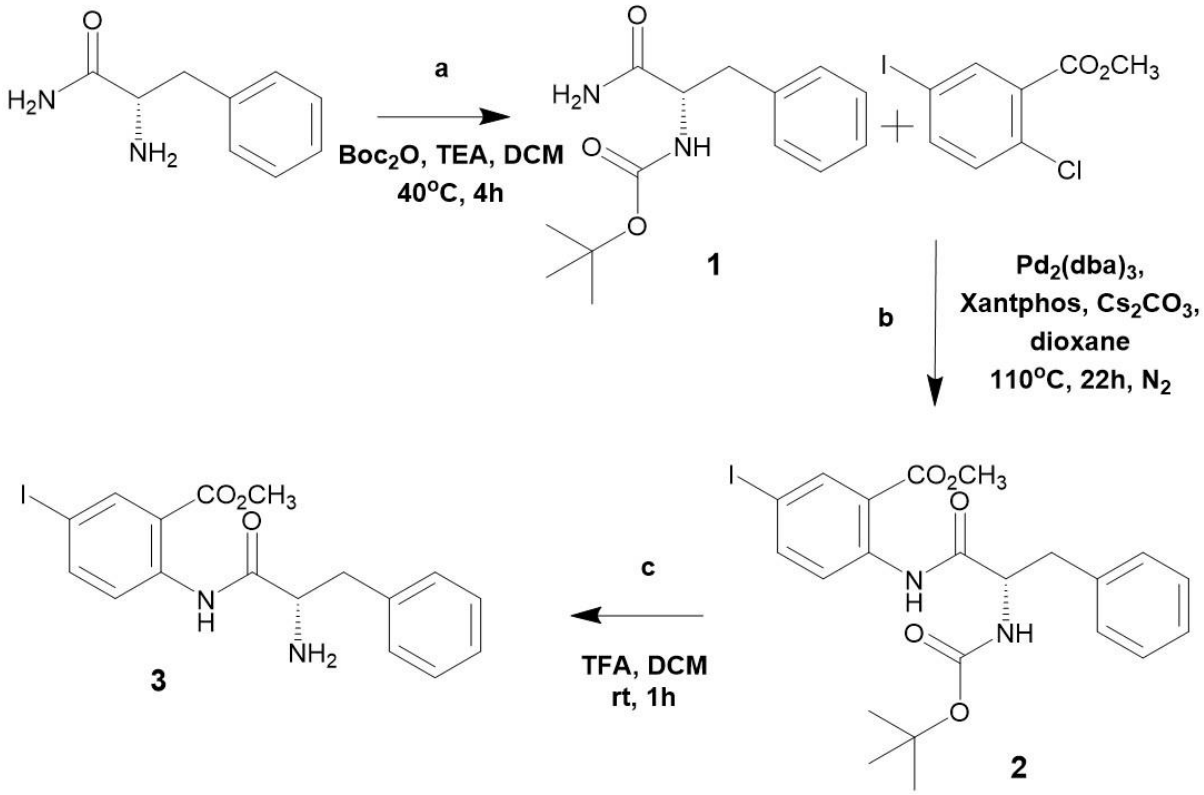

Reaction a. Boc Protection (Appendix 1)

Di-tert-butyl dicarbonate (4.37 g, 20 mmol, 1 eqv) and L-Phenylalaninamide (3.30 g, 20 mmol, 1 eqv) were dissolved in 100 mL of DCM and stirred. Triethylamine (5.58 mL, 40 mmol, 2 eqv) was added and refluxed at 40°C for 4 hrs.

The reaction was cooled and washed thrice with 30 mL water. The compound was extracted from water ten times with 30 mL DCM each time. The product formed a white crust on glassware and even entered the aqueous layer but was extracted with DCM. The compound was dried over Na_2SO_4 and filtered, then evaporated by rotary evaporator and dried in vacuo to produce compound **1**, a fluffy white solid called Boc-phenylalaninamide.

Yield= 91%

Mr= 264.32 g/mol

R.f.= 0.7 (DCM)

^{1}H-NMR (400MHz, $CDCl_3$)= Δ ppm: 1.41 (s, CH_3, 9H), 3.08 (s, CH_2, 2H), 4.42 (s, CH, 1H), 5.20 (d, NH, 1H), 5.81 (s, $RONH_a$, 1H), 6.05 (s, $RONH_b$, 1H), 7.24 (d, *Ar*H, 2H), 7.28 (d, *Ar*H, 1H), 7.32 (t, *Ar*H, 2H).

Reaction b. Buchwald-Hartwig Coupling (Appendix 2)

A two necked flask and three vials were oven dried at 150^{o}C for 1 hour and sealed upon retrieval. Under an inert atmosphere, $CsCO_3$ (74.61 mg, 0.229 mmol, 1.5 eqv) and $Pd(Dba)_3$ (14.95 mg, 0.0163 mmol, 10% eqv) were weighed out and dissolved in 2 mL anhydrous dioxane. Xantphos (9.4 mg, 0.0163 mmol, 10% eqv), Boc-phenylalaninamide (compound **1**) (50 mg, 0.196 mmol, 1.2 eqv) and Methyl-2-chloro-5-iodobenzoate (48.32 mg, 0.163 mmol, 1 eqv) were also dissolved in anhydrous dioxane and stirred. The flask was evacuated twice under vacuum and refilled with N_2 before being refluxed at 110^{o}C for 22 hours under N_2.

The reaction was cooled and diluted with 10mL ethyl acetate and washed thrice with 10mL brine, then extracted from the water thrice with 10mL ethyl acetate. The organics were pooled and dried over $MgSO_4$ and filtered. The compound was evaporated by rotavapor and dried *in vacuo* to produce a thick orange oil. The mixture was separated by Flash Silica Chromatography using 10% ethyl acetate in hexane. The fractions were combined and evaporated by rotary evaporator and dried *in vacuo* to produce compound **2**, an orange oil called Methyl-2-(Boc-phenylalaninamido)-5-iodobenzoate. In large amounts, the oil dissolves poorly in 10% ethyl acetate in hexane, and so should be deposited into the silica column for purification dissolved in DCM before separating with 10% ethyl acetate in hexane.

Yield= 100%

Mr= 524.36 g/mol

R.f.= 0.5 (10% EtOAc in hexane)

^{1}H-NMR (400MHz, $CDCl_3$)= Δ ppm:. 1.44 (s, CH_3, 9H), 3.15 (m, CH_2, 2H), 3.937 (s, OCH_3, 3H), 4.50 (d, CH, 1H), 5.20 (s, NH, 1H), 7.23 (s, *Ar*H, 1H), 7.25 (d, *Ar*H, 2H), 7.31 (d, *Ar*H, 2H), 7.37 (d, *Ar*H, 1H), 7.55 (q, *Ar*H, 1H), 7.84 (d, *Ar*H, 1H).

Reaction c. TFA Cleavage (Appendix 3)

Methyl-2-(Boc-phenylalaninamido)-5-iodobenzoate (compound **2**) (393.80 mg, 0.751 mmol, 1 eqv) was dissolved in 1 mL of DCM (min. 10 eqv) and stirred. TFA (trifluoroacetic acid) (1 mL, min. 10 eqv) was added and left to stir at R.T for 1 hr.

The DCM, TFA and side products were evaporated *in vacuo*, with the gaseous extract collected in a liquid nitrogen trap to leave a sticky brown oil. This was then dissolved in 1 mL DCM, evaporated by rotary evaporator and dried again *in vacuo* to produce compound **3**, a brown solid called Methyl-2-(phenylalaninamide)-5-iodobenzoate, as a TFA salt.

Yield= 100%

Mr= 538.26 g/mol in salt form. 424.24 g/mol free amine.

R.f.= 0.0 (DCM)

^{1}H-NMR (400MHz, DMSO-d6)= Δ ppm:. 3.15 (m, CH_2, 2H), 3.87 (s, OCH_3, 3H), 4.18 (s, CH, 1H), 7.26 (t, *Ar*H, 3H), 7.32 (t, *Ar*H, 2H), 7.575 (d, *Ar*H, 1H), 7.71 (q, *Ar*H, 1H), 8.01 (d, *Ar*H, 1H), *10.71 (s, CF_3CO_2H, 1H)*.

Producing a Free Amine from the TFA Salt (Appendix 4)

The free amine form of Methyl-2-(phenylalaninamido)-5-iodobenzoate (compound **3**) was obtained from the TFA salt produced above by diluting the relevant amount of the TFA salt form in 5 mL DCM with 1% triethylamine, then washing that thrice with 5 mL of 0.2M NaOH solution. The NaOH solutions were then pooled and extracted from thrice with 5 mL DCM with 1% triethylamine, which was dried over Na_2SO_4 and filtered, before being evaporated by rotavapor to produce a white solid.

Analogue Synthesis

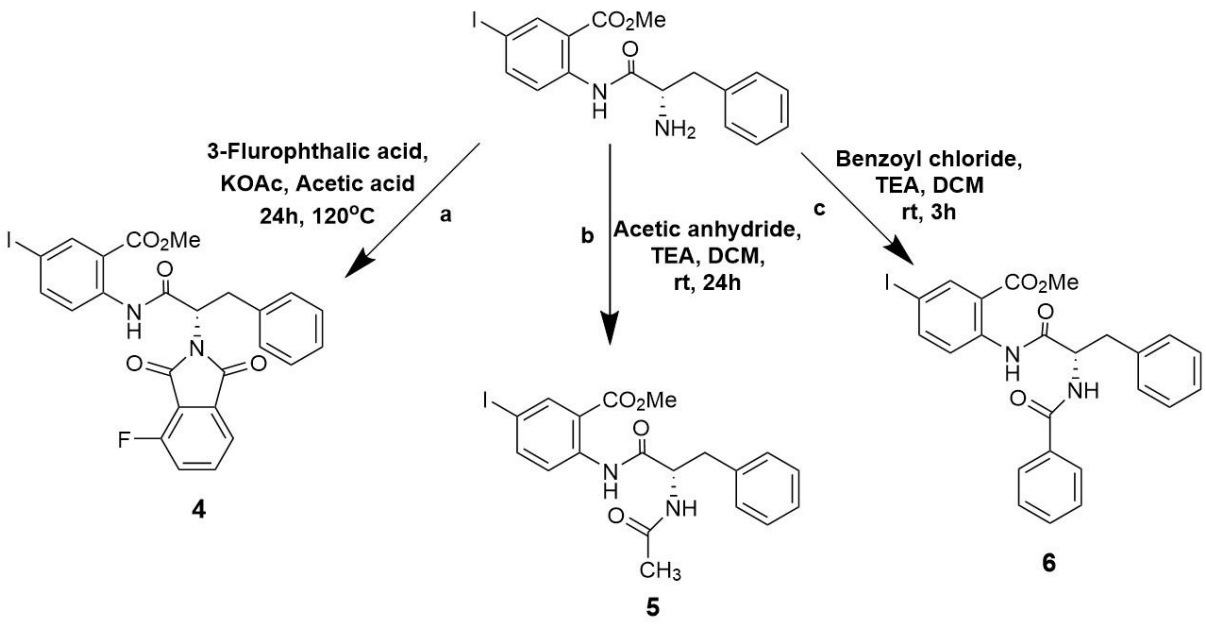

Reaction a. Phthalimide Protection (Appendix 5)

Methyl-2-(phenylalaninamido)-5-iodobenzoate (compound **3**) as an amine (15 mg, 0.035 mmol, 1 eqv), 3-fluorophthalic acid (5.81 mg, 0.035 mmol, 1 eqv) and potassium acetate (34.35 mg, 0.035 mmol, 1 eqv) were dissolved in 1 mL of acetic acid and refluxed at 120°C for 24 hrs.

The reaction was cooled and diluted with 5 mL DCM and washed thrice with 5 mL water. The water was extract from thrice with 5 mL DCM. The organics were pooled, dried over Na_2SO_4, filtered, evaporated by rotavapor and dried in vacuo to produce a beige crust before being separated by Flash Silica Chromatography with a solvent system progressing from 0-10% methanol in DCM. The combined fractions were then evaporated by rotavapor and dried *in vacuo* to produce a beige solid, methyl (S)-2-(2-(3-fluoro-phthalimido)-3-phenylpropanamido)-5-iodobenzoate (compound **4**).

Yield= 30%

Mr= 450.28 g/mol

R.f.= 0.8 (10% MeOH in DCM)

^{1}H-NMR (400MHz, $CDCl_3$)= Δ ppm:. 3.70 (m, CH_2, 2H), 3.99 (m, OCH_3, 3H), 5.27 (s, CH, 1H), 7.23 (m, *Ar*H, 1H), 7.43 (t, *Ar*H, 4H), 7.68 (m, *Ar*H, 3H), 7.78 (m, *Ar*H, 1H), 7.91 (m, *Ar*H, 1H), 8.28 (s, *Ar*H, 1H).

Reaction b. Nucleophilic Addition-Elimination (Appendix 6)

Methyl-2-(phenylalaninamido)-5-iodobenzoate (compound **3**) as an amine (15 mg, 0.035 mmol, 1 eqv) and triethylamine (4.65 µL, 0.105 mmol, 3 eqv) were dissolved in 1 mL of DCM and stirred at R.T for 15mins. An excess of acetic anhydride (4.96 µL, 0.052 5mmol, 1.5 eqv) was added and stirred at R.T for 24 hrs.

The reaction was diluted with 5 mL DCM and washed thrice with 5 mL water. The water was extracted from thrice with 5 mL DCM. The pooled organics were dried over Na_2SO_4, filtered, evaporated by rotavapor and dried in vacuo to produce a beige crust before being separated by Flash Silica Chromatography with a solvent system progressing from 0-10% methanol in DCM. The combined fractions were then evaporated by rotavapor and dried *in vacuo* to produce a beige solid, methyl (S)-2-(2-(acetamido)-3-phenylpropanamido)-5-iodobenzoate (compound **5**).

Yield= 50%

Mr= 595.87 g/mol

R.f.= 0.6 (10% MeOH in DCM)

^{1}H-NMR (400MHz, $CDCl_3$)= Δ ppm:. 2.04 (m, CH_3, 3H), 3.13 (m, CH_2, 2H), 3.95 (s, OCH_3, 3H), 4.96 (s, CH, 1H), 6.51 (dd, *Ar*H, 1H), 7.16 (d, *Ar*H, 1H), 7.20 (d, *Ar*H, 2H), 7.25 (m, *Ar*H, 2H), 7.28 (s, *Ar*H, 1H), 7.37 (t, *Ar*H, 1H), 7.60 (m, *Ar*H, 1H), 7.88 (d, *Ar*H, 1H).

Reaction c. Nucleophilic Addition-Elimination (Appendix 7)

Methyl-2-(phenylalaninamido)-5-iodobenzoate (compound **3**) TFA salt (15 mg, 0.0286 mmol, 1 eqv) and triethylamine (8.27 µL, 0.0572mmol, 2 eqv) were dissolved in 1 mL of DCM and

stirred at R.T for 15 mins. A slight excess of Benzoyl chloride (9.49 µL, 0.031 mmol, 1.08 eqv) was added and stirred at R.T for 3 hrs.

The reaction was diluted with 5 mL DCM and washed thrice with 5 mL water, which was extracted water thrice with 5 mL DCM. The organics were pooled and dried over Na_2SO_4, filtered, evaporated by rotavapor and dried in vacuo to produce a beige crust. The compound was separated by Flash Silica Chromatography using 5% methanol in DCM. The fractions were combined, evaporated by rotavapor and dried *in vacuo* to produce a beige solid, methyl (S)-2-(2-(benzamido)-3-phenylpropanamido)-5-iodobenzoate (compound **6**).

Yield= 67%

Mr= 528.59 g/mol

R.f.= 0.9 (5% MeOH in DCM)

^{1}H-NMR (400MHz, $CDCl_3$)= Δ ppm:. 3.21 (m, CH_2, 2H), 3.90 (m, OCH_3, 3H), 5.19 (m, CH, 1H), 6.51 (dd, *Ar*H, 1H), 7.03 (d, *Ar*H, 1H), 7.20 (t, *Ar*H, 2H), 7.26 (m, *Ar*H, 2H), 7.36 (t, *Ar*H, 1H), 7.47 (t, *Ar*H, 2H), 7.57 (m, *Ar*H, 2H), 7.77 (t, *Ar*H, 2H), 7.88 (t, *Ar*H, 1H), 9.00 (d, *Ar*H, 1H).

2.2. Materials

Solutions and Buffers

PBS (Sigma-Aldrich, St-Louis, MO)

PBS-Tween (PBS + 0.1% Tween-20)

Laemmli Buffer (50mM Tris pH 6.8, 2% SDS, 10% Glycerol)

Running Buffer (25mM Tris, 192mM Glycine, 0.1% SDS)

Transfer Buffer (25mM Tris pH 8.3, 192mM Glycine)

10x SDS-PAGE Loading Buffer (1M DTT, 1% Bromophenol Blue)

Amersham ECL Rainbow marker (Merck, Kenilworth, NJ)

Poly-Acrylamide Gel Electrophoresis

Nitrocellulose membrane

Blotting tissue

Milk Powder

Ponceau Stain

Tris

20% 1:1 Acrylamide: Bis-Acrylamide

TEMED

BCA Assay

BSA

BCA reagent A

BCA reagent B

Cell Fixing and Staining

Moviol

DAPI

Goat Serum

Ethanol

Methanol

16% Paraformaldehyde

Triton x-100

Goat Serum

Crystal Violet

Propidium Iodide

RNAse A

Gene Transfection

KIFC1_4 siRNA (QIAGEN, Hilden, Germany)

KIFC1_5 siRNA (QIAGEN, Hilden, Germany)

All Stars Negative Control siRNA (QIAGEN, Hilden, Germany)

RNAiMax Transfection Reagent

OptiMEM

Cell Culture

RPMI Media

FCS

Pen/Strep

Trypsin

Primary Antibodies

KIFC1 (Rb) (Abcam, Cambridge, UK)

GAPDH (Mo) (Abcam, Cambridge, UK)

Alpha-Tubulin (Mo) (Sigma-Aldrich, St-Louis, MO)

Alpha-Tubulin (Rt) (Merck Millipore, Burlington, MA)

Centrin (Mo) (Merck Millipore, Burlington, MA)

Pericentrin (Rb) (Abcam, Cambridge, UK)

Caspase 3 (Rb) (Cell Signalling Technology, Danvers, MA)

Survivin (Rb)

Immunofluorescent Secondary antibodies

Goat anti-Mouse IgG (H+L)

Alexa Fluor 555 nm Goat anti-Rabbit IgG (H+L) (Invitrogen, Carlsbad, CA)

Alexa Fluor 647 nm Goat anti-Rat IgG (H+L) (Invitrogen, Carlsbad, CA)

Alexa Fluor 488 nm Goat anti-Mouse (H+L) (Invitrogen, Carlsbad, CA)

Western blotting secondary antibodies

Donkey anti-Mouse IgG (H+L), IRDye 680RD (LiCOR Biosciences, Lincoln, NE)

Donkey anti-Rabbit IgG (H+L), IRDye 800CW (LiCOR Biosciences, Lincoln, NE)

Structure-Activity Relationship Kinesin Assay

HTS kinesin ATPase Endpoint Assay Biochem Kit (Cytoskeleton, Denver, CO)

Cell lines

Omm2.3 (Courtesy of the Sarah Coupland Lab, University of Liverpool)

Omm2.5 (Courtesy of the Sarah Coupland Lab, University of Liverpool)

Mel270 (Courtesy of the Sarah Coupland Lab, University of Liverpool)

3. Centrosome Amplification and KIFC1 Function in Primary and Metastatic Uveal Melanoma Cells

3.1. Results I

Metastatic Uveal Melanoma Cells Show High Levels of Centrosome Amplification

It is known that cancer cells of many different types display centrosome amplification (Godinho et al., 2009). Recently, a large study of the NCI-60 panel of cancer and tissue-matched normal cell lines was undertaken, with the prevalence of *bona-fide* centrosome amplification in each cell line identified by dual staining with two centriole/centrosome markers. The average frequency of centrosome amplification in non-cancerous cells was found to be 7 ± 3%. Therefore 13% (Mean + 2 SD) was defined as the cut-off point for classifying cells as having centrosome amplification (Marteil et al., 2018).

To explore if centrosome amplification occurred in uveal melanoma, a set of cell lines derived from the same patient (Mel270 from a primary tumour, Omm2.3 and Omm2.5 cells from two distinct liver metastases) were examined by immunofluorescence.

Mel270, Omm2.3 and Omm2.5 cells were grown on coverslips and 48 hours later, the cells were fixed, stained for immunofluorescence with DAPI and a combination of anti-tubulin (to identify spindles), anti-centrin (centriole marker) and anti-pericentrin (pericentriolar material marker) antibodies were used to detect *bona-fide* extra centrosomes along with bipolar and multipolar mitosis. To quantify the extent of centrosome amplification, multiple images were taken of fields of all three cell lines where mitosis and centrosome amplification would clearly be visible. From these images, cells with more than two centrosomes were counted (Figure 3.1).

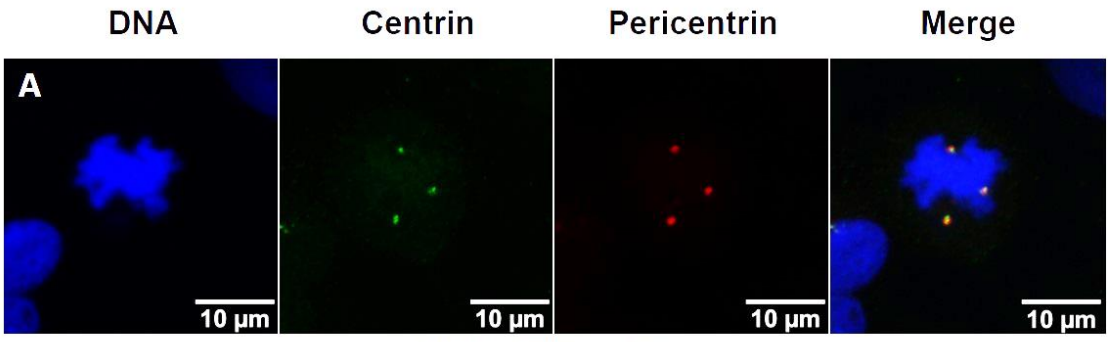

Mel 270 – Multipolar Mitosis

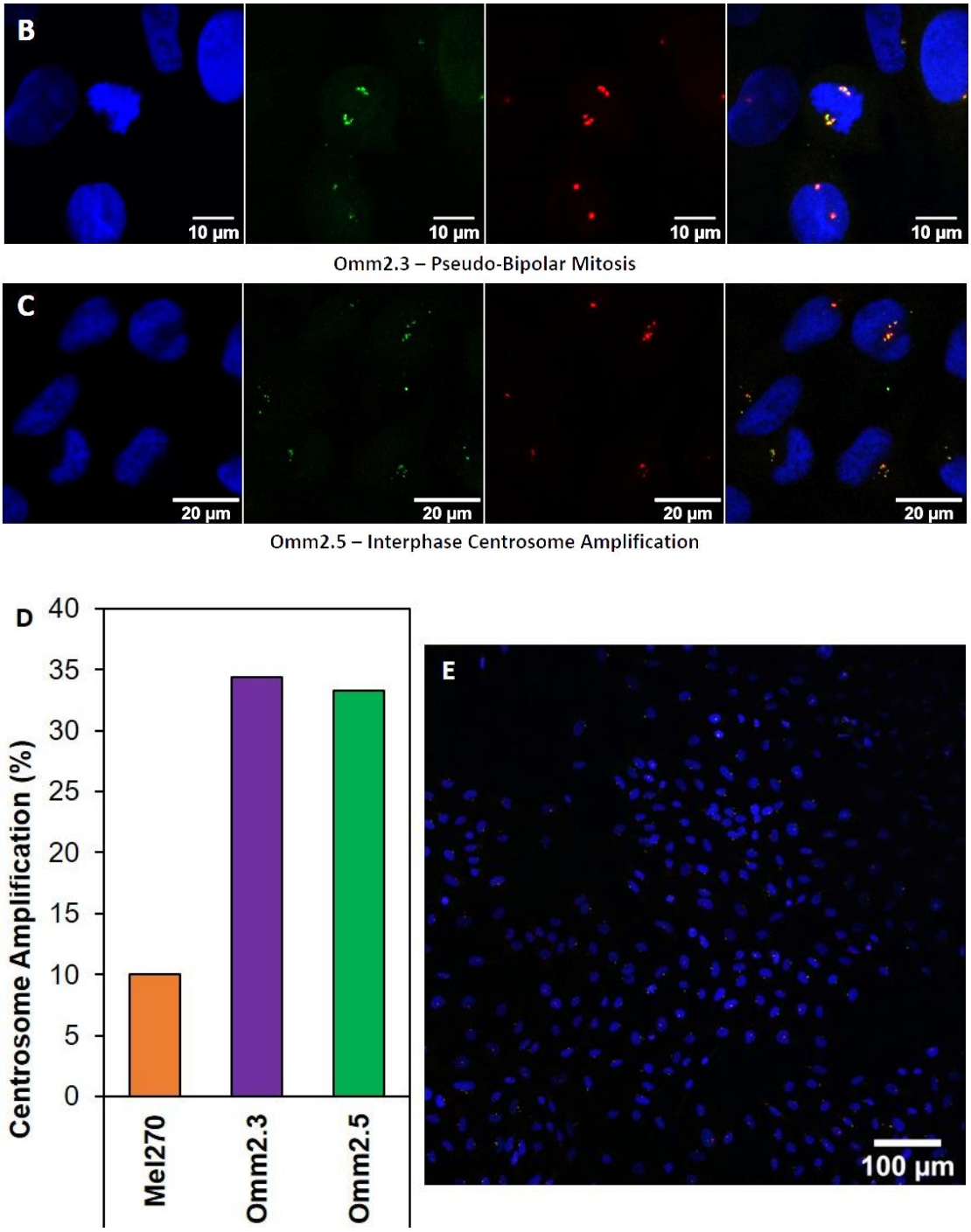

Figure 3.1. Metastatic Uveal Melanoma Cell Lines Contain Amplified Centrosomes. *A) Immunofluorescence microscopy of Mel270 cells. B) Immunofluorescence microscopy of Omm2.3 cells. C) Immunofluorescence microscopy of Omm2.5 cells. Cells were grown on coverslips for 48 h, processed for immunofluorescence and stained with anti-centrin antibody and 488 nm-conjugated secondary (to stain centrioles green), anti-pericentrin antibody and 555 nm-conjugated secondary (to stain centrosomes red) and DAPI (to stain DNA blue). D) Quantification of centrosome amplification detected by immunofluorescence microscopy. Fields of cells were imaged by confocal microscopy to visualise the centrosomes as above. The total number of cells on each field was counted using ImageJ, while cells in mitosis with more than 2 centrosomes were counted and plotted as frequency of centrosome amplification. Between 3000 and 7000 cells were counted for each cell line. E) Example of image used to quantify centrosome amplification displaying a field of Omm2.3 cells.*

Upon imaging fields of cells by confocal microscopy, the number of cells with amplified centrosomes were counted. As the coverslips were not stained in a way that cells in G1 and G2 could not be discriminated between, there was no way to know whether a cell with 2 centrosomes was in G1 with centrosome amplification or was in G2 with a normal number of centrosomes. Therefore, the number of obviously mitotic cells with more than two centrosomes were counted as positives against the total number of mitotic cells.

Examination of uveal melanoma cell lines by immunofluorescent confocal microscopy showed that Omm2.3 (Figure 3.1B) and Omm2.5 (Figure 3.1C) cells harboured extra centrosomes. As shown in figure 3.2D, it was shown that Omm2.3 and Omm2.5 had similar levels of centrosome amplification at 34% and 33% respectively, whereas Mel270 had lower levels of centrosome amplification at 10%. In comparison to the analysis of the NCI-60 panel, it can be concluded that the metastatic uveal melanoma cells examined here have a very high level of centrosome amplification, as only 8 of the 53 cancer cell lines examined had >30% cells displaying centrosome amplification. In contrast, Mel270 has a much lower level of centrosome amplification, below the 13% threshold proposed by Marteil et al., 2018.

Metastatic Uveal Melanoma Cells Undergo Efficient Centrosome Clustering

Cells with centrosome amplification require their centrosomes to be clustered to avoid multipolar mitosis and aneuploidy. To explore if multipolar mitosis occurred in uveal melanoma, Mel270, Omm2.3 and Omm2.5 cells were further examined by immunofluorescence.

Mel270, Omm2.3 and Omm2.5 cells were grown on coverslips and 48 hours later, the cells were fixed, stained for immunofluorescence with DAPI and a combination of anti-tubulin (to identify spindles), anti-centrin (centriole marker) and anti-pericentrin (pericentriolar material marker) antibodies were used to detect *bona-fide* extra centrosomes along with bipolar and multipolar mitosis. To quantify the extent of multipolar mitosis, multiple images were taken of fields of all three cell lines where mitosis and the centrosomes would clearly be visible. From these images, cells undergoing multipolar mitosis were counted (Figure 3.12).

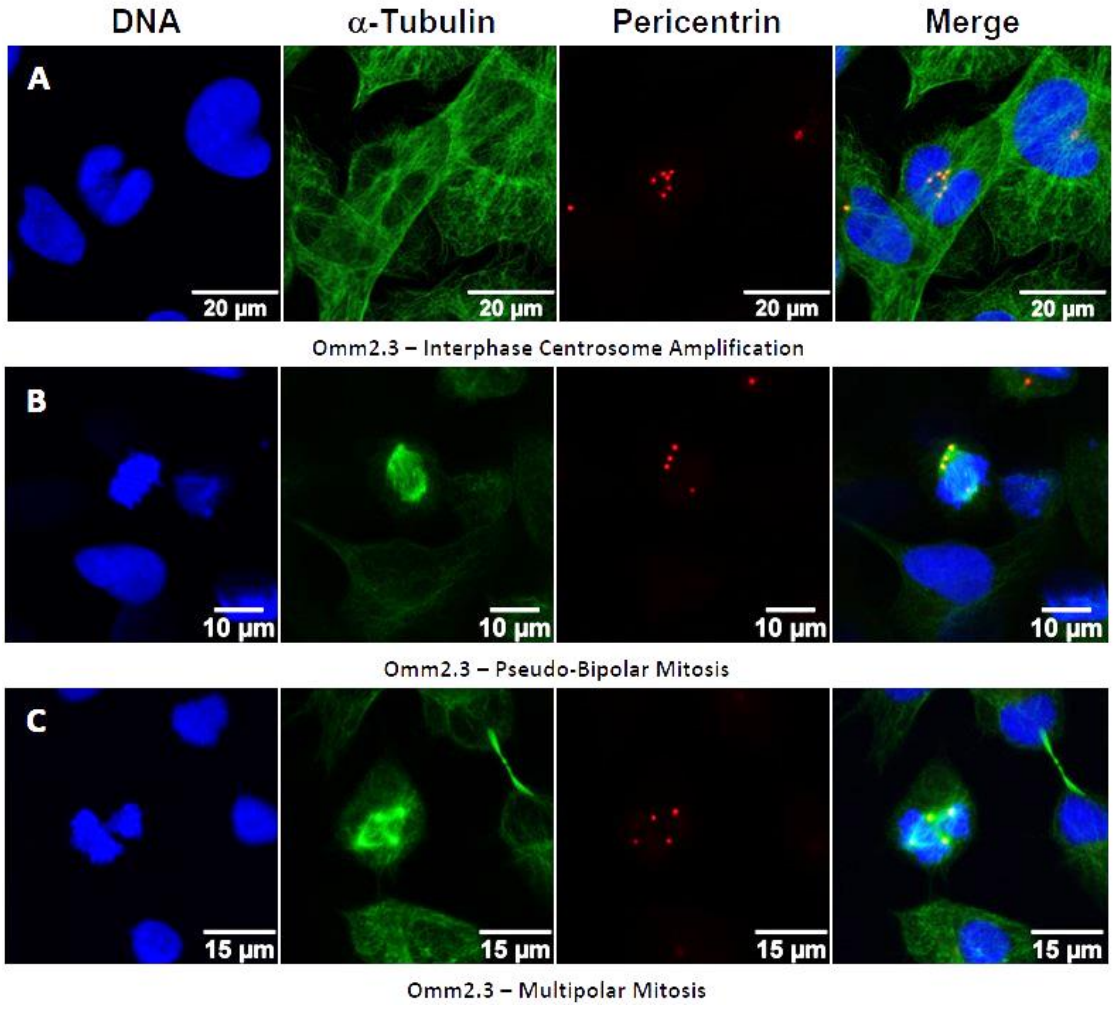

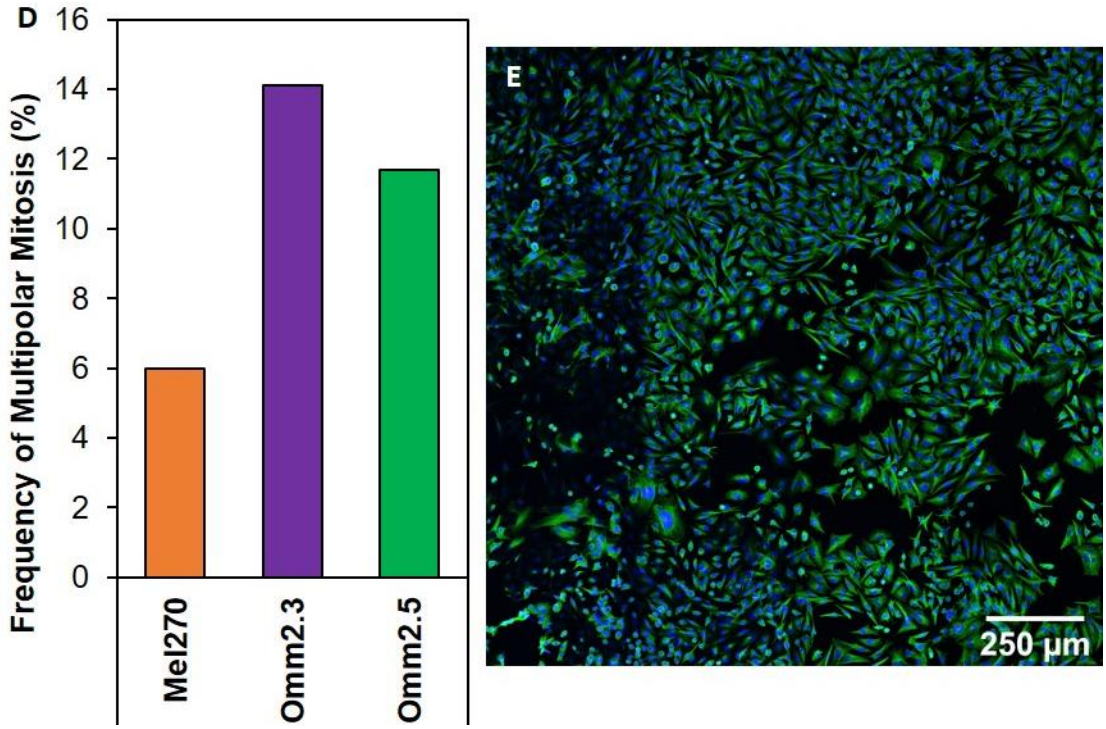

Figure 3.2. Metastatic Uveal Melanoma Cell Lines Cluster Centrosomes and Undergo Multipolar Mitosis Relatively Infrequently. A) *Immunofluorescence microscopy of an Omm2.3 cell with amplified centrosomes.* ***B)*** *Immunofluorescence microscopy of an Omm2.3 cell with clustered centrosomes undergoing pseudo-bipolar mitosis.* ***C)*** *Immunofluorescence microscopy of an Omm2.3 cell undergoing multipolar mitosis. Cells were grown on coverslips for 48 h, processed for immunofluorescence and stained with anti-α-tubulin antibody and 488 nm-conjugated secondary (to stain microtubules green), anti-pericentrin antibody and 555 nm-conjugated secondary (to stain centrosomes red) and DAPI (to stain DNA blue). D) Quantification of multipolar mitosis detected by immunofluorescence microscopy. Fields of cells were imaged by confocal microscopy to visualise mitotic cells as above. The total number of cells on each field was counted using ImageJ, while cells in mitosis with more than 2 spindle poles were counted and plotted as frequency of multipolar mitosis. Between 3000 and 7000 cells were counted for each cell line. E) Example of image used to quantify centrosome amplification displaying a field of Omm2.3 cells.*

Examination of uveal melanoma cell lines by immunofluorescent confocal microscopy showed that Mel270 (Figure 3.2A), Omm2.3 (Figure 3.2B) and Omm2.5 (Figure 3.1C) underwent multipolar mitosis. Upon imaging fields of cells by confocal microscopy, the number of cells undergoing multipolar mitosis were counted. The frequency of multipolar mitosis was calculated by counting the number of multipolar mitotic cells against the total number of mitotic cells. As shown in figure 3.2D, it was found that Omm2.3 had the highest incidence of multipolar mitosis at 14% of the time, followed by Omm2.5 at 12%, followed by Mel270 at 6% of the time. The fact that the frequency of multipolar mitosis always remains below the

frequency of centrosome amplification shows that centrosome clustering is a fairy efficient process.

Although this shows that Mel270 undergoes multipolar mitosis the most infrequently, together the results shown in figures 3.1D and 3.2D show that Mel270 is the least proficient in clustering its amplified centrosomes, clustering them 40% of the time, as opposed to 60% in Omm2.3 and 66% of the time in Omm2.5, calculated by taking the proportion of cells undertaking multipolar mitosis and dividing that by the proportion of cells with centrosome amplification. All in all, this data shows that Mel270 has the lowest levels of centrosome amplification and multipolar mitosis but is also the least proficient in clustering amplified centrosomes. Incidentally, this is to be expected as tumour grade is associated to centrosome amplification and clustering capacity (Denu et al., 2016). Omm2.3 and Omm2.5 cells are secondary metastases of Mel270, a primary tumour, which means that it is reasonable to assume that they are of a higher tumour grade than Mel270 and thus also more likely to be proficient in clustering centrosomes to pseudo-bipolar spindles.

KIFC1 is Expressed and Localises to the Spindle During Mitosis in Uveal Melanoma Cell Lines

Having found that uveal melanoma cells have centrosome amplification, the focus shifted onto the role of KIFC1 in this process, as is it often an invaluable protein in clustering extra centrosomes during mitosis (Reviewed by Xiao and Yang, 2016). To explore KIFC1 dynamics in uveal melanoma, Mel270, Omm2.3 and Omm2.5 cells were further examined by immunofluorescence (Figure 3.3).

Mel270, Omm2.3 and Omm2.5 cells were grown on coverslips and 48 hours later, the cells were fixed, stained for immunofluorescence with DAPI and anti-tubulin and anti-KIFC1 antibodies were used to detect KIFC1.

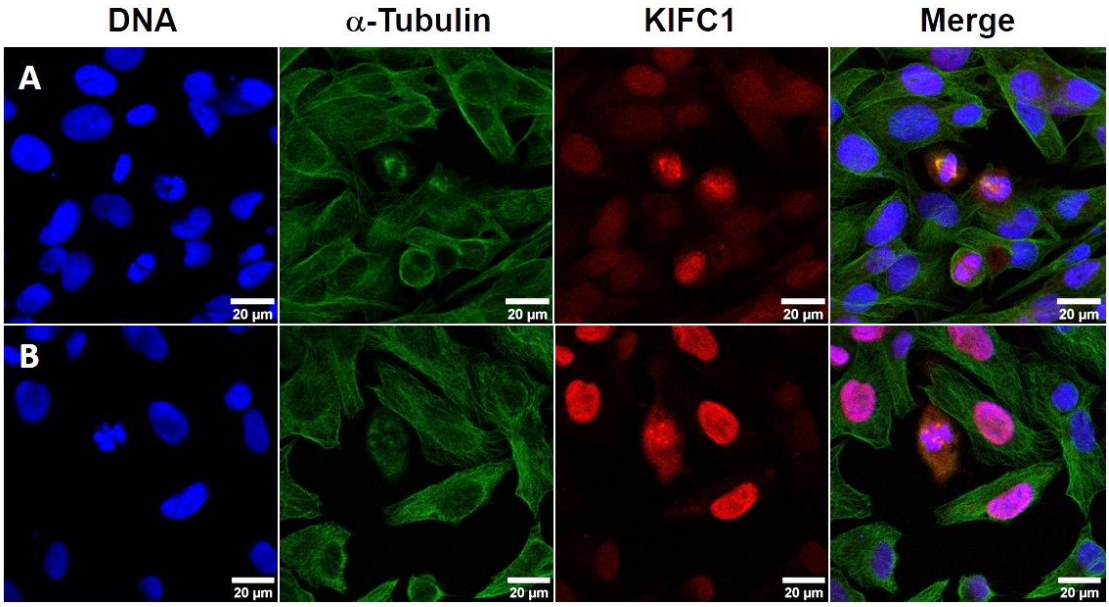

Figure 3.3. KIFC1 is Expressed and Localises to the Spindle During Mitosis in Uveal Melanoma Cell Lines. *A) Immunofluorescence microscopy showing a group of Omm2.3 cells with a cell undergoing bipolar mitosis. B) Immunofluorescence microscopy showing a group of Omm2.3 cells with a cell under multipolar mitosis - Note how KIFC1 is localised most intensely to the spindle in cells in mitosis. Mel270, Omm2.3 and Omm2.5 cells were grown on coverslips for 48 h, processed for immunofluorescence and stained with anti-α-tubulin antibody and 488 nm-conjugated secondary (to stain microtubules green), anti-KIFC1 antibody and 555 nm-conjugated secondary (to stain KIFC1 red) and DAPI (to stain DNA blue).*

KIFC1 is differentially expressed in cells across the cell cycle. As seen in figure 3.3, KIFC1 is present in the nucleus throughout interphase before being translocated to the mitotic spindle during mitosis. This occurs in both bipolar mitosis (Figure 3.3A) and multipolar mitosis (Figure 3.3B).

Two Independent KIFC1 siRNAs Efficiently Deplete KIFC1 in Uveal Melanoma Cell Lines

To understand the role of KIFC1 in uveal melanoma cells, Mel270, Omm2.3 and Omm2.5 were treated with anti KIFC1 siRNA. Western blots were carried out to confirm whether the siRNA transfection worked and KIFC1 protein levels were depleted satisfactorily (Figure 3.4).

Mel270, Omm2.3 and Omm2.5 cells were mock transfected, transfected with a control siRNA or with one of two independent siRNAs against KIFC1 and left to grow before the cells were lysed and processed to perform Western blots.

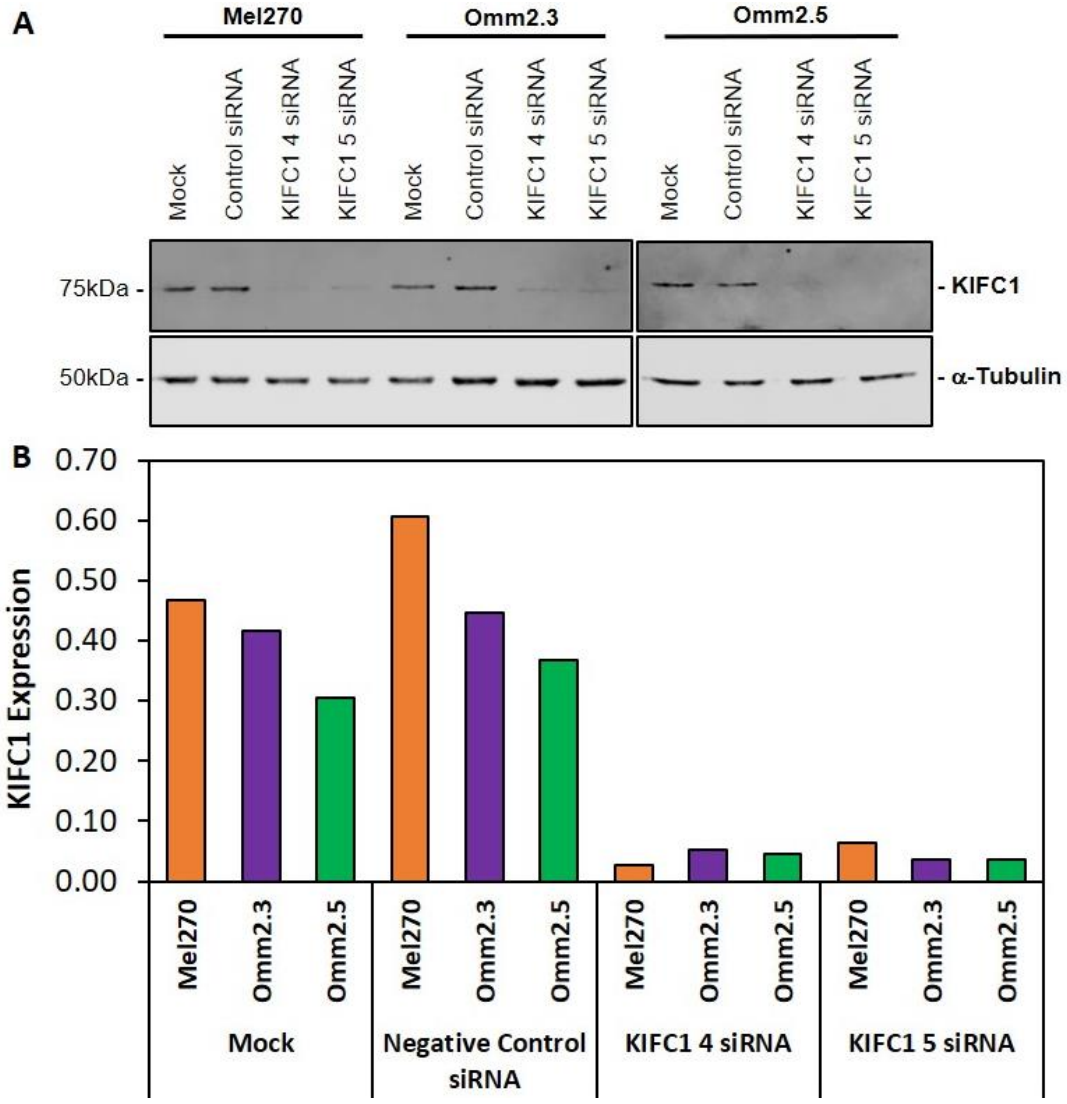

Figure 3.4. **Two Independent KIFC1 siRNAs Efficiently Deplete KIFC1 in Uveal Melanoma Cell Lines.** *Mel270, Omm2.3 and Omm2.5 cells were plated and transfected with either KIFC1 4 siRNA, KIFC1 5 siRNA, negative control siRNA or were mock transfected. 48 h post siRNA transfection, cells were hot lysed with Laemmli buffer and run on SDS-PAGE gels made with 10% acrylamide before being transferred to nitrocellulose membrane.*

The nitrocellulose blots were probed with anti-KIFC1 antibody and Donkey anti-Rabbit IRDye 680RD secondary antibody, along with anti-α-tubulin antibody (loading control) and Donkey anti-mouse IRDye 800CW secondary antibody before imaging using a LiCOR Odyssey Fc machine (A).

The intensity for each band was quantified and the intensity values for KIFC1 expression were normalised against the intensity values for α-tubulin, the loading control protein, and plotted in a graph (B).

As shown in Figure 3.4, KIFC1 4 siRNA and KIFC1 5 siRNA efficiently deplete KIFC1 expression in Mel270, Omm2.3 and Omm2.5 cells. Furthermore, the negative control siRNA does not affect KIFC1 expression. These siRNAs were deemed suitable to use in further experiments.

It is important to note, however, that Omm2.3 and Omm2.5 cells seem to express no more KIFC1 in mock conditions than Mel270 cells, and maybe even express KIFC1 slightly less (Figure 3.4B), despite the increased centrosome amplification and frequency of multipolar mitosis. This also may imply that any mutations to amplify KIFC1 (assuming KIFC1 is overexpressed) may be early mutations that occurred before metastasis. Although there has been no study published which looks specifically at KIFC1 expression in uveal melanoma, it is known that Mel270 cells contain four copies of chromosome 6p, which is where the KIFC1 gene is located (Reviewed by Jager et al., 2016). It may be reasonable to assume that these amplifications are still present in the secondary Omm2.3 and Omm2.5 cells.

KIFC1 Knockdown Decreases the Mitotic Index of Uveal Melanoma Cell Lines

Aside from clustering extra centrosomes, existing evidence also implicates KIFC1 as having a role in cell proliferation (Pannu et al., 2015b). To begin to understand whether this was the case in Mel270, Omm2.3 and Omm2.5 cells, KIFC1 was knocked down and the mitotic indices of these cell lines were calculated by immunofluorescence imaging (Figure 3.5).

Mel270, Omm2.3 and Omm2.5 cells were grown on coverslips and mock transfected, transfected with a control siRNA or with one of two independent siRNAs against KIFC1. 48 hours later, the cells were fixed, stained for immunofluorescence with DAPI and anti-tubulin and anti-pericentrin antibodies were used to detect mitotic cells.

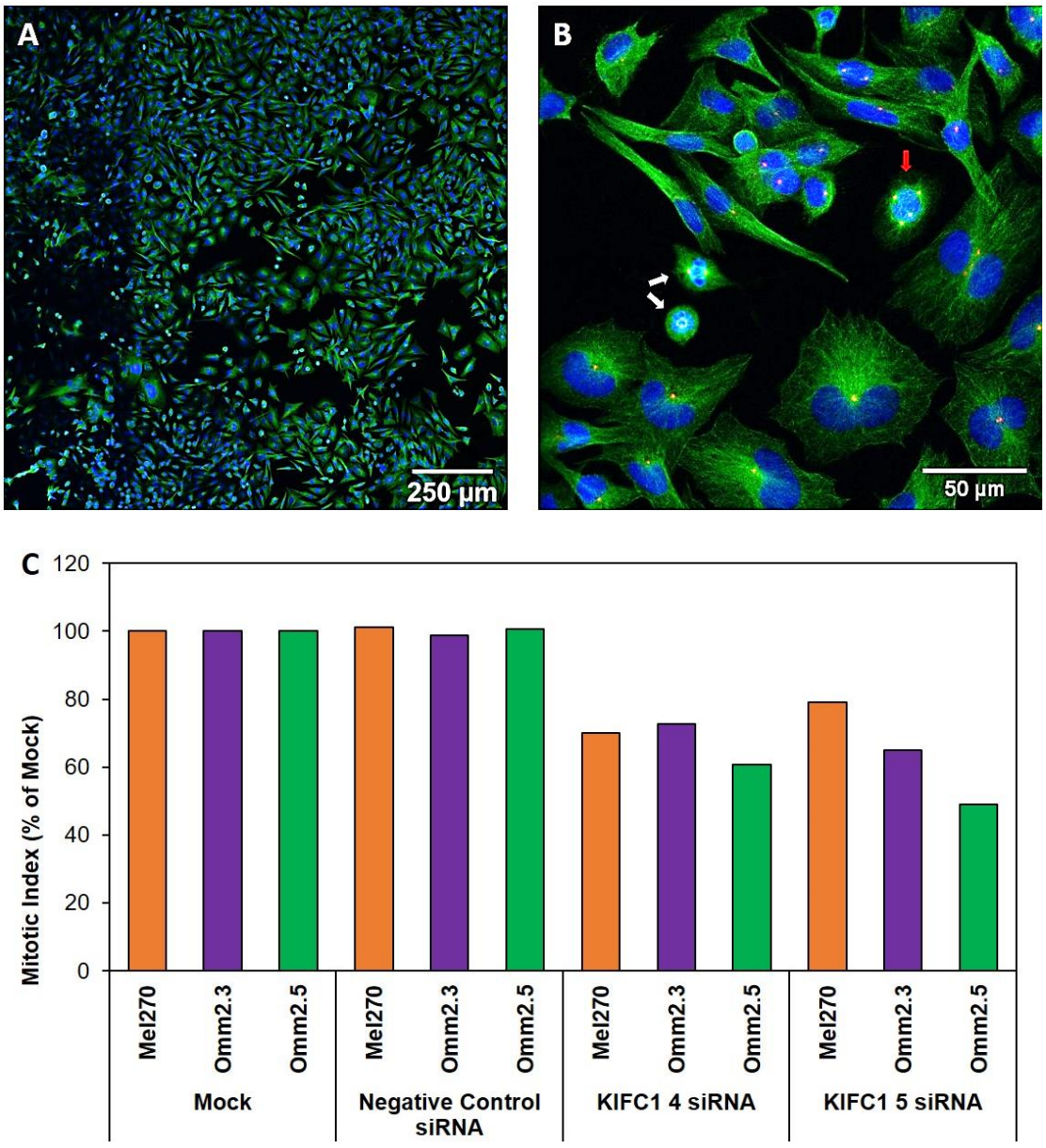

Figure 3.5. KIFC1 Knockdown Decreases the Mitotic Index of Uveal Melanoma Cell Lines. *A) Immunofluorescence microscopy of a field of Omm2.3 cells treated with negative control siRNA. B) A close-up of the field of Omm2.3 cells treated with negative control siRNA - Note the relative ease of identifying bipolar mitotic (white arrows) and multipolar mitotic cells (red arrow) among non-mitotic cells. Cells were grown on coverslips and transfected with either KIFC1 4 siRNA, KIFC1 5 siRNA, negative control siRNA or were mock transfected. 48 h post siRNA transfection, cells were processed for immunofluorescence and stained with anti-α-tubulin antibody and 488 nm-conjugated secondary (to stain microtubules green), anti-pericentrin antibody and 555 nm-conjugated secondary (to stain centrosomes red) and DAPI (to stain DNA blue). D) Quantification of mitotic index detected by immunofluorescence microscopy. The total number of cells on each field was counted using ImageJ, while cells visibly in mitosis were counted by eye and the percentages plotted relative to mock. Between 3000 and 19,000 cells counted for each condition.*

Examination of uveal melanoma cell lines by counting the number of visibly mitotic cells (Figure 3.5B) on images of cell fields obtained by immunofluorescence imaging (Figure 3.5A) and comparing them to the total number of cells showed that KIFC1 knockdown negatively affected the mitotic index of all three cell lines (Figure 3.5C). Furthermore, it was found that Omm2.3 and Omm2.5 had similar mitotic indices of 1.51 and 1.55 respectively, followed by Mel270 at 0.77 (Figure 3.6).

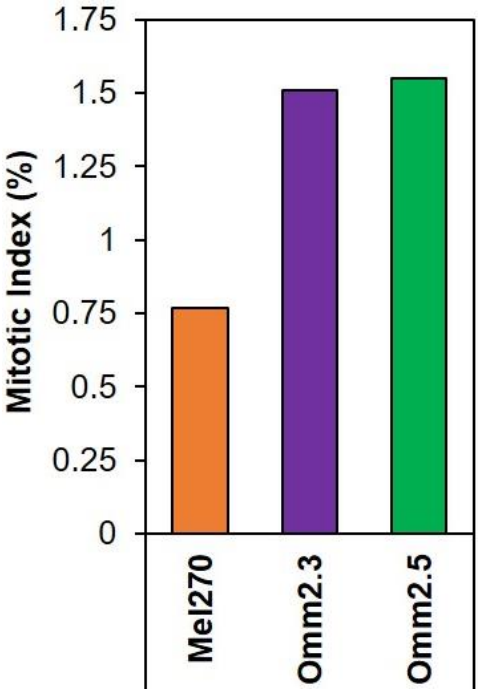

Figure 3.6. Mitotic Index of Uveal Melanoma Cell Lines. *Mel270, Omm2.3 and Omm2.5 cells were grown on coverslips mock transfected. 48 h post siRNA transfection, cells were processed for immunofluorescence and stained with anti-α-tubulin antibody and 488nm-conjugated secondary (to stain microtubules green), anti-pericentrin antibody and 555nm-conjugated secondary (to stain centrosomes red) and DAPI (to stain DNA blue). Immunofluorescence images were taken by confocal microscopy showing field images of Mel270, Omm2.3 and Omm2.5 treated with mock transfection conditions. The total number of cells on each field was counted using ImageJ, while cells visibly in mitosis were counted by eye and plotted as a percentage of the total number of cells. Between 4000 and 13,000 cells counted for each cell line.*

KIFC1 knockdown reduced the mitotic index of all three cell lines (Figure 3.5C). Omm2.5 seemed to be the most sensitive to KIFC1 knockdown, with a 40% and 50% decrease upon treatment with KIFC1 4 siRNA and KIFC1 5 siRNA respectively. Omm2.3 followed with 27%

and 35% decreases, while Mel270 followed with 30% and 20% decreases in mitotic index upon treatment with KIFC1 4 and 5 siRNAs respectively.

In relation to cells expressing KIFC1 to avoid multipolar mitosis, these results are as expected as Mel270 had the lowest levels of centrosome amplification (Figure 3.2C) and lowest clustering ability (Figure 3.2D), implying that it required KIFC1 the least. Meanwhile, Omm2.3 and Omm2.5, which had high centrosome amplification and were proficient in clustering centrosomes had higher decreases in mitotic index upon KIFC1 knockdown, showing that they relied on it more.

KIFC1 Knockdown Reduces Proliferation in Mel270 Cells

To explore the effects of KIFC1 knockdown on cell proliferation upon KIFC1 knockdown and verify the decrease in mitotic index in Mel270, Omm2.3 and Omm2.5, an MTT cell proliferation assay was carried out (Figure 3.7). This would allow comparison of the metabolic activity of a group of cells, which would indicate the number of cells present.

Mel270, Omm2.3 and Omm2.5 cells were mock transfected, transfected with a control siRNA or with one of two independent siRNAs against KIFC1 and plated. Cell numbers were then estimated over 5 days by colorimetry.

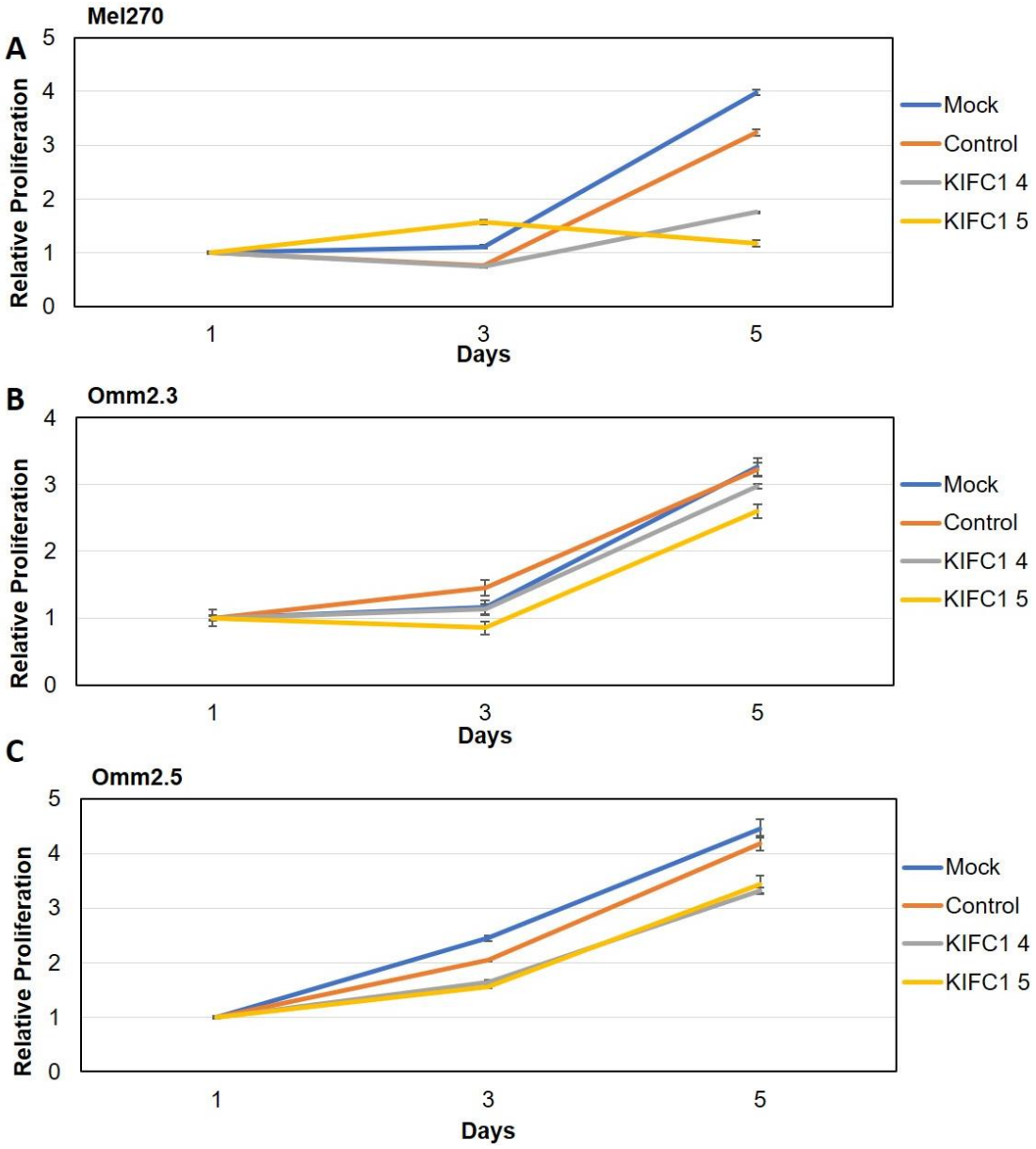

Figure 3.7. KIFC1 Knockdown Reduces Proliferation in Mel270 Cells*. A) Line graph showing growth of Mel270 cells at day 1, 3 and 5 post mock (blue), negative control siRNA (orange), KIFC1 4 siRNA (grey) or KIFC1 5 siRNA*

(yellow) treatment. B) Line graph showing growth of Omm2.3 cells at day 1, 3 and 5 post mock (blue), negative control siRNA (orange), KIFC1 4 siRNA (grey) or KIFC1 5 siRNA (yellow) treatment. C) Line graph showing growth of Omm2.5 cells at day 1, 3 and 5 post mock (blue), negative control siRNA (orange), KIFC1 4 siRNA (grey) or KIFC1 5 siRNA (yellow) treatment. Mel270, Omm2.3 and Omm2.5 cells were seeded in 96 well plates and transfected with either KIFC1 4 siRNA, KIFC1 5 siRNA, negative control siRNA or were mock transfected. One, three and five days post siRNA transfection, MTT reagent was added and the cells were left for 4 hours before the cells were processed for colorimetry and scanned at 590 nm. Cell proliferation decreased in all cell lines upon KIFC1 knockdown but was most pronounced in Mel270. Readings averaged and normalised against background, expressed relative to day 1. Error bars plotted as 1 standard deviation. Technical repeats=6.

The five-day MTT assay showed that siRNA knockdown of KIFC1 decreased growth relative to mock and negative control groups in Mel270 (Figure 3.7A), Omm2.3 (Figure 3.7B) and Omm2.5 (Figure 3.7C). This is expected considering the change in mitotic index outlined earlier. However, the extent of change varied across cell lines. Omm2.3 and Omm2.5 showed modest decreases in cell proliferation relative to the negative control group upon KIFC1 4 and KIFC1 5 siRNA treatment, showing reductions of 8% and 20% respectively in Omm2.3 and reductions of 21% and 19% respectively in Omm2.5. Meanwhile, Mel270 showed much greater decreases of 46% and 64% compared to the negative control group when treated with KIFC1 4 and KIFC1 5 siRNAs respectively.

This was unexpected, as the low-level centrosome amplification and clustering in Mel270 in wild-type conditions implied that KIFC1 would be relatively dispensable, especially when compared to Omm2.3 and Omm2.5. Although there is some variation between the negative controls and between the KIFC1 4 and 5 siRNAs in Mel270, it is clear that Mel270 cells are affected by KIFC1 knockdown more than Omm2.3 and Omm2.5, which is unexpected.

KIFC1 Knockdown Reduces Clonogenicity in Uveal Melanoma Cell Lines

To further explore how KIFC1 knockdown affected cell growth, an alternative method to measure cell proliferation, the clonogenic assay, was used to assess change in clonogenic capacity of Mel270, Omm2.3 and Omm2.5 cells upon KIFC1 knockdown (Figure 3.8).

Mel270, Omm2.3 and Omm2.5 cells were mock transfected, transfected with a control siRNA or with one of two independent siRNAs against KIFC1 and plated at a low density. 21 days later, the cells were fixed and stained with crystal violet to visualise colonies, which were imaged and analysed using a GelCount colony counter.

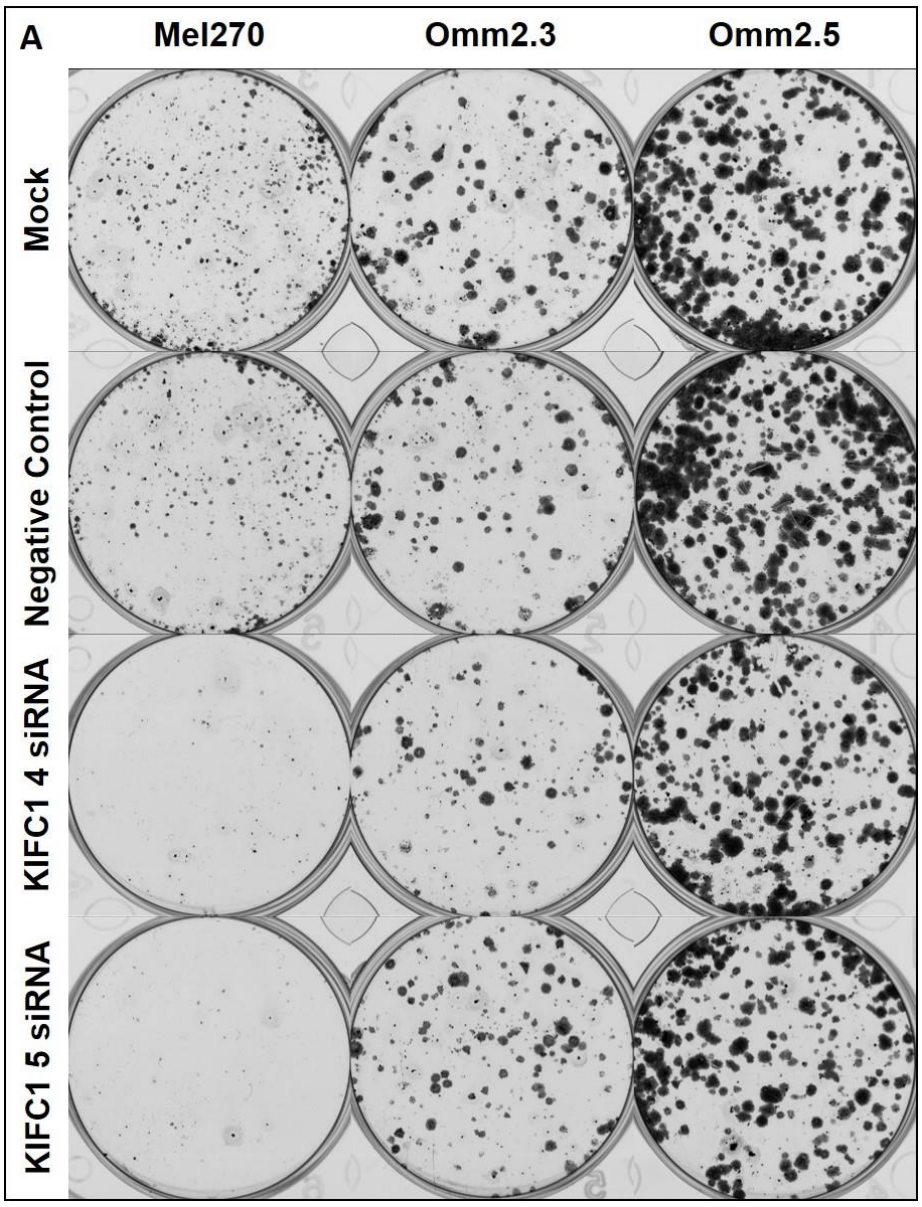

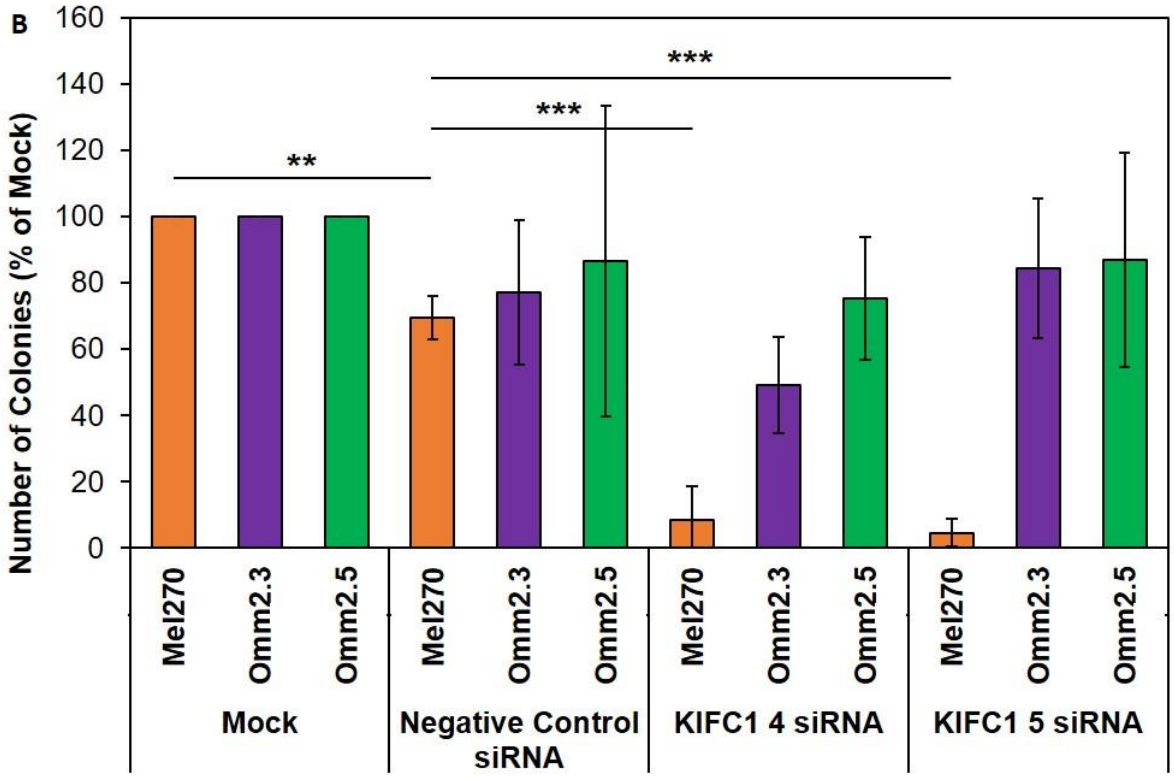

Figure 3.8. KIFC1 Knockdown Reduces Clonogenicity in Uveal Melanoma Cell Lines. *A) image of one set of three clonogenic plates stained with crystal violet. Mel270, Omm2.3 and Omm2.5 cells were transfected with either KIFC1 4 siRNA, KIFC1 5 siRNA, negative control siRNA or were mock transfected and seeded at very low density. 21 days later, the cells were fixed, stained with Crystal Violet and the number of colonies were counted. B) A graph showing number of colonies in Mel270, Omm2.3 and Omm2.5 upon mock or negative control siRNA, KIFC1 4 siRNA or KIFC1 5 siRNA treatment. Error bars plotted as 1 standard deviation. Independent biological repeats=3. Statistics were performed in OriginPro 2019b. A Shapiro-Wilk test was used to test for normality of each set of data. This showed that the data for the Negative Control, KIFC1 4 siRNA and KIFC1 5 siRNA was significantly drawn from a normally distributed population at the 0.05 level, although there was not enough information to draw a conclusion for the Mock as the data was normalised to Mock readings. A repeated measures, One-Way ANOVA with Dunnett's multiple comparison test was then used to test for significance between the Negative Control and KIFC1 4 and KIFC1 5 siRNAs. **p<0.001, ***p<0.0001. KIFC1 knockdown affects clonogenicity of Mel270 but not Omm2.3 and Omm2.5.*

The clonogenic growth assay in uveal melanoma cell lines showed that KIFC1 knockdown negatively affected the colony forming ability of Mel270 (Figure 3.8). Mirroring the results from the MTT assay, Mel270 cells were far more sensitive to KIFC1 knockdown by KIFC1 4 and KIFC1 5 siRNA treatment than Omm2.3 and Omm2.5. Counting of colonies showed that the number of colonies formed by Mel270 when treated by KIFC1 4 and 5 siRNA fell by 88% and 93% respectively when compared to negative control groups. As this data was normally distributed, a repeated measures, One-Way ANOVA with Dunnett's multiple comparison test showed that there was a significant difference between Mel270 cells treated with Negative

Control siRNA and Mel270 cells treated with KIFC1 siRNAs at $p<0.0001$. Importantly however, there was also a significant difference between mock Mel270 cells and negative control Mel270 cells at $p<0.001$.

In contrast, there was no significant difference in the clonogenicity of Omm2.3 and Omm2.5 treated with KIFC1 4 siRNA and KIFC1 5 siRNA when compared to the negative control treated cells. Coupled with the large variability in results across the 3 independent repeats for Omm2.3 and Omm2.5, this indicates that these cell lines are not very sensitive to KIFC1 depletion when forming colonies. However, as shown by the MTT assays, Omm2.3 and Omm2.5 cells have a higher metabolism than Mel270 and so the question arises whether the KIFC1 depletion effect was maintained throughout the 21 days, or whether these cells merely recovered after the KIFC1 siRNA effect was sufficiently diluted within the cells.

KIFC1 Knockdown Has No Effect on Cell Cycle Dynamics in Uveal Melanoma Cell Lines

Evidence exists that KIFC1 depletion slows down the cell cycle (Pannu et al., 2015b) and delays mitotic exit (Kim and Song, 2013). To see if this was the case in Mel270, Omm2.3 and Omm2.5 cells, changes in the cell cycle upon KIFC1 knockdown were explored.

Mel270, Omm2.3 and Omm2.5 cells were mock transfected, transfected with a control siRNA or with one of two independent siRNAs against KIFC1. 48 hours later, cells were fixed, stained with propidium iodide and the cell cycle was analysed by flow cytometry (Figure 3.9).

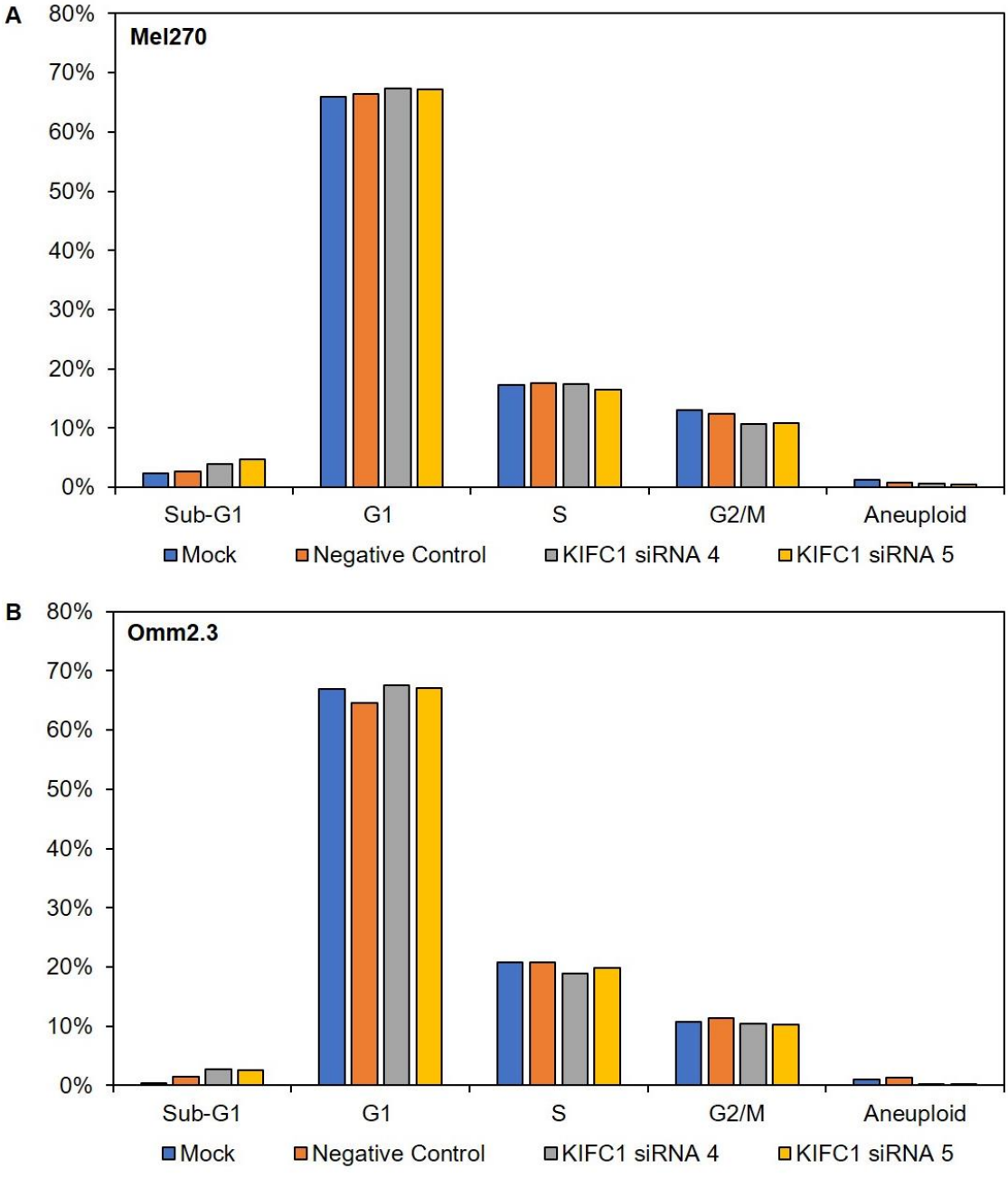

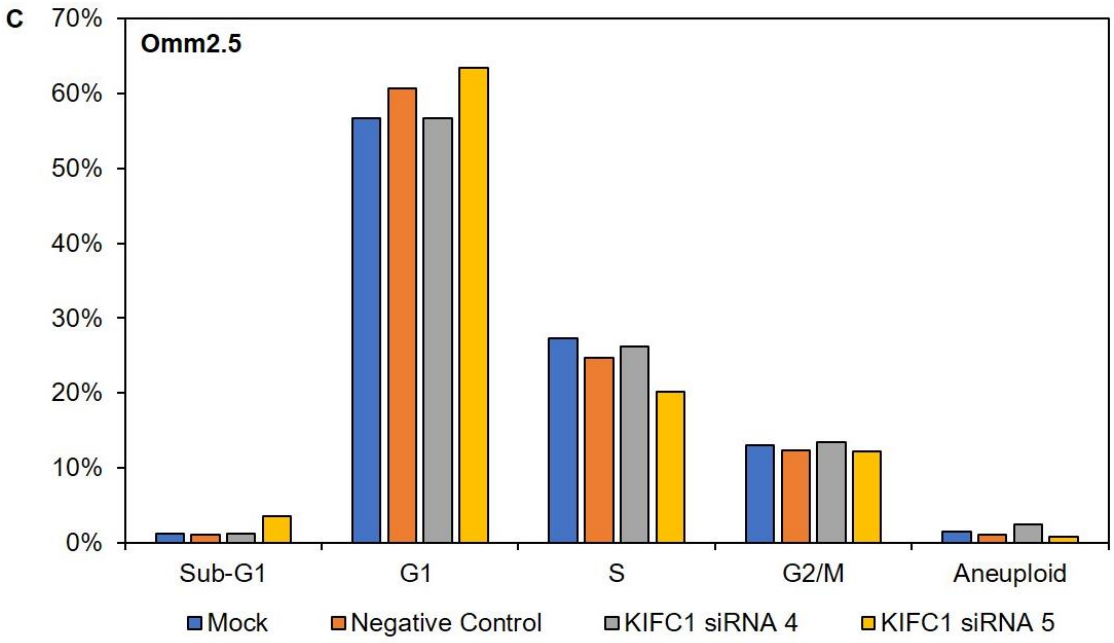

Figure 3.9. KIFC1 Has No Effect on the Cell Cycle in Uveal Melanoma Cells. *A) Bar graph showing cell cycle distribution of Mel270 cells. B) Bar graph showing cell cycle distribution of Omm2.3 cells. C) Bar graph showing cell cycle distribution of Omm2.5 cells with mock (blue), negative control siRNA (orange), KIFC1 4 siRNA (grey) or KIFC1 5 siRNA (yellow) treatment. Mel270, Omm2.3 and Omm2.5 cells were transfected with either KIFC1 4 siRNA, KIFC1 5 siRNA, negative control siRNA or were mock transfected and seeded at very low density. The cells were fixed with ice cold methanol, treated with RNAse A, stained with propidium iodide and analysed by flow cytometry.*

As shown in figure 9, KIFC1 depletion had no profound effect on the cell cycle distribution of Mel270, Omm2.3 and Omm2.5. Although KIFC1 depletion has been shown to affect cyclin expression and cell cycle distribution in some cancer types (Pannu et al., 2015b), it has also been shown to have no effect in other cancer types (Fu et al., 2018).

Under mock conditions, the proportion of cells in G2/M were similar in all three cell lines, ranging between 10-13%. However, Omm2.5 had the highest proportion of cells in S phase (27%) and the fewest proportion of cells in G1 (57%) when compared to Omm2.3 (67% and 21%) and Mel270 (66% and 17%).

KIFC1 Knockdown Increases Apoptosis in Uveal Melanoma Cell Lines

KIFC1 overexpression has been shown to reduce apoptosis in cancer cells, both by limiting multipolar mitosis as well as by increasing survival signalling (Pannu et al., 2015b). Therefore, to understand how KIFC1 knockdown changed cell proliferation and colony formation in Mel270, Omm2.3 and Omm2.5 cell lines without changing cell cycle dynamics, the effect of KIFC1 depletion on apoptosis was examined by immunofluorescence imaging (Figure 3.10).

Mel270, Omm2.3 and Omm2.5 cells were grown on coverslips and mock transfected, transfected with a control siRNA or with one of two independent siRNAs against KIFC1. 48 hours later, the cells were fixed, stained for immunofluorescence with DAPI and an anti-cleaved caspase 3 antibody was used to detect apoptotic cells due to the role of cleaved caspase-3 in apoptosis (McIlwain et al., 2013).

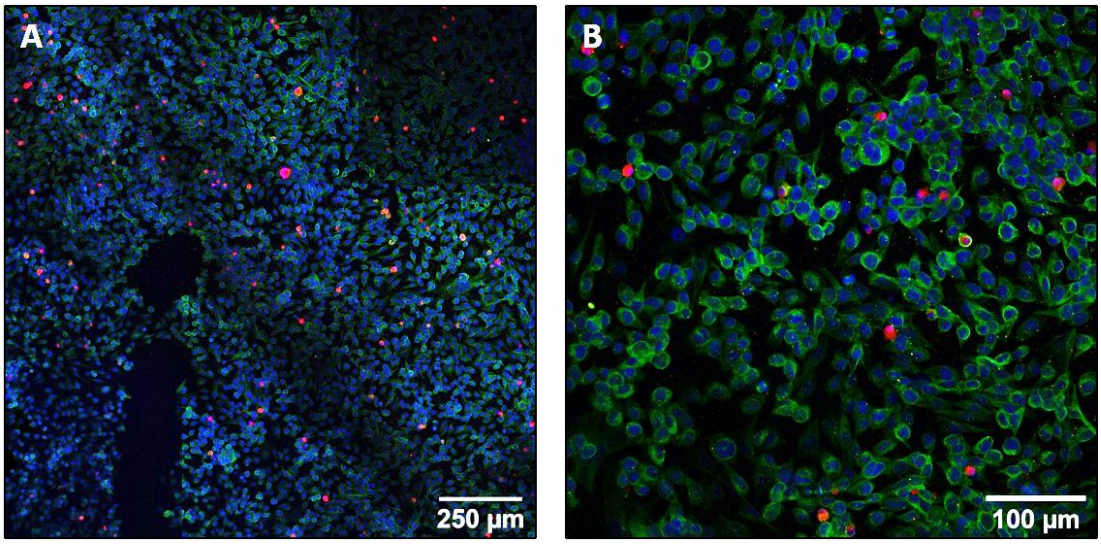

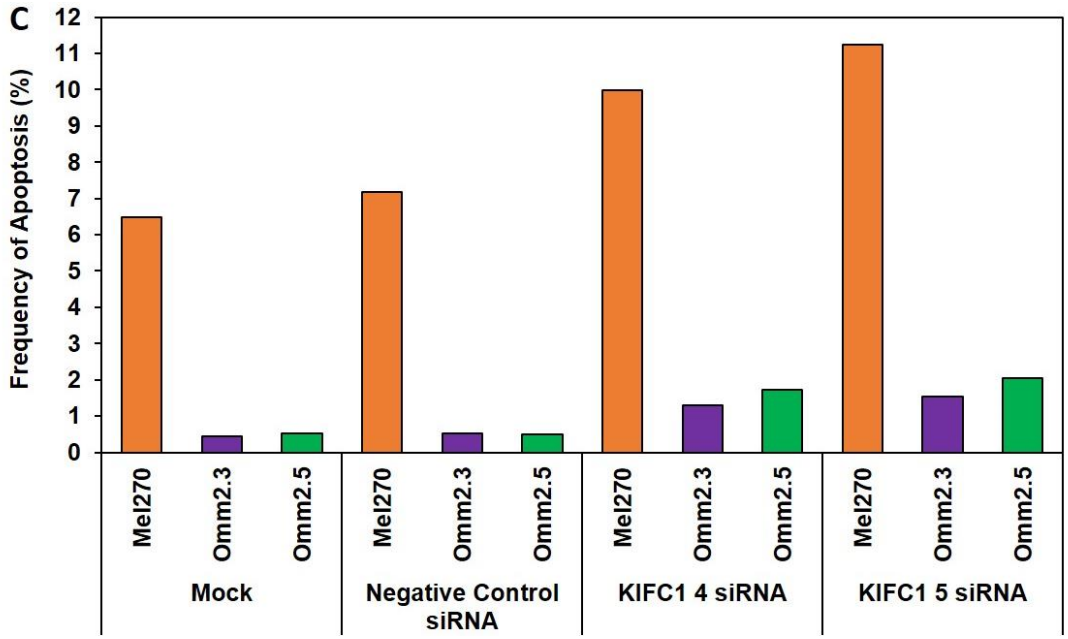

Figure 3.10. KIFC1 Knockdown Increases Apoptosis in Uveal Melanoma Cells. *A) Immunofluorescence microscopy of a field of Omm2.5 cells treated with KIFC1 5 siRNA. B) Close-up of the field of Omm2.5 cells treated with KIFC1 5 siRNA. Mel270, Omm2.3 and Omm2.5 cells were grown on coverslips and transfected with either KIFC1 4 siRNA, KIFC1 5 siRNA, negative control siRNA or were mock transfected. 48 h post siRNA transfection, cells were processed for immunofluorescence and stained with anti-α-tubulin antibody and 488 nm-conjugated secondary (to stain microtubules green), anti-cleaved caspase-3 antibody and 555 nm-conjugated secondary (as apoptotic marker, red) and DAPI (to stain DNA blue). D) Quantification of apoptosis detected by immunofluorescence microscopy. The total number of cells on each field was counted using ImageJ, while cells stained red were counted by eye and the percentages plotted relative to mock. Between 300 and 12,000 cells were counted for each condition. Red cells indicated cleaved caspase-3 expression and were counted as positive apoptosis signals and plotted as % apoptotic cells for each cell line. The frequency of apoptosis increased upon KIFC1 knockdown in Mel270, Omm2.3 and Omm2.5.*

Examination of apoptosis in uveal melanoma cell lines by counting cleaved capase-3 positive cells on images obtained by confocal microscopy showed that the basal apoptosis level of Mel270 was more than 10-fold higher than the basal apoptosis level of Omm2.3 and Omm2.5 (Figure 3.10C).

Furthermore, transfection with KIFC1 siRNA markedly increased the proportion of apoptotic cells in Mel270, Omm2.3 and Omm2.5 cells when compared to mock and negative control treated cells. The frequency of cleaved caspase-3 expression increased in Omm2.5 the most, showing 240% and 300% increases over mock cells when treated with KIFC1 4 and KIFC1 5 siRNAs. Omm2.3 showed a smaller increase in the frequency of cleaved caspase-3 expression, with 200% and 260% increases, while Mel270 showed the smallest increase, with 50% and 70% increases compared to mock cells when treated with KIFC1 4 and KIFC1 5 siRNAs respectively.

Nevertheless, although Mel270 showed the smallest % increase in apoptosis upon KIFC1 depletion, the absolute frequency of apoptosis rose to greater than 10% following KIFC1 depletion, which means KIFC1 knockdown is far more likely to induce a cell growth effect in Mel270. This is in comparison to an absolute level of 2% apoptosis in Omm2.3 and Omm2.5 after KIFC1 depletion, which may have relatively little effect on cell proliferation. However, these results seemingly disagreed with the results of the cell cycle distribution analysis by flow cytometry, in which the population of sub-G1 group did not substantially increase as expected in Mel270.

KIFC1 Knockdown Increases Multipolar Mitosis in Mel270

One possible explanation for the stark negative effect of KIFC1 knockdown on Mel270, especially when compared to Omm2.3 and Omm2.5, is that the frequency of multipolar mitosis in Mel270 may increase upon KIFC1 knockdown. Therefore, the effect of KIFC1 knockdown on Mel270 was examined by immunofluorescence (Figure 3.11).

Mel270 cells were grown on coverslips and mock transfected, transfected with a control siRNA or with one of two independent siRNAs against KIFC1. 48 hours later, the cells were fixed, stained for immunofluorescence with DAPI and anti-α-tubulin, anti-centrin and anti-pericentrin antibodies were used to identify cells undergoing mitosis and visualise the centrosomes.

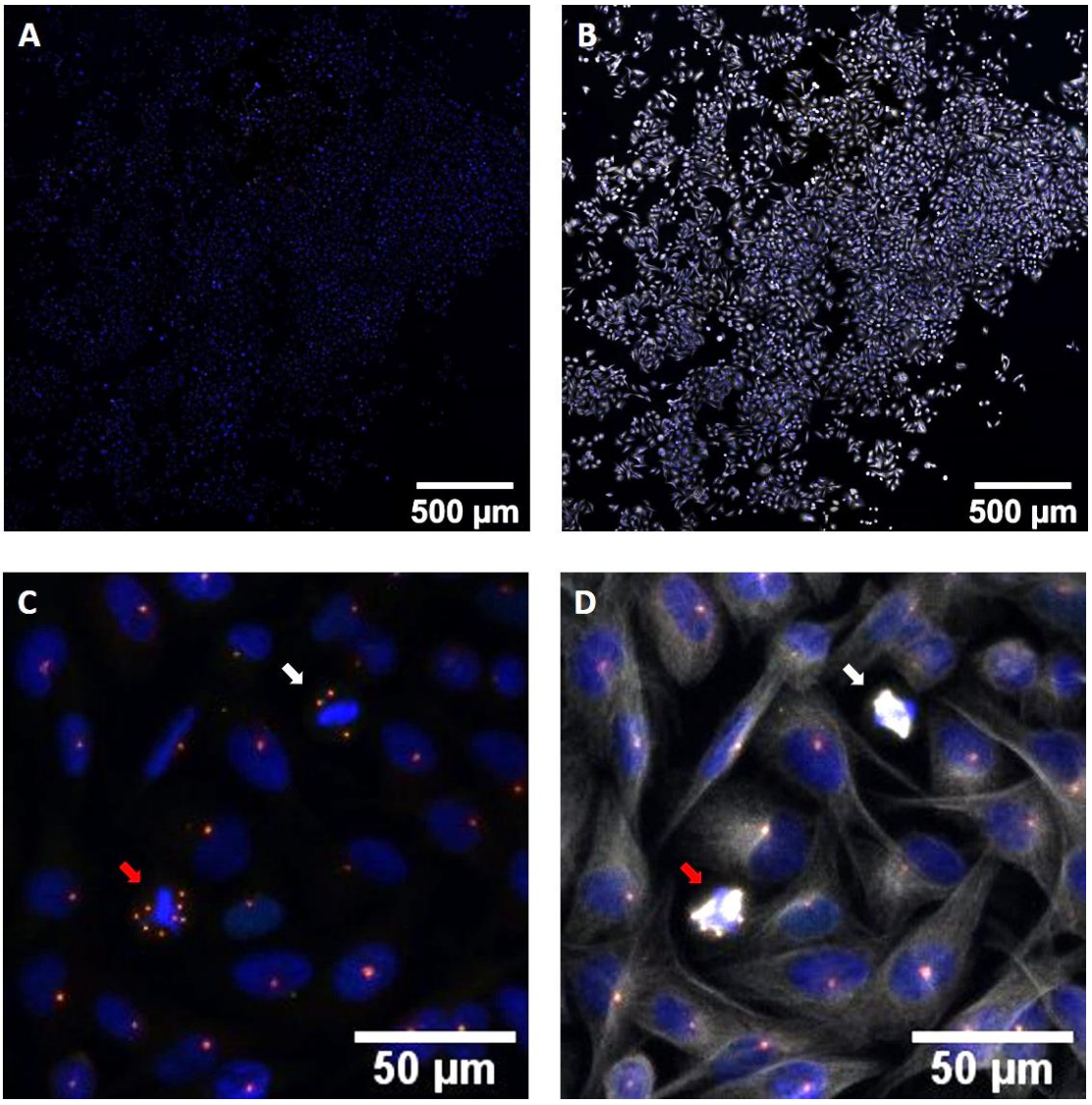

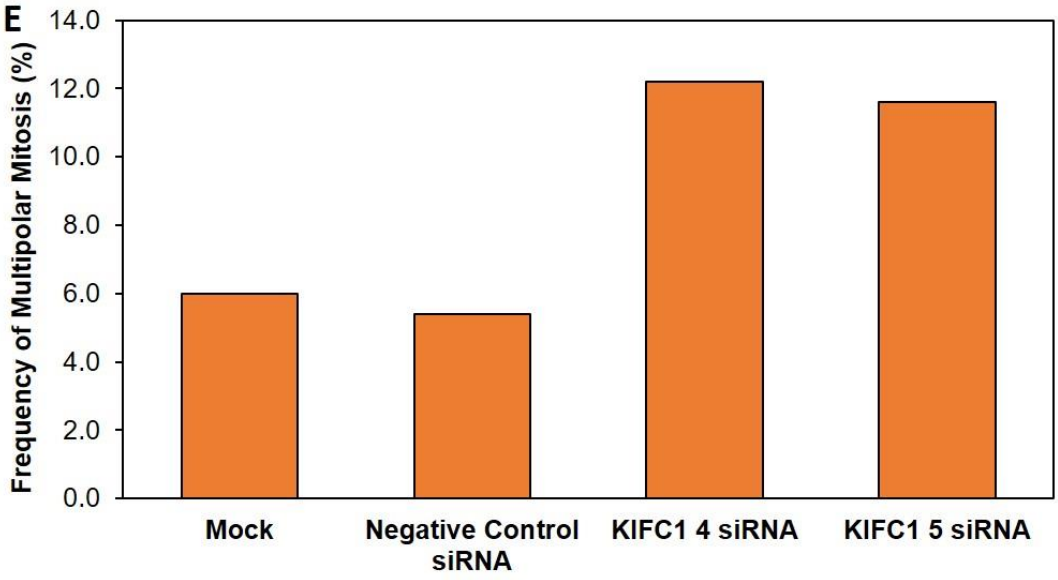

Figure 3.11. KIFC1 Knockdown Increases Multipolar Mitosis in Mel270. *A) Immunofluorescence microscopy showing a field of Mel270 cells with mock treatment made up of merged DNA, centrin and pericentrin channels. B) Immunofluorescence microscopy showing the same field of Mel270 cells made up of merged DNA, centrin, pericentrin and α-tubulin channels. Image A allows examination of the centrosome, while image B allows identification of mitosis. C) Zoomed in image of micrograph A to show close ups of pseudo-bipolar (white arrow) and multipolar (red arrow) spindles. D) Zoomed in image of micrograph B to show close ups of pseudo-bipolar (white arrow) and multipolar (red arrow) mitosis. Mel270 cells were grown on coverslips and transfected with either KIFC1 4 siRNA, KIFC1 5 siRNA, negative control siRNA or were mock transfected. 48 h post siRNA transfection, cells were processed for immunofluorescence and stained with anti-centrin antibody and 488 nm-conjugated secondary (to stain centrioles green), anti-pericentrin antibody and 555 nm-conjugated secondary (to stain centrosomes red), anti-α-tubulin antibody and 647 nm-conjugated secondary (to stain microtubules grey) and DAPI (to stain DNA blue. E) Quantification of multipolar mitosis detected by immunofluorescence microscopy. Cells in multipolar mitosis were counted by eye, compared to the total number of mitotic cells and plotted relative to mock. Between 37 and 50 mitotic cells counted for each condition. KIFC1 knockdown increased multipolar mitosis in Mel270.*

Examination of the frequency of multipolar mitosis among the population of mitotic Mel270 cells showed that KIFC1 knockdown increases multipolar mitosis. This is expected, as KIFC1 is known to cluster amplified centrosomes prior to anaphase (Kwon et al., 2008). As seen in figure (Figure 3.11E), the incidence of multipolar mitosis increases from approximately 6% in mock and negative control siRNA treated cells to 12.2% and 11.6% upon treatment with KIFC1 4 and KIFC1 5 siRNAs respectively.

Uncorrected multipolar mitosis usually leads to apoptosis, either due to prolonged mitotic arrest or massive aneuploidy in daughter cells. A twofold increase in multipolar mitosis in Mel270 could potentially double the number of cell deaths which occur due to multipolar

mitosis. However, the increase in multipolar mitosis would only affect cells undergoing mitosis, which occur at a relatively low rate (Figure 3.6), and so is unlikely to explain the large increase in Mel270 cells undergoing apoptosis or the huge decrease in cell proliferation observed on the clonogenic and MTT assays.

An unexpected finding from this experiment was that the frequency of multipolar mitosis upon KIFC1 knockdown (12%) was higher than the amounts of centrosome amplification in Mel270 reported in Figure 3.2 (10%). Although this increase is unlikely to be statistically significant given the number of cells counted in these experiments, it does raise the possibility that a process other than centrosome amplification was causing multipolar mitosis. Assuming this might be the case, it was hypothesised that a possible cause of the high incidence of multipolar mitosis may be the formation of acentriolar spindle poles.

Mel270 Does Not Contain Acentriolar Spindle Poles

One possibility for the relatively high incidence of multipolar mitosis upon KIFC1 knockdown in Mel270 when compared to the relatively low levels of centrosome amplification is that Mel270 may harbour acentriolar spindle poles. Acentriolar spindle poles are MTOCs which contain clusters of pericentrin, but do not contain centrioles and therefore are not true centrosomes. These work as viable spindles poles and can be clustered by KIFC1 and so take part in multipolar mitosis upon KIFC1 knockdown (Kleylein-Sohn et al., 2012).

To explore whether this was the case, cells stained with anti-α-tubulin, anti-centrin and anti-pericentrin antibodies were imaged at a higher magnification to confirm or deny the presence of acentrosomal spindle poles in Mel270.

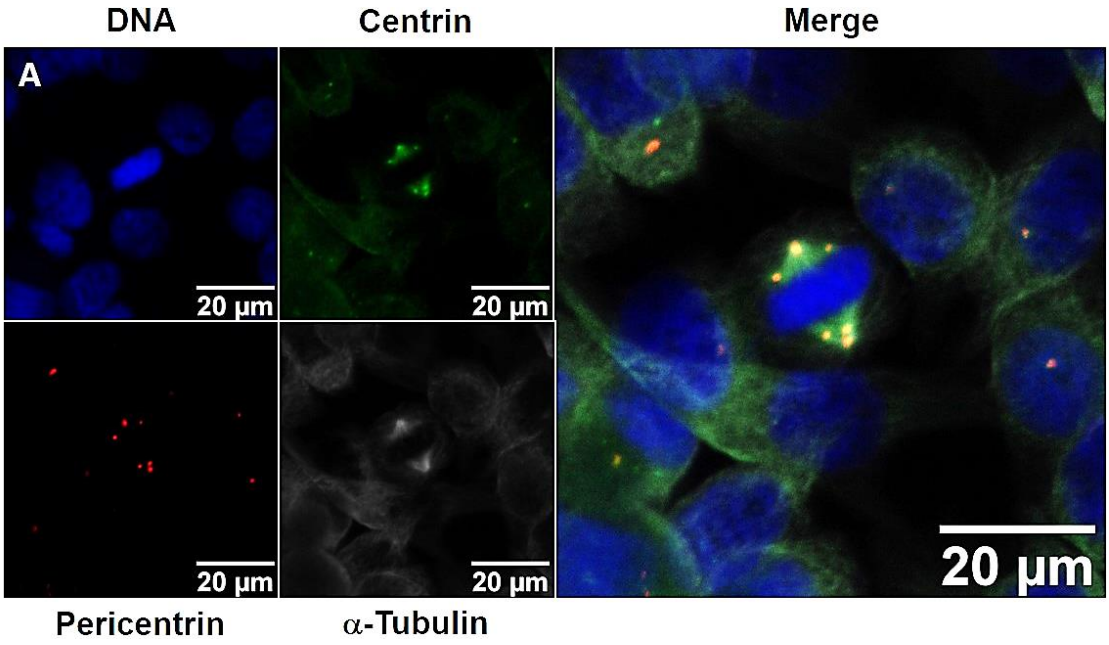

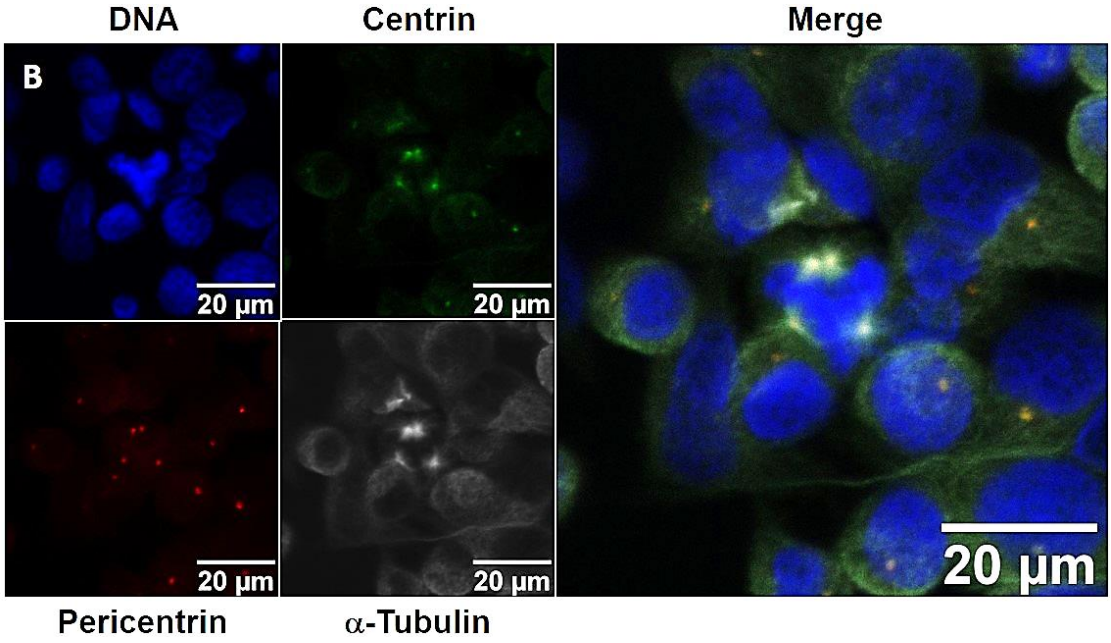

Figure 3.12. Mel270 Does Not Contain Acentriolar Spindle Poles. *A) Immunofluorescence microscopy of Mel270 under mock conditions undergoing pseudo-bipolar mitosis. B) Immunofluorescence microscopy of Mel270 treated with KIFC1 5 siRNA undergoing multipolar mitosis. Mel270 cells previously processed for immunofluorescence and stained with anti-centrin antibody and 488 nm-conjugated secondary (to stain centrioles green), anti-pericentrin antibody and 555 nm-conjugated secondary (to stain centrosomes red), anti-α-tubulin antibody and 647 nm-conjugated secondary (to stain microtubules grey) and DAPI (to stain DNA blue) were imaged at a high magnification to clearly view the spindles during mitosis. These images show the presence of centrin (green), a key component of centrioles, in each centrosome, and thus the lack of acentriolar spindles.*

Upon closer examining the slides shown in figure 3.11 for mitotic cells whose spindle poles contained no centrioles, also known as acentriolar spindle poles, it was found that Mel270 cells do not hold acentriolar spindle poles. Most cells undergoing mitosis, be it bipolar, pseudo-bipolar or multipolar mitosis, resembled the cells shown in figure 3.12.

While this experiment did further characterise the relatively unknown Mel270 cells, it provided no answers as to whether the greater incidence of multipolar mitosis in KIFC1-depleted Mel270 cells compared to the levels of overall centrosome amplification was the product of another process, such as acentriolar spindle formation.

3.2. Discussion I

3.2.1. Centrosome Amplification and Multipolar Mitosis in Uveal Melanoma Cells

Uveal Melanoma Cells Harbour Extra Centrosomes and Undergo Centrosome Clustering

To analyse whether Mel270 (primary uveal melanoma), Omm2.3 and Omm2.5 (liver metastases from the original Mel270 primary tumour) had centrosome amplification, the cells were imaged and analysed by immunofluorescent microscopy. As shown in figure 3.1, the metastatic uveal melanoma cell lines have a high degree of centrosome amplification when compared to the primary Mel270 cells. As these cell lines are from the same patient, they present a good model as to how centrosome amplification may develop in cancer. Omm2.3 undergoes multipolar mitosis most frequently at 14%, followed by Omm2.5 at 12% and Mel270 at 6% of mitoses. The fact that the proportion of cells undergoing multipolar mitosis is smaller than the proportion of cells undergoing centrosome amplification shows that centrosome clustering is mostly an efficient process.

In a large-scale screen of the extent of centrosome amplification in a panel of 60 representative cancer cell lines termed the NCI-60, including five non-transformed matched cell lines, it was found that 7% ± 3% of normal cells had centrosome amplification. Setting the cut-off at two standard deviations above the mean suggested that greater than 13% of cells with centrosome amplification would be considered for a cell line to have significant centrosome amplification (Marteil et al., 2018). Based on this, our data shows that Mel270 would be considered to have insignificant centrosome amplification (10%), while Omm2.3 (34%) and Omm2.5 (33%) would be considered to have extremely high centrosome amplification and would rank 7th and 8th highest if placed amongst the NCI-60.

Nevertheless, although Mel270 undergoes multipolar mitosis the most infrequently, together these results show that Mel270 clusters its amplified centrosomes the least efficiently when compared to Omm2.3 and Omm2.5, as 60% of Mel270 cells with extra centrosomes undergo multipolar mitosis, as opposed to 40% and 34% of Omm2.3 and Omm2.5 cells with amplified centrosomes. Overall, this data shows that Mel270 has the lowest levels of centrosome amplification and multipolar mitosis but is also the least proficient in clustering amplified centrosomes. This was not unexpected as centrosome amplification causes high-grade features, and higher levels of centrosome amplification are associated with poor prognosis

(Denu et al., 2016). Afterall, Omm2.3 and Omm2.5 cells are secondary metastases of the primary tumour that Mel270 was derived from.

In fact, it would not be surprising that centrosome amplification matches the difference in grade between Mel270 and Omm2.3 and Omm2.5. This is because although centrosome amplification can occur very early in cancer and can initiate tumorigenesis during transplantation experiments (Basto et al., 2008), (Levine et al., 2017), it also dictates higher grade (Denu et al., 2016). However, in a bioinformatics screen of nearly 10,000 tumours from TGCA datasets spanning over 30 cancer types, the centrosome amplification-linked transcriptomic signature of primary uveal melanoma was relatively low compared to other cancers (de Almeida et al., 2019). Despite this, it is important to mention that the TGCA data are not yet available for metastatic uveal melanoma, and so the results from our matched cell model would predict a higher expression of centrosome amplification-linked genes in metastatic uveal melanoma.

Furthermore, there is good evidence to suggest that centrosome amplification can drive metastatic phenotypes. It is possible that the increased centrosome amplification and associated genomic instability enabled cells to detach from the primary tumour and successfully metastasise, later becoming the Omm2.3 and Omm2.5 lines. Amplified centrosomes alter microtubule dynamics inside cells and alter directional migration (Reviewed by Ogden et al., 2013), and through increased centrosomal microtubule nucleation, disrupt adhesion to promote invasion (Godinho et al., 2009). Centrosome amplification can also induce invasiveness in a non-cell autonomous manner, where adding media in which cells with centrosome amplification had previously grown increases cell invasiveness in cells without centrosome amplification (Arnandis et al., 2018).

In this experiment, only cells in mitosis were analysed to assess whether they had centrosome amplification as mitosis was easily identified by microscopy, while cells in G1 could not be differentiated with cells in G2. This is important because a cell with two visible centrosomes in G1 would be considered to have centrosome amplification, whereas a cell in G2 with two centrosomes would have a normal number of centrosomes. To improve this experiment, cells could be stained with cyclin D, which is expressed up until the S-phase boundary before it is degraded (Reviewed by Alao, 2007) which would allow analysis of every cell on a field image, thus increasing the statistical power of the results.

KIFC1 knockdown in Mel270 Increases the Frequency of Multipolar Mitosis

To understand why KIFC1 depletion disproportionately affects the growth of Mel270, Mel270 cells were treated with KIFC1 siRNA and the frequency of multipolar mitosis was analysed by immunofluorescence. Figure 3.11 shows that KIFC1 knockdown increases the frequency of multipolar mitosis twofold.

This is expected as it is well known that KIFC1 clusters amplified centrosomes to bipolar spindles, while depletion of KIFC1 induces multipolar mitosis in cells with amplified centrosomes (Kwon et al., 2008). Although it is not known exactly how KIFC1 clusters centrosomes, a mechanism has been proposed that KIFC1 does so during prometaphase (Reviewed by Xiao and Yang, 2016). Without the clustering ability of KIFC1, it is likely that Mel270 cells would improperly complete centrosome clustering and instead undergo multipolar mitosis.

The increase in multipolar mitosis upon KIFC1 knockdown in Mel270 partially explains the decrease in proliferation seen in Mel270 upon KIFC1 knockdown, shown in figure 3.7, as it is well known that multipolar mitosis almost always causes apoptosis or growth arrest. When the progeny of spontaneous multipolar mitoses in a range of cancer cells were tracked over four days, it was found that most of the first generation died, while a few went into growth arrest and approximately a fifth successfully divided again. However, the entirety of the second generation died or underwent growth arrest, thus eliminating the progeny of multipolar mitotic cells regardless of the tissue of origin (Ganem et al., 2009).

The incidence in multipolar mitosis upon KIFC1 knockdown in Mel270 (approx. 12%, Figure 3.11) matches or slightly exceeds the incidence of centrosome amplification in mock Mel270 cells (approx. 10%, Figure 3.1). If these figures were found to be statistically significant in the future, there would be three possible explanations for this observation. The first and perhaps most likely is that without KIFC1, cells with centrosome amplification are unable to cluster their centrosomes and therefore close to 100% of the cells with centrosome amplification display multipolar mitoses. The two remaining possibilities are that either KIFC1 knockdown increased centrosome amplification, which has been shown to not occur in other models

(Kleylein-Sohn et al., 2012), or that Mel270 may harbour alternative, acentriolar microtubule organising complexes (MTOCs) following KIFC1 depletion.

Mel270 Does Not Harbour Acentriolar Spindle Poles

As KIFC1 knockdown is not known to increase the incidence of centrosome amplification in cancer cells (Kleylein-Sohn et al., 2012), it was somewhat surprising to see that the frequency of multipolar mitosis upon KIFC1 knockdown in Mel270 (12%, Figure 3.11) increased slightly beyond the incidence of centrosome amplification in mock Mel270 cells (10%, Figure 3.1). Although this increase may not be significant, it does suggest that KIFC1 knockdown resulted in nearly 100% of Mel270 cells with centrosome amplification being unable to cluster their centrosomes. However, if the slight increase in multipolar mitosis beyond centrosome amplification was significant, a hypothesis of how this occurs could be by the formation of acentriolar spindle poles. Also known as acentrosomal spindles poles, they are MTOCs formed independently of centrioles (Schuh and Ellenberg, 2007). These are normally seen in cells without centrosomes, such as female germ cells, higher plants or cells artificially depleted of centrosomes. In these cells, a Ran-GTP gradient accumulates around chromosomes relative to the cytoplasm to induce nucleation of microtubules around the chromosomes (Reviewed by Kalab and Heald, 2008), while also promoted and organised by Augmin-HAUS. The resulting structure is then incorporated into a bipolar spindle by kinesins including KIFC1 and act like bona-fide centrosomes in cells with more than two spindle poles, being focused for pseudo-bipolar mitosis. Furthermore, depletion of KIFC1 in cells with acentriolar spindles causes defective spindle assembly and pole focussing, causing spindle poles to fragment and thus induce multipolar mitosis (Kleylein-Sohn et al., 2012).

For this experiment, acentriolar spindles were characterised as a nucleation of microtubules surrounded by pericentrin but devoid of centrin, a key component of centrioles. Therefore, immunofluorescent images of cells stained for DNA, α-tubulin, centrin and pericentrin were taken and analysed for the presence of a cell undergoing mitosis in which a spindle pole contained pericentrin but not centrioles. It was found that neither Mel270, Omm2.3 or Omm2.5 contained acentriolar spindles, rather most cells undergoing mitosis had centrosomes resembling those presented in figure 3.12. Although this gave an interesting

insight into these cell lines, it provided no answer as to how KIFC1 depletion increased the frequency of multipolar mitosis beyond the level of centrosome amplification in mock Mel270 cells.

It has recently been discovered that in cancer cells, KIFC1 is involved in regulation of nuclear membrane maintenance, chromatin distribution and participates in DNA synthesis (Zou et al., 2014). Therefore, an alternative explanation could be that KIFC1 knockdown and the resultant improper division of the chromosomes induced chromosomal aberrations, DNA damage or mutations to critical components of the centrosome cycle, thus inducing further centrosome amplification. However, we do not have evidence that this is occurring in Mel270 cells. Overall then, more work needs to be carried out to understand if KIFC1 depletion is causing an increase centrosome amplification in Mel270 cells and if so, how this might occur.

3.2.2. KIFC1 Depletion Negatively Affects Growth in Uveal Melanoma Cells

KIFC1 Depletion Reduces Mitotic Index

Confocal microscopy and subsequent analysis of primary and secondary uveal melanoma cell lines showed that KIFC1 depletion reduced the mitotic index of these cell lines. As presented in figure 3.5, treatment with KIFC1 4 and KIFC1 5 siRNA decreased mitotic index by 40% and 50% in Omm2.5, 27% and 35% in Omm2.3 and 20% and 30% in Mel270 respectively when compared to mock treatment. This was expected, as it has been well established that KIFC1 affects cancer cell proliferation. However, the difference in the effect of KIFC1 knockdown on mitotic index (Figure 3.5C) between Mel270 and the Omm cell lines was not proportional to the differences in centrosome amplification and multipolar mitosis (Figure 3.1D and 3.2D). This was the first indication that KIFC1 had a function other than centrosome clustering in uveal melanoma cells, and especially in Mel270 cells. Although this is the first study to examine the role of KIFC1 in uveal melanoma cells, only once has it been reported that cells with and without artificial centrosome amplification both overexpressed proliferation markers upon overexpression of KIFC1 (Pannu et al., 2015b). Conversely, many studies regarding the role of KIFC1 in cancer use cell lines with centrosome amplification.

The measured mitotic index in this case was defined as the number of observable cells undergoing mitosis in a certain field divided the total number of cells in the field, presented as a percentage. Mitotic index is used commonly in grading classifications, for example the Elston-Ellis grading system for breast cancers, the French Federation of Cancer Centres Sarcoma Group and to distinguish between different neuroendocrine tumours (Kriegsmann and Warth, 2016).

Mitotic index is generally calculated as the number of cells between prophase and telophase divided by the total number of cells (Kim et al., 2007). However, as seen in figure 3.5B, the staining conditions are such that it is not always obvious what constitutes a cell in prophase or telophase. This, along with the subjective nature of identifying mitotic figures likely means that cells early in prophase and very late in telophase may be missed, possibly underestimating the reported mitotic indexes. However, consistent counting means that any underestimates will likely apply across all cell lines and conditions, and thus comparisons between these likely still stand. Nevertheless, this experiment could have been improved by

staining for a target expressed very soon after G2, a criterion fulfilled by Phosphohistone H3. Incidentally, World Health Organisation (WHO) grading classifications which rely on mitotic indexes recommend using phosphohistone H3 as a proliferation marker, which has been shown to yield greater sensitivity than the Ki67 labelling index, another common proliferation index (Kim et al., 2007).

KIFC1 Depletion Reduces Proliferation

To understand whether the observed decrease in mitotic index upon KIFC1 depletion would manifest long term, an MTT assay was carried out. As shown in figure 3.7, KIFC1 knockdown reduced cell proliferation in all three cell lines after five days. Mel270 showed a much greater reduction in proliferation upon KIFC1 knockdown compared to Omm2.3 and Omm2.5, which showed modest decreases in proliferation. Nevertheless, the observation that KIFC1 depletion reduces proliferation has been reported in other cancer cell lines. For example, similar proliferation assays have shown that KIFC1 depletion caused an approximately 80% decrease in proliferation in breast cancer cells (Li et al., 2015), while also reducing viability in gastric cancer spheres (Oue et al., 2016) (Zhang et al., 2016a), lung cancer cells (Liu et al., 2016), prostate cancer spheres (Sekino et al., 2017) and a variety of other cancer types (Imai et al., 2017), (Li et al., 2018), (Patel et al., 2018), (Fu et al., 2018), (Han et al., 2019).

The results observed in this experiment were unexpected, as Mel270 had the lowest centrosome amplification and incidence of multipolar mitosis but had the highest reduction in proliferation. As previously discussed, the negative effect of KIFC1 depletion on proliferation does not seem to correlate with the extent of centrosome amplification and multipolar mitosis. This further lends credence to the theory that KIFC1 has pro-mitogenic effects in uveal melanoma cells, most strikingly in Mel270.

The MTT assay was run in 96 well plates to assess the fold-change in the number of cells present after one, three and five days after KIFC1 knockdown, compared to negative control and mock-treated cells, the latter of which was arbitrarily set as 100% proliferation. The assay works by assessing cell metabolic activity, which acts as a proxy to reflect the number of cells present. The assay involves incubating cells with MTT, a tetrazolium dye, which is reduced to insoluble formazan crystals inside, and sometimes outside the cell. This means that different

cell types cannot be directly compared due to differing metabolic activities. This effect was visually obvious at the endpoint of the MTT assay, as Mel270 cells would show relatively little purple coloration at the end of the assay, whereas the Omm cells showed strong purple coloration. Simple visual analysis by light microscopy also showed the presence of much larger crystals in the Omm cells. Nevertheless, this was not an issue in this study as relative changes within cell type were assessed and then compared between cell lines, rather than raw absorbance readings. The MTT-reducing function is often credited to NADH-dependent oxidoreductase enzymes in the mitochondria, but it is also actually reduced in endosome/lysosome compartment. The fact that MTT is endocytosed, reduced and then exocytosed to the cell surface, where it forms crystals, still makes this assay valid as it measures endocytosis, a fundamental feature of living cells (Liu et al., 1997). Nevertheless, care must be taken to avoid using reducing agents or compounds that inhibit endocytosis and uncouple the electron transport chain. In this case, siRNAs were used rather than small molecule inhibitors, which means off target effects on these functions were relatively unlikely.

Nevertheless, this experiment could have been improved. One procedural limitation could be that to solubilise the formazan crystals and kill the cells at the end of the assay, slightly acidified isopropanol was added to the wells and mixed well. This also converts the pH-sensitive phenol red to yellow, avoiding interference at 590 nm, but the process requires rigorous mixing to fully solubilise the formazan and may require microscopy to verify that the crystals are fully dissolved. During this process, evaporation of the isopropanol and subsequent concentration of the formazan may skew results. An alternative could be to use MTS, another tetrazolium salt which does not require solubilisation and so can be directly analysed after incubation. Furthermore, because the MTT assay measures metabolic activity, the assay would be most useful when cells are at their most active in the growth phase and not at low confluence or very high confluence and thus approaching senescence. Although the initial cell number in this experiment was optimised by running the experiment multiple times loading 400, 1000, 2500, 5000, 7500 and 10,000 cells, if I were to repeat this experiment, I would begin by performing a growth curve assay to identify a suitable initial concentration of cells which would reach log phase by five days. Furthermore, the variation between the results for Mel270 mock and Mel270 negative control cells, which in theory

would be expected to be quite small, may have been attenuated by carrying out independent repeats of the assay. Repeats were attempted, but the experiments failed and were not attempted again due to time constraints.

KIFC1 Depletion Reduces Clonogenicity

Considering the results of the MTT assay, a clonogenic assay was employed to verify whether such effects would translate long term and affect clonogenicity. The clonogenic assay tested whether every plated cell retained the capacity to undergo indefinite mitosis to produce colonies over 21 days after KIFC1 knockdown. As shown in figure 3.8, Mel270 cells were most negatively affected by treatment with KIFC1 4 siRNA and KIFC1 5 siRNA with 88% and 93% reductions in clonogenicity, which were significantly different to negative control cells at $p<0.0001$. This means that without KIFC1, only 12% and 7% of cells retained the ability to undergo indefinite mitosis compared to cells treated with negative control siRNA. It has been reported that KIFC1 affects clonogenicity in many cancer types, for example, KIFC1 overexpression in HCC cell lines increased the number of clones produced compared to mock cell lines, whereas KIFC1 knockdown reduced the number of clones produced (Han et al., 2019). However, the fall in clonogenicity of Omm2.3 and Omm2.5 upon KIFC1 depletion was nowhere near as drastic compared to the negative control siRNA treated cells. The lack of significant difference between the negative controls and the KIFC1 siRNA treated cells meant that the clonogenicity of these cells may not be sensitive to KIFC1 knockdown.

One weakness of the methodology of this experiment is that KIFC1 siRNA was only applied on day 0 of the experiment. The fact that Omm2.3 and Omm2.5 cells have a higher metabolism that Mel270 cells, as evidenced by the MTT assays, may mean that upon subsequent divisions, the KIFC1 siRNA molecules were diluted to an ineffective concentration sooner than in Mel270, and so had more time to recover their populations. If this experiment were to be repeated, it could be done so that KIFC1 siRNA is reapplied regularly throughout the 21 days.

When considering the results of the MTT assays, the clonogenic assays and the changes in mitotic index, the fact that the changes in cell proliferation upon KIFC1 knockdown in Mel270 compared to Omm2.3 and Omm2.5 do not correlate with the extent of centrosome amplification and multipolar mitosis indicates that KIFC1 seems to have an important role in

proliferation in uveal melanoma cells. This effect is much more pronounced in Mel270 cells, which were derived from a primary uveal melanoma tumour, whereas Omm2.3 and Omm2.5 were derived from independent liver metastases originating from the Mel270 tumour (Jager et al., 2016). This likely means that the metastatic cells carry more adaptations to pursue a more aggressive proliferation, shown by the mitotic indexes in mock conditions (Figure 3.6). This could be due to mutations in alternative proliferation pathways making KIFC1-mediated proliferation redundant to an extent.

Recent evidence shows that KIFC1 has a role in cell proliferation. *In silico* studies predicted that KIFC1 interacts with a variety of proteins involved in progressing the cell cycle, assembling the spindle or regulating the spindle assembly checkpoint in ovarian cancer cells (Pawar et al., 2014) (Mittal et al., 2016). Furthermore, KIFC1 overexpression reduced doubling times in breast cancer cells (Pannu et al., 2015b), while RCC cells treated with KIFC1 produced smaller tumours when transplanted in mice compared to control RCC cells (Li et al., 2018). Proof that KIFC1 had centrosome clustering-independent roles in the proliferation of cancer cells was first published in 2015 (Pannu et al., 2015b), but since then, a concrete mechanism has not been proposed. Nevertheless, observations of potential networks of protein interactions have been reported.

One example of such a network of interactions is that overexpression of KIFC1 induced expression of PI3K and AKT (Li et al., 2018), while knockdown of KIFC1 reduces expression of phosphorylated AKT and PI3K (Fu et al., 2018). Furthermore, KIFC1 increased the expression of HIF1α, Aurora B kinase, although their expression was not reduced upon KIFC1 knockdown (Pannu et al., 2015b). The fact that KIFC1 knockdown did not decrease expression of these proteins implies that KIFC1 is not normally a regulator of such proliferative pathways, which is supported by the fact that KIFC1 is dispensable for viability in normal cells (Godinho et al., 2009). This led Pannu *et al.* to hypothesise that KIFC1 is part of an oncogenic axis with HIF1α and Aurora B kinase which thrusts cells into “overdrive” by employing an alternative function. Interestingly, this was observed in HeLa cells with only 3% centrosome amplification, which confirms that such functions are centrosome clustering-independent (Pannu et al., 2015b).

Furthermore, KIFC1 overexpression upregulated survivin signalling but its knockdown did not decrease survivin signalling. KIFC1 also coprecipitated with survivin, proving an interaction between the two. Furthermore, immunoblotting revealed that KIFC1 overexpression reduced polyubiquitination signals at the survivin band, despite the increased survivin expression, strongly indicating that high levels of KIFC1 bind to and protect survivin from ubiquitination-dependent degradation (Pannu et al., 2015b). This is important as survivin is widely expressed in cancers and has a dual role as both an Inhibitor of Apoptosis (IAP). First, it binds and inactivates "executioner" caspases (Tamm et al., 1998). It also takes part in the cell cycle as one of the four proteins in the Chromosomal Passenger Complex (CPC), one of the most important master regulators of mitosis (Carmena et al., 2012). Incidentally, survivin increases the expression and activity of Aurora B Kinase (Chen et al., 2003), which is also part of the CPC (Carmena et al., 2012), while HIF1α upregulates expression of Survivin (Wu et al., 2010). The fact that KIFC1 overexpression increases the expression of Aurora B Kinase, HIF1α and Survivin, and even shares common E2F upstream transcription factors (Jiang et al., 2004) raises the possibility that KIFC1 may be involved in upregulation of the CPC.

KIFC1 Depletion Increases Apoptosis in Mel270 Cells

To understand how KIFC1 knockdown mediated the reduction in proliferation in uveal melanoma cells, the rate of apoptosis was observed. This was done by immunostaining for the expression of cleaved capsase-3 for observation by immunofluorescence. As shown in figure 3.10, KIFC1 knockdown increased the percentage of cells expressing cleaved caspase-3 in all three cell lines. This means that KIFC1 knockdown increased apoptosis in all three cell lines as caspase-3 is an executioner caspase zymogen, whose cleavage and subsequent activation in cells induces apoptosis (McIlwain et al., 2013). Omm2.3 and Omm2.5 showed more than two-fold increases in the rate of apoptosis, while Mel270 showed 50% and 70% increases in the rate of apoptosis upon treatment with KIFC1 4 and KIFC1 5 siRNA when compared to mock cells. However, even though Mel270 had the smallest percentage increase, the fact that Mel270 had a more than 10-fold basal apoptotic rate compared to Omm2.3 and Omm2.5 meant that its relatively small increase in apoptosis upon KIFC1 knockdown brought the frequency up to above 10% of all cells. On the other hand, in Omm2.3 and Omm2.5, the frequency of apoptosis only rose to around 2% of all cells. This means that

Mel270 is far more likely to show an effect in cell growth upon KIFC1 knockdown. Furthermore, questions do remain regarding how much of an effect 12% apoptosis would have on a real tumour *in vivo* upon KIFC1 inhibition.

It is also important to note that the increases in apoptosis upon KIFC1 knockdown were not replicated in the sub G1 population of cells upon flow cytometry, which is one of the reasons why this experiment should be repeated.

One aspect of this experiment that could have been improved was that the preparation of immunofluorescent samples included growing cells on coverslips and then washing the coverslips before fixing the cells. Even though this was done as carefully as possible to avoid washing cells away, apoptotic cells are known to shrivel up and become loose or even detach from the growing surface. This meant that the numbers recorded were possible underestimates. Nevertheless, the consistent processing and counting technique likely meant that such an underestimate was carried over to all the conditions and cell lines, and so comparisons between conditions were unlikely to change.

It has been shown that cancer cells with KIFC1 depletion expressed more caspase-3 after UV-C irradiation compared to control cells and cancer cells with KIFC1 overexpression (Pannu et al., 2015b). Furthermore, KIFC1 knockdown was shown decrease Bcl-2 expression and increase proapoptotic Bax, p53 (Fu et al., 2018) and c-PARP expression (Sekino et al., 2019). The enhanced survival effects of KIFC1 are likely to be mediated by survivin, which was found to co-precipitate with KIFC1, implying an interaction between the two. Furthermore, KIFC1 overexpression reduced the poly-ubiquitination signals associated with survivin, implying that KIFC1 protected survivin from APC-C-mediated degradation (Pannu et al., 2015b), allowing cancer cells to better resist apoptosis signalling. However, it is worth noting that the nature of the polyubiquitin signals were not characterised, and so it cannot be said with certainty that the reduced polyubiquitin signal was the cause of reduced survivin degradation.

It is known that Omm2.3 and Omm2.5 overexpress survivin compared to Mel270 (Li et al., 2006), which may explain the increased overall levels of apoptosis in Mel270. However, it has also been reported that KIFC1 knockdown does not decrease levels of survivin in HeLa cells (Pannu et al., 2015b), which does not explain the increases in apoptosis upon KIFC1 knockdown in uveal melanoma cell lines. To explore whether KIFC1 knockdown decreased

survivin expression in uveal melanoma cell lines, lysates of Mel270, Omm2.3 and Omm2.5 with and without KIFC1 knockdown were immunoblotted for survivin, albeit unsuccessfully, while low antibody stocks and time constraints prevented optimisation of the staining process.

KIFC1 Depletion Does Not Affect Cell Cycle Distribution

Although KIFC1 depletion had been shown to decrease proliferation and clonogenicity, analysis of DNA content to determine cell cycle distribution in Mel270, Omm2.3 and Omm2.5 showed no changes upon KIFC1 depletion (Figure 3.9). Although unexpected, this has been reported before in HCC cells where KIFC1 depletion reduced proliferation and increased apoptosis but did not change cell cycle distribution (Fu et al., 2018). This may imply that KIFC1 has cell cycle-independent effects in uveal melanoma cell lines which still affect proliferation and clonogenicity. Furthermore, the lack of significant change in the sub-G1 region, which implies little change in apoptotic cells, may be due to gating out of cell debris produced apoptosis when setting parameters for data collection. Thus, repeats would need to be conducted before conclusions are to be drawn from this experiment.

3.2.3. Conclusion

Taken together, it seems that KIFC1 has many roles beyond the original theory of providing protection against multipolar mitosis-induced apoptosis or arrest for cancer cells with amplified centrosomes, while providing no significant benefit to those without. Instead, recent research initially alluded to by Kleylein-Sohn *et al.* in 2012, expanded upon by Pannu *et al.* in 2015 and now further evidenced by the work in this thesis shows that KIFC1 depletion inhibits cell proliferation and induces apoptosis in a manner largely independent of centrosome amplification status. There is now a good base of evidence that KIFC1 depletion does have cancer-specific effects on cell growth. This suggests that KIFC1 may take part in oncogenic signalling networks yet to be uncovered and is a more suitable cancer-specific therapeutic target than originally thought, as it may be effective regardless of centrosome amplification status. However, repeats of many experiments are still required for the conclusions to be accepted and questions still remain regarding whether the effects observed in uveal melanoma cells are strong enough to produce acceptable clinical responses.

4. Towards a KIFC1 PROTAC: Synthesis and *In-Vitro* Testing of CW069 Analogues

4.1. Results II

4.1.1. CW069 Synthesis

The results presented in section 3.1.1. showed that KIFC1 is a viable therapeutic target in treating uveal melanoma, especially in the primary tumour. These results also show that KIFC1, previously thought to be dispensible in cells with little or no centrosome amplification, can actually be essential in cells with centrosome amplification, thus broadening the range of tumours in which it could be targetted.

KIFC1 inhibitors do exist, but they tend to be effective only at higher doses and are thought to suffer from poor specificity. Two such inhibitors, CW069 and AZ82, induce cell death in Mel270, Omm2.3 and Omm2.5 (Andrew Fielding, unpublished results). To combat the low specificity and high dosages required, the inhibitor could be used as part of a proteolysis-targeting chimaera, known as a PROTAC.

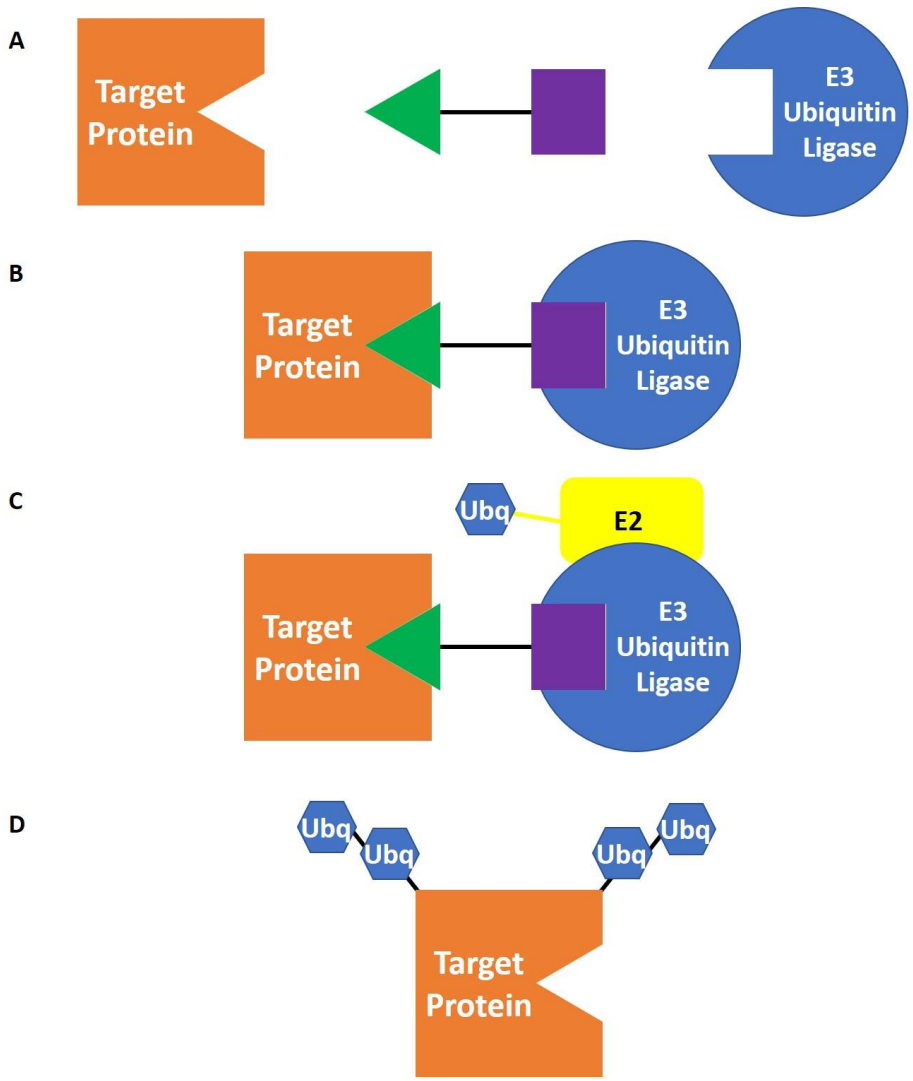

Figure 4.1. A Crude Representation of PROTAC Action. *A) PROTACs are bifunctional and so incorporate recruiters for both the target protein and an E3 ubiquitin ligase. B) By binding both the target protein and the E3 ubiquitin ligase to form a ternary complex, the PROTAC brings the two proteins in to proximity with each other. Novel intermolecular protein interactions between the two proteins can further stabilise the complex. C) An E2 ubiquitin-conjugating enzyme binds to the E3 ubiquitin ligase and delivers activated ubiquitin molecules. D) The target protein is now polyubiquitinated and ready for degradation by the 26S proteasome.*

PROTACs are bifunctional molecules that link together a ubiquitin E3 ligase recruiter and a target inhibitor (Schneekloth et al., 2008). These molecules form a ternary complex between the E3 ligase and the target, causing the ubiquitination and degradation of the latter (Figure 4.1). To accomplish this a flexible linker must be substituted on to the inhibitor in an appropriate location so as to not disrupt binding to the target.

In this study, CW069 was chosen as the inhibitor of choice to build a PROTAC around. Initially, CW069 would be synthesised and then a series of different analogues of CW069 would be synthesised to explore options for PROTAC design. These analogues would contain different functional groups and tested in a structure-activity relationship assay using KIFC1 motor protein to test which alterations to CW069 could be used to build a PROTAC from while still allowing effective binding to KIFC1.

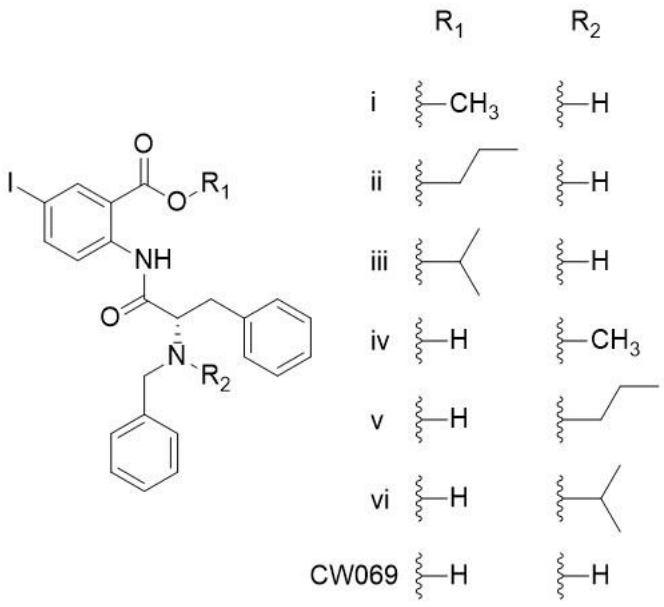

Figure 4.2. Initial Plan for CW069 Analogues. *A schematic to show the various analogues of CW069 proposed to ascertain which functional groups were dispensible while still maintaining KIFC1 binding capabilities.*

The synthesis of CW069 had already been published (Watts et al., 2013) and so the same reaction scheme was employed (Figure 4.3).

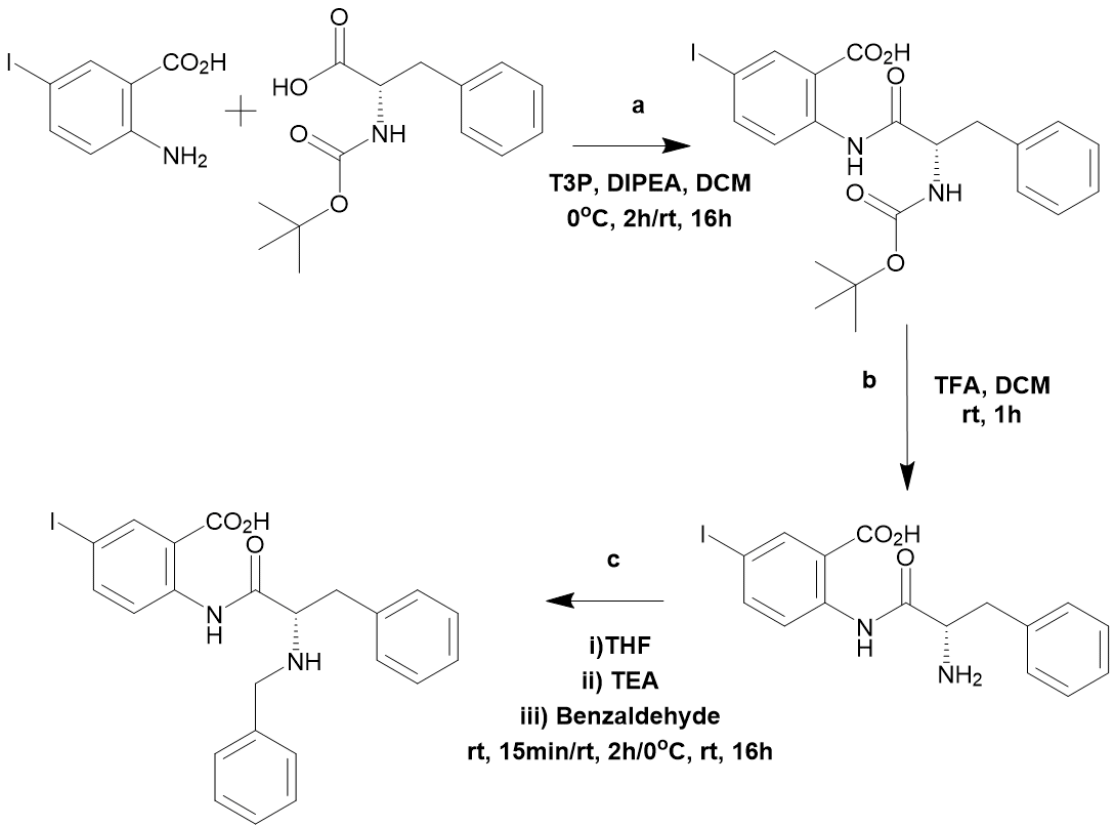

Figure 4.3. Initial Synthetic Pathway for CW069. *A three-step process for the production of KIFC1 inhibitor CW069 described by Watts et al., 2013 starting with the reaction* ***a****, an amide coupling of 2-Amino-5-iodobenzoic acid and N-Boc-phenylalanine, followed by* ***b****, a Boc deprotection reaction using TFA and concluded with a reductive amination using benzaldehyde.*

Reaction **a,** an amide coupling reaction, was published to have been completed with a 1:1:2 ratio between reactants and DIPEA, the base, and a slight excess of T3P, the coupling agent, relative to N-Boc-phenylalanine. However, after two attempts, NMR data showed that the reaction had not worked. To optimise conditions for the reaction, ratios were increased to 1:2:6:2.5 between 2-Amino-5-iodobenzoic acid, N-Boc-phenylalanine, DIPEA and T3P, to no avail.

Thin layer chromatography indicated that N-Boc-phenylalanine may have coupled to T3P, but not reacted any further with 2-Amino-5-iodobenzoic acid, so HATU was used as an alternative coupling agent, but again, NMR data showed that the reaction did not proceed to the desired product.

One possible reason for the lack of reactivity may be insufficient electronegativity of the nitrogen atom in amine group (-NH_2) of 2-Amino-5-iodobenzoic acid, leading it to lack the sufficient nucleophilicity to react with the activated N-Boc-phenylalanine-derived intermediate. To force the reaction to completion, 2-Amino-5-iodobenzoic acid was switched out to its ethylester, Ethyl-2-Amino-5-iodobenzoate. The logic for this decision was that the ester group is less electron withdrawing than a carboxylic acid group, leaving the amine group more nucleophilic and thus more likely to react with the activated N-Boc-phenylalanine-derived intermediate.

This reaction was carried out using both HATU and T3P separately as coupling agents, but NMR data showed that this reaction had also failed. Again, thin layer chromatography indicated that the N-Boc-phenylalanine had coupled with the coupling agent in each case, but had not reacted any further.

At this stage, the decision was made to shift away from this reaction scheme. Another synthetic pathway for CW069 had been published (Watts et al., 2013), labelled by the authors as the “optimised pathway”, which was adopted. However, even though this reaction scheme was reported to have produced higher yields, it contained more steps and the specific reaction conditions and purifications were not reported, so these required optimisations at each step.

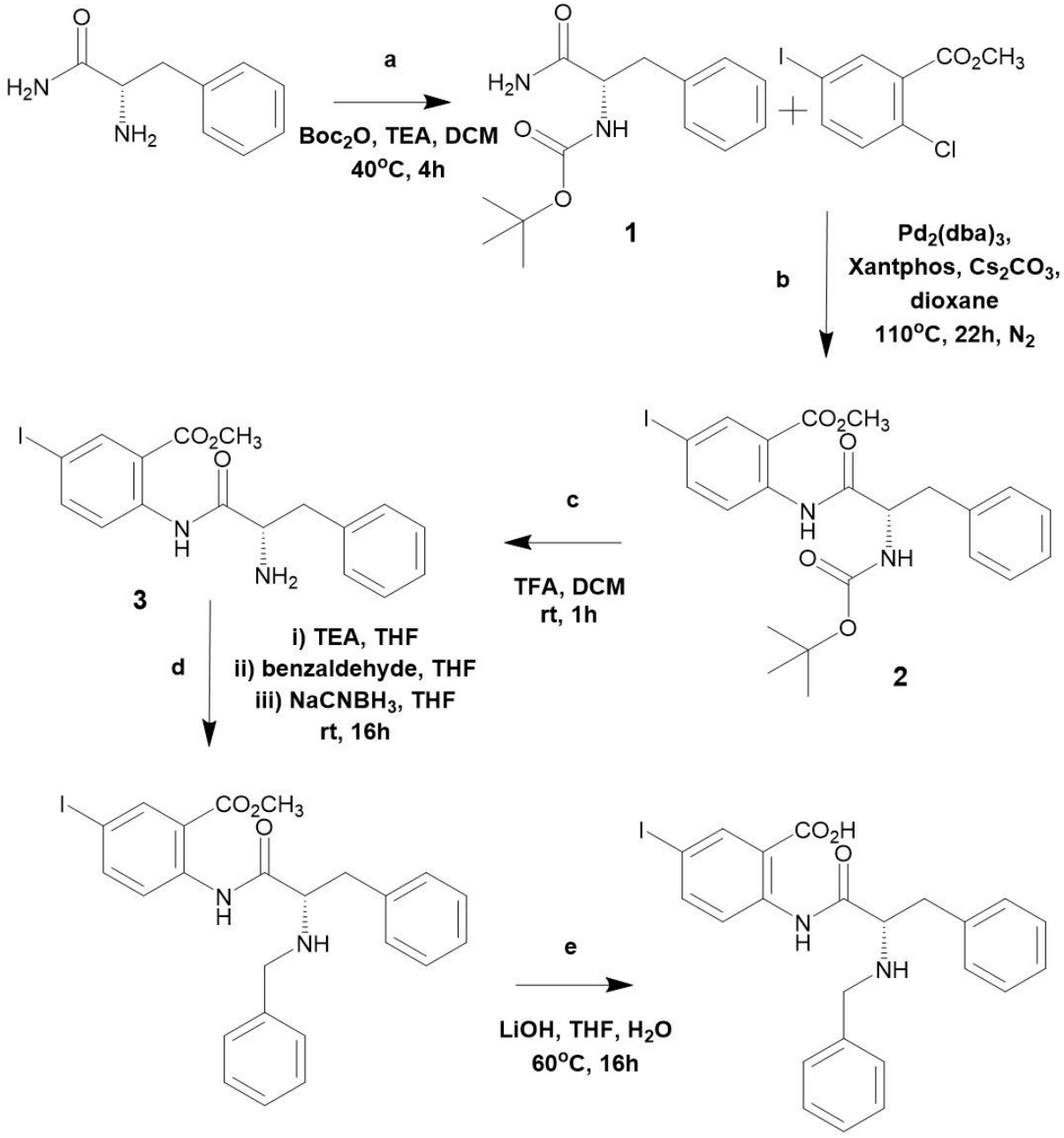

Figure 4.4. Alternative Synthetic Pathway for CW069. *A five-step process for the production of KIFC1 inhibitor CW069 described by Watts et al. (2013), starting with the reaction* ***a****, a Boc protection of phenylalaninamide with di-tert butyl dicarbonate to produce compound 1, followed by* ***b****, a Buchwald-Hartwig coupling reaction with methyl-2-chloro-5-iodobenzoate to produce compound 2. Reaction* ***c****, a Boc deprotection using TFA was carried out to produce compound 3 and then followed by reaction* ***d****, a reductive amination with benzaldehyde and then reaction* ***e****, an ester hydrolysis with LiOH and* H_2O.

Reaction **a**, shown in figure 4.4, produced a 91% yield, while reaction **b**, a Buchwald-Hartwig coupling reaction, produced only a 2% yield along with an unexpected yellow gum at the bottom of the flask. This reaction required a palladium catayst and Cs_2CO_3 base, both of which are highly sensitive to oxygen and atmospheric levels of water. Even though the reaction was

carried out in oven-dried glassware in a nitrogen atmosphere, it was suspected that the solvent, dioxane, may have contained tiny amounts of water which oxidised the catalyst and base. Reapeating the reaction with anhydrous dioxane gave a 24% yield, which still fell short of the published yield of 90%. In the work done by Watts *et al*., the catalyst and ligand were required at molar equivalence with the reactants to give their observed yield (Watts et al., 2013). As such a ratio would suggest that the reaction was not actually catalytic in their hands, we concluded that greater amounts of catalyst and ligand may be required. An increased concentration of palladium catalyst and its Xantphos ligand from 2% each to 10% molar concentration gave a 100% yield. Subsequent scale-ups of the reaction with higher amounts of reactants and 10% and 20% catalyst/ligand concentrations gave 31% and 16% yields respectively due to loss of compound 2 during purification. It was found that significantly less compound would be lost if loaded into the silica column dissolved in DCM before purification with 10 % ethyl acetate in hexane. Nevertheless, enough of the compound had been produced to proceed to reaction **c**, a Boc-deprotection reaction that consistently produced 100% yields.

Reaction **d**, a reductive amination reaction with benzaldehyde was carried out and thin layer chromatography and NMR data indicated that the reaction had failed. It was expected that the amine group would react with the benzaldehyde by nucleophilic attack, but this had not occurred. An alternative method would be to activate the benzaldehyde by addition of acetic acid, which would allow the amine to undertake a nucleophilic attack. Again, this reaction did not work.

Up until this point, the direct product of reaction **c** was being used. Being cleaved by TFA left the amine as a TFA salt, which merited the addition of triethylamine, a base, at the beginning of the reaction to basify compound 3 to a free amine. It was thought that basifying the amine before the reaction to leave a free amine group would eliminate the need for a base in the reaction and so would allow the acidic conditions to activate the benzaldehyde. Nevertheless, the reaction also failed. The same reaction was then tried with formic acid, a stronger acid, but still did not work.

Another possibility was that the benzaldehyde and amine were reacting as expected to form an imine, but the imine was not being reduced to fully complete the reaction. Imines are extremely unstable and so would deompose to their original reactants before analysis with

thin layer chromatography. Therefore, the reducing agent $NaCNBH_3$ was switched out to $NaBH_4$, a stronger reducing agent, to increase the likelihood of a successful final reduction. Nevertheless, the reaction failed. At this stage, time constraints dictated that work on analogues was to begin, especially as the aim was to generate CW069 analogues rather than CW069 itself.

4.1.2. CW069 Analogue Synthesis

In silico predictions of how CW069 bound to KIFC1 stated that KIFC1 interacted with the amino group, carboxylate group and exposed benzyl group of CW069 (Watts et al., 2013). Analogues were therefore made to alter or eliminate these groups (Figure 4.5). Furthermore, the suitability of building viable PROTACS directly onto the amine group was tested by producing compound **4**, which has a PROTAC linker region bound directly to the amine of the CW069 precursor.

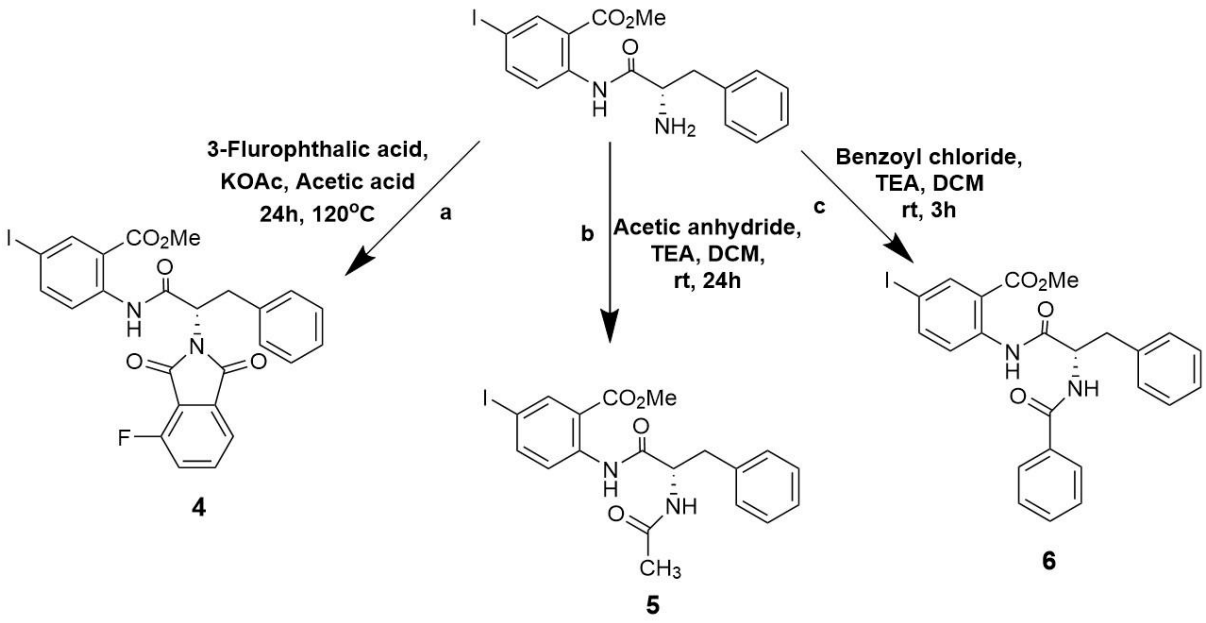

Figure 4.5. Initial Synthetic Pathway for CW069. *A scheme showing the three analogues of the CW069 precursor. Reaction **a** was a phthalimide protection synthesis to produce compound **4**, a phthalimide from an amine and phthalate. Reaction **b** was a nucleophilic addition-elimination reaction with acetic anhydride to form compound **5**, an acetamide, while reaction **c** was also a nucleophilic addition-elimination reaction to form compound **5**, a benzamide.*

Reaction **a**, a phthalimide protection worked well, producing a phthalimide with a 30% yield. Furthermore, reaction **b**, an Eschweiler-Clarke reductive methylation also worked, giving a yield of 50%, while reaction **c**, a nucleophilic addition-elimination reaction gave a yield of 67%.

4.1.3. Structure-Activity Relationship Kinesin Assay

For the CW069 analogues to be suitable for building a PROTAC around, they would need to be able to bind to KIFC1 and inhibit its ATPase activity. To test this, the KIFC1 motor domain (His_6-KIFC1305–673; provided by Morgan Gadd) was to be tested in a biochemical assay with the analogues and microtubulues to test the amount of ATP hydrolysed, using the HTS kinesin ATPase Endpoint Assay Biochem Kit (Cytoskeleton).

Before testing the analogues, the KIFC1 motor domain was to be verified as functional by the production of inorganic phosphate. Between 0.16 µg and 0.8 µg of KIFC1 motor protein was tested, along with KIFC1 incubated without mictrotubules, acting as negative controls. Similarly, a control kinesin motor protein was loaded with and without microtubules.

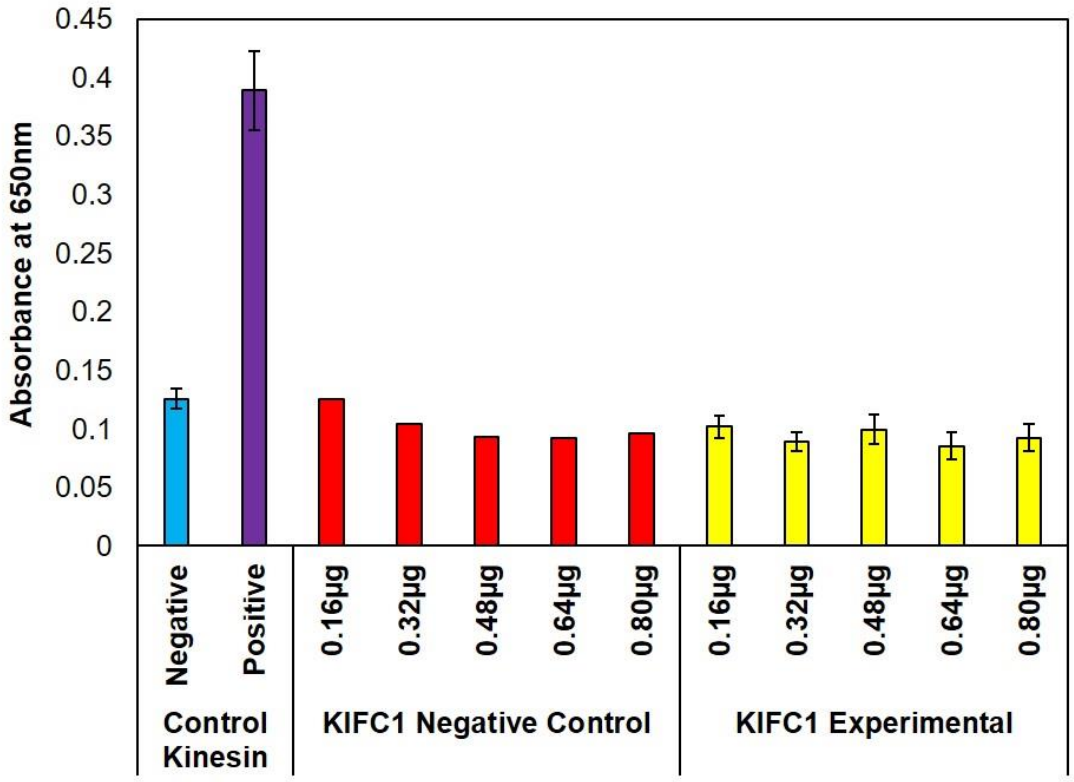

Figure 4.6. KIFC1 ATPase Test Assay 1. *A graph showing the absorbance at 650 nm after a kinesin ATPase assay. Differing amounts of KIFC1 were loaded with ATP into wells and incubated with (KIFC1 Experimental) or without (KIFC1 Negative Control) preformed microtubules. The activity of the KIFC1 assay was compared to 0.2 µg of Control Kinesin incubated with ATP with (Positive Control) or without (Negative Control). Error bars plotted as one standard deviation.*

The data presented in figure 4.6 shows that the KIFC1 motor protein either did not work or had undetectable activity, as it showed no more absorbance than the control kinesin negative control and KIFC1 negative controls, implying no more ATP hydrolysis. One possibility was that not all of the protein in the sample was KIFC1, or that only part of the KIFC1 in the sample was active. Thus, the protein was concentrated centricon.

The assay was rerun, but with wells loaded with between 0.9 µg and 4.5 µg of KIFC1.

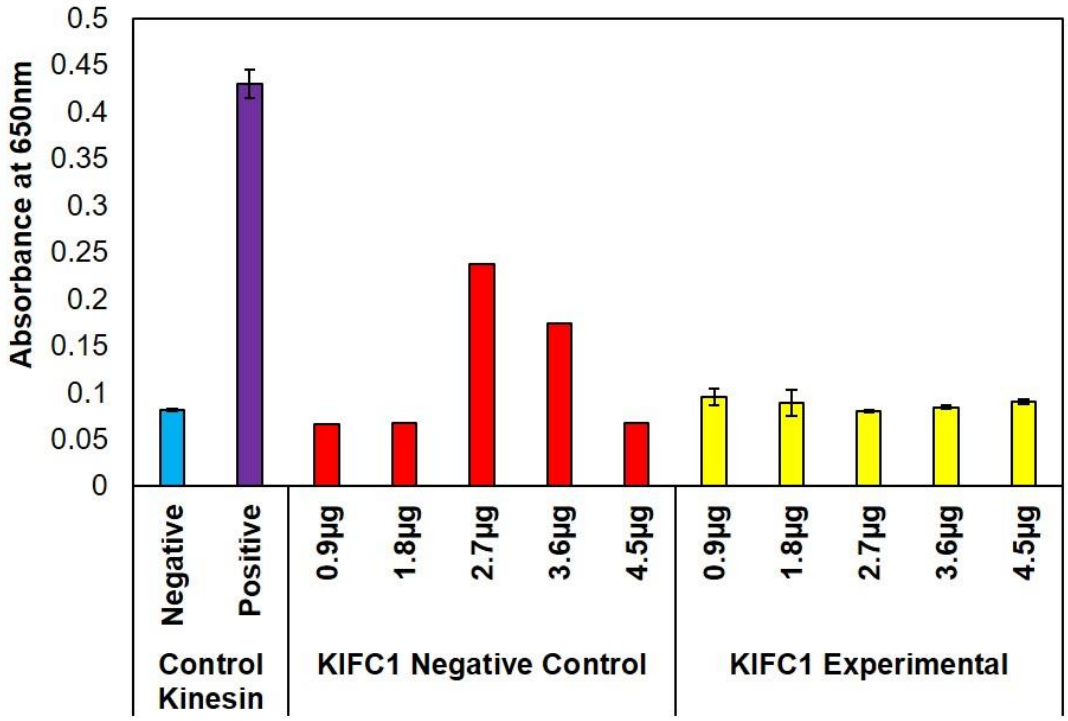

Figure 4.7. KIFC1 ATPase Test Assay 2. *A graph showing the absorbance at 650 nm after a kinesin ATPase assay. Differing amounts of KIFC1 was loaded with ATP into wells and incubated with (KIFC1 Experimental) or without (KIFC1 Negative Control) preformed microtubules. The activity of the KIFC1 assay was compared to 0.2 µg of Control Kinesin incubated with ATP with (Positive Control) or without (Negative Control). Error bars plotted as 1 standard deviation.*

As seen in figure 4.7, higher concentrations of KIFC1 hydrolysed no more ATP than the negative controls. It was surmised that KIFC1 may possibly work at a different pH than the pH 6.7 solutions used in the kit. Therefore, seven different buffers ranging between pH 6.5 to pH 7.1 were made up to test whether the activity of KIFC1 would change at different pH conditions. Furthermore, the lack of KIFC1 activity might have been due to the fact that the concentrated KIFC1 solution was estimated to contain approximately 150 mM of salt, as

opposed to the 20 mM in the buffer provided by the kit manufacturer. Therefore, KIFC1 was dialysed using dialysis tubing in an identical buffer, but with a 10 mM concentration of salt.

Unfortunately, complete sample loss during dialysis prevented these parameters from being explored further, and time constraints precluded the possibility of attempting the assays following expression and purification of a new batch of KIFC1 protein.

4.2. Discussion II

CW069 was chosen as the KIFC1 inhibitor to build a PROTAC around. This was because, at least in theory, it had the shortest synthetic pathway with simpler and safer chemical reactions of all the KIFC1 inhibitors. Furthermore, the relative inefficiencies of CW069 in the form of high dosage requirement (Watts et al., 2013) and suspected off target effects (Yukawa et al., 2018) meant that it would benefit the most from being assembled into a PROTAC.

PROTACs consist of a target binder linked to an E3 ubiquitin ligase recruiter via a linker molecule. In this case, the target would be KIFC1 and the target binder would be CW069. However, the linker would attach to (and thus alter) a functional group on CW069. Therefore, the purpose of producing CW069 analogues was to alter various functional groups to understand which groups were crucial to the binding of KIFC1. The effect of these changes would be assessed by a Structure-Activity Relationship (SAR) assay, and the functional groups to which changes were best tolerated would then be selected to attach a linker to.

In silico predictions of how CW069 bound to KIFC1 indicated that the carboxylate group of CW069 interacted with the guanidinium group of Arg521 of KIFC1, while the exposed phenyl group of CW069 interacts with the alkyl side chain of Arg521. Furthermore, the amine and carboxylic acid groups of CW069 were thought to interact with the respective backbone amide and carbonyl groups of Gly423 and Leu517. In particular, the interactions with Arg521 were predicted to be critical for the reported selectivity of CW069 to KIFC1 (Watts et al., 2013).

The implied lack of interactions between KIFC1 and the exposed benzylamine group of CW069 meant that this group may be dispensable in binding KIFC1, and so could be used to attach a linker. To determine whether this is the case, compound **5** was produced where the benzyl group was replaced with an acetamide group (Figure 4.8). This way it could be tested to see if the aromatic ring was dispensable.

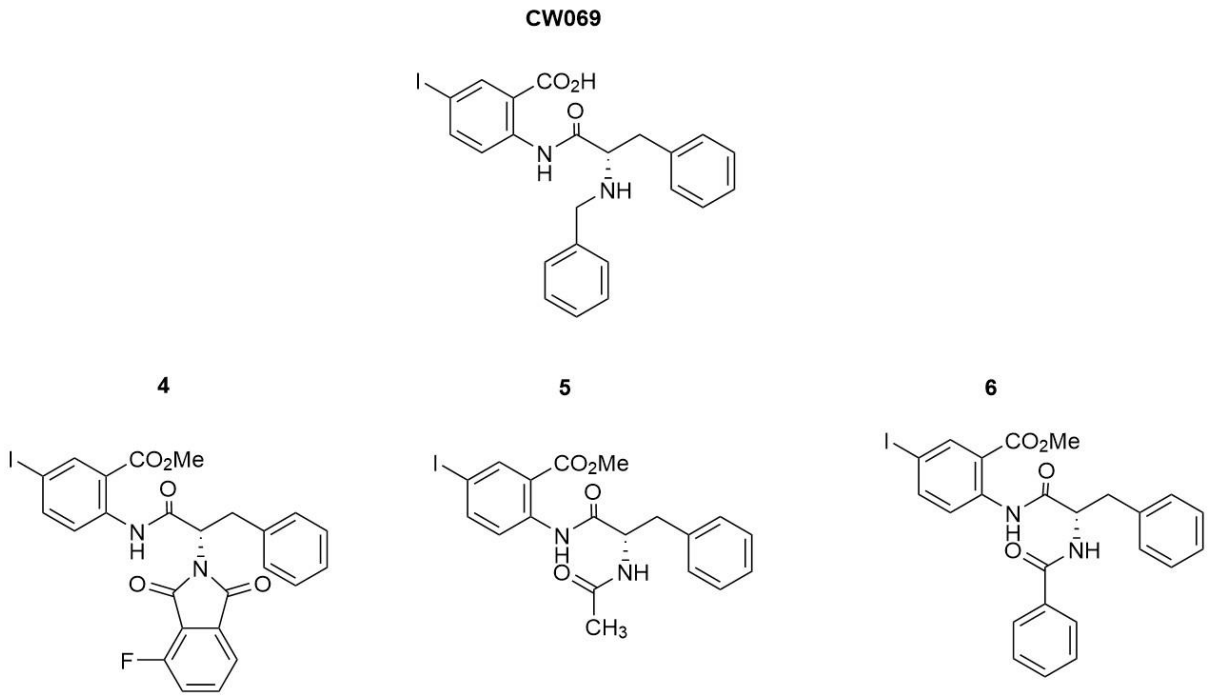

Figure 4.8. CW069 and CW069 Analogues. *A diagram to compare the differences in structures between CW069 and analogues synthesised. Compound **4** was formed so that the fluoride group would be amenable to nucleophilic aromatic substitution. Compound **5** was formed to test whether the benzyl ring was required for KIFC1 binding, while compound **6** was formed to see whether the molecule could tolerate a benzamide substitution in the place of benzylamine, and still bind KIFC1. All three analogues also had a methyl ester instead of the carboxylic of CW069, which, if required, could easily be removed to see if the carboxylic acid group was important for KIFC1 binding.*

As explained in the results section, CW069 was not synthesised, rather analogues were made from a common upstream molecule. These molecules were produced to mimic CW069, but with important alterations that would make the attachment of linker vastly easier.

For example, compound **6** is very similar to CW069, the only difference being that CW069 has a benzyl group attached to the amine to form a benzylamine, whereas compound **6** has a benzoyl group attached to the amine, forming a benzamide. This is important because amide coupling reactions are commonly used to attach linkers to ligands (Figure 4.9).

Similarly, analogue **a** was produced to eliminate the amine group and produce a phthalimide. This molecule preserves all aspects of CW069, but as a phthalimide it engineers even greater conformational rigidity via the imide attachments to the phenyl ring. If this molecule was found to be suitable, it would relatively easy to attach a linker using nucleophilic aromatic

substitution via the fluorine group, without the possibility for undesired side reactions (Figure 4.9).

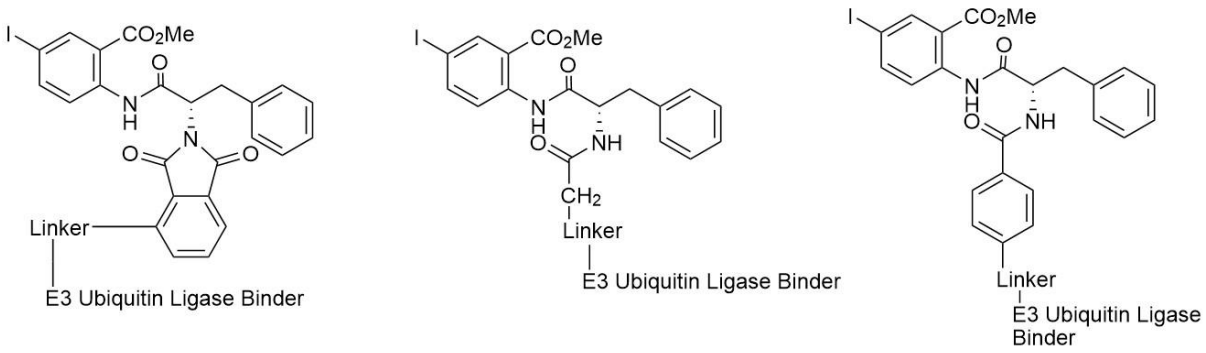

Figure 4.9. Proposed Structure of PROTACs Derived from CW069 Analogues. *A diagram to show how the three analogues would look as PROTAC molecules, assuming they had been found to suitably bind to KIFC1. Between the KIFC1 binder (analogue) and the E3 ubiquitin ligase binder would be a linker, which could be as simple as a hydrocarbon chain. Similarly, any variety of E3 ubiquitin ligase binder could be used.*

The region where a carboxylic acid group was situated in CW069 was left as a methyl ester group in the analogues. This was left as a protecting group to stop unwanted side reactions in the formation of the analogues. To cleave the ester to a carboxylic acid would simply require refluxing with an acid (Watts et al., 2013) to hydrolyse the molecule into CW069 and methanol. Comparisons between carboxylic acids and esters would also prove whether the carboxylic acid was definitively required for binding to KIFC1.

To test the activity of the CW069 analogues on KIFC1, an ATPase activity assay was undertaken. The assay would measure the amount of ATP hydrolysed by a KIFC1 motor domain (His_6-KIFC1305–673; provided by Morgan Gadd). However, before testing the analogues, verification of the ATPase activity of the KIFC1 motor domain revealed that it did not work. Concentrations of KIFC1 comparable to the control kinesin did not hydrolyse any more ATP than the KIFC1 negative controls (Figure 4.6). Furthermore, higher concentrations of KIFC1 showed the same lack of activity (Figure 4.7).

This lack of activity could be due to various reasons but due to time constraints, we could not produce more KIFC1 so investigations into why the assay did not work were not carried out.

It is unlikely that the protein construct itself was non-functional, as the same KIFC1 motor domain has been published to have yielded ATPase activity (Wu et al., 2013). However, one possible reason could have been that the protein was improperly folded or had become unfolded, and that its intricate tertiary structure was lost. To determine if this were the case, this could have been deduced by a 1D proton NMR or circular dichroism (CD).

In a proton NMR, each peak would correspond to a particular proton, and each protein would have multiple protons with many peaks overlapping, which would make interpreting a 1D NMR of an average sized protein a difficult task. However, a basic principle is that a well-folded protein would show sharp and narrow peaks over a large range of chemical shifts (Page et al., 2005). Conversely, an unfolded or poorly folded protein would show broad peaks with little chemical shift range. This is because the protons in a folded protein are likely to be contained in distinct conformations as a result of their intramolecular interactions, leaving the same protons in the same positions across multiple molecules, producing sharp peaks across a large range of chemical peaks. On the other hand, protons in unfolded proteins adopt their conformations at random, and as chemical shift is an average of a proton's environment, the average of multiple different positions produces broad peaks over a narrow range (Page et al., 2005).

An alternative method is CD spectroscopy, an approach based on the principle that a beam of light consists of electric and magnetic fields oscillating perpendicular to each other (Greenfield, 2006). When polarised, the electric field can be made to oscillate sinusoidally in a single plane which, when viewed from the front, can be visualised as the result of two equal vectors oscllating 90 degrees out of phase, rotating either clockwise or anticlockwise. These waves are absorbed by asymmetric molecules to different degrees, and also have different refractive indeces. Circular dichroism is therefore the unequal absorption of circularly polarised light, spectroscopy of which measures the differences in absorption between clockwise and anticlockwise rotating light. Based on amide chromophores in peptide backbones of proteins, different characteristic circular dichroism spectra are produced by diferent structural elements in proteins, allowing unfolded and disordered proteins with no structural characteristics to be identified, as opposed to globular proteins with significant components of alpha or beta structure (Greenfield, 2006).

Another reason that KIFC1 may have been non-functional is that it may have aggregated. Similar to misfolding, aggregation can disturb protein tertiary structure and may disrupt protein function. Protein aggregates normally form by self-association of a few proteins which serve as nucleation foci for growth and formation of larger aggregates. Generally, aggregation can occur during recombinant protein expression due to a variety of reasons, ranging from too high an expression rate and incompatible strain of recombinant bacteria to unfavourable temperature and pH during purification (Reviewed by Lebendiker and Danieli, 2014). To assess whether proteins were aggregated, they could by separated by size using size-exclusion chromatography (SEC) and then the mass of eluting proteins would be measured using multi angle light scattering (MALS). SEC-MALS works by first running a protein solution through a column of porous beads, allowing larger complexes and molecules to elute first. As the protein molecules elute from the column, a monochromatic light beam would be used to illuminate the protein suspension (Hong et al., 2012). The intensity of the scattered light is proportional to to both overall mass and the mass of individual particles (either complexes or monomers), meaning that aggregated proteins would produce more intense signals even with the same total number of protein monomers in a solution (Hong et al., 2012).

Alternatively, the assay may have failed due to suboptimal conditions for KIFC1 ATPase function. A similar assay using the same KIFC1 construct was used successfully in the discovery of AZ82 (Wu et al., 2013). In this assay, KIFC1 was run in a similar buffer of similar concentration to the assay carried out in our study. However, the pH of the buffer used in the production of AZ82 was pH 7.0, whereas the pH used in our study was pH 6.7. It may be that KIFC1 works in a very small pH range, and experiments at a range of pHs were planned to be carried out prior to the loss of KIFC1 protein.

5. Conclusion

The work presented in this thesis shows for the first time that metastatic uveal melanoma cells lines display rampant centrosome amplification. This is important as amplified centrosomes present a novel cancer-specific therapeutic target in liver metastatic uveal melanoma. The fact that uveal melanoma metastasis to the liver has such poor survival rates in part due to no effective therapeutic options means that investigations into the role of amplified centrosomes in metastatic uveal melanoma warrant further pursuit.

Furthermore, this work has also shown that KIFC1 depletion reduces proliferation in primary and metastatic uveal melanoma cell lines, while increasing the frequency multipolar mitosis. This has important implications. Firstly, the negative effects of KIFC1 depletion in Mel270 cells, despite the lack of significant centrosome amplification, further lends credence to the theory that KIFC1 has centrosome clustering-independent roles in cancer growth. Additionally, speculation by Pannu *et al.* (2015b) that KIFC1 may gain function as part of an "oncogenic axis" in a cancerous environment may also be the case in uveal melanoma. However, the relatively modest increases in apoptosis in uveal melanoma cells upon KIFC1 depletion may leave much to be desired in a clinical setting, while the resistance of metastatic uveal melanoma cells to KIFC1 depletion with regards to clonogenicity means that any clinical targeting of KIFC1 may only be relevant for primary uveal melanoma cells.

The fact that KIFC1 has centrosome amplification-independent effects in primary uveal melanoma cells means that development of PROTACs targeting KIFC1 may have increased significance as they could be used to treat a larger range of cancers. Although the admittedly ambitious project aim of synthesising a functional CW069-derived PROTAC was not fully achieved due to time constraints and difficulties in this project, the work presented in this thesis has for the first time outlined the concept of using small-molecule KIFC1 inhibitors to produce PROTACs which target KIFC1. The analogues developed in this thesis will provide the starting point for developing future KIFC1-targeting PROTACs using the multitude of linkers and E3 ubiquitin ligase binders available.

6. Bibliography

Abbas, T. & Dutta, A. (2009). P21iIn Cancer: Intricate Networks and Multiple Activities. *Nat Rev Cancer,* 9**,** 400-14.

Akutsu, M., Dikic, I. & Bremm, A. (2016). Ubiquitin Chain Diversity at a Glance. *J Cell Sci,* 129**,** 875-80.

Alao, J. P. (2007). The Regulation of Cyclin D1 Degradation: Roles in Cancer Development and the Potential for Therapeutic Invention. *Mol Cancer,* 6**,** 24.

An, S. & Fu, L. (2018). Small-Molecule PROTACs: An Emerging and Promising Approach for the Development of Targeted Therapy Drugs. *Ebiomedicine,* 36**,** 553-562.

Arnandis, T., Monteiro, P., Adams, S. D., Bridgeman, V. L., Rajeeve, V., Gadaleta, E., Marzec, J., Chelala, C., Malanchi, I., Cutillas, P. R. & Godinho, S. A. (2018). Oxidative Stress in Cells with Extra Centrosomes Drives Non-Cell-Autonomous Invasion. *Dev Cell,* 47**,** 409-424 E9.

Bakhoum, M. F. & Esmaeli, B. (2019). Molecular Characteristics of Uveal Melanoma: Insights from The Cancer Genome Atlas (TCGA) Project. *Cancers (Basel),* 11.

Basto, R., Brunk, K., Vinadogrova, T., Peel, N., Franz, A., Khodjakov, A. & Raff, J. W. (2008). Centrosome Amplification Can Initiate Tumorigenesis in Flies. *Cell,* 133**,** 1032-42.

Bondeson, D. P., Mares, A., Smith, I. E., Ko, E., Campos, S., Miah, A. H., Mulholland, K. E., Routly, N., Buckley, D. L., Gustafson, J. L., Zinn, N., Grandi, P., Shimamura, S., Bergamini, G., Faelth-Savitski, M., Bantscheff, M., Cox, C., Gordon, D. A., Willard, R. R., Flanagan, J. J., Casillas, L. N., Votta, B. J., Den Besten, W., Famm, K., Kruidenier, L., Carter, P. S., Harling, J. D., Churcher, I. & Crews, C. M. (2015). Catalytic In Vivo Protein Knockdown by Small-Molecule PROTACs. *Nat Chem Biol,* 11**,** 611-7.

Bononi, A., Giorgi, C., Patergnani, S., Larson, D., Verbruggen, K., Tanji, M., Pellegrini, L., Signorato, V., Olivetto, F., Pastorino, S., Nasu, M., Napolitano, A., Gaudino, G., Morris, P., Sakamoto, G., Ferris, L. K., Danese, A., Raimondi, A., Tacchetti, C., Kuchay, S., Pass, H. I., Affar, E. B., Yang, H., Pinton, P. & Carbone, M. (2017). BAP1 Regulates IP3R3-Mediated Ca(2+) Flux to Mitochondria Suppressing Cell Transformation. *Nature,* 546**,** 549-553.

Boveri, T. (2008). Concerning the Origin of Malignant Tumours by Theodor Boveri. Translated and Annotated by Henry Harris. *J Cell Sci,* 121 Suppl 1**,** 1-84.

Braun, M., Lansky, Z., Bajer, S., Fink, G., Kasprzak, A. A. & Diez, S. (2013). The Human Kinesin-14 HSET Tracks the Tips of Growing Microtubules In Vitro. *Cytoskeleton (Hoboken),* 70**,** 515-21.

Bremm, A., Moniz, S., Mader, J., Rocha, S. & Komander, D. (2014). Cezanne (OTUD7b) Regulates HIF-1alpha Homeostasis in a Proteasome-Independent Manner. *Embo Rep,* 15**,** 1268-77.

Buhimschi, A. D., Armstrong, H. A., Toure, M., Jaime-Figueroa, S., Chen, T. L., Lehman, A. M., Woyach, J. A., Johnson, A. J., Byrd, J. C. & Crews, C. M. 2018. Targeting the C481s Ibrutinib-Resistance Mutation in Bruton's Tyrosine Kinase Using PROTAC-Mediated Degradation. *Biochemistry,* 57**,** 3564-3575.

Cai, S., Weaver, L. N., Ems-Mcclung, S. C. & Walczak, C. E. (2009). Kinesin-14 Family Proteins

HSET/XCTK2 Control Spindle Length by Cross-Linking and Sliding Microtubules. *Mol Biol Cell,* 20**,** 1348-59.

Carmena, M., Wheelock, M., Funabiki, H. & Earnshaw, W. C. (2012). The Chromosomal Passenger Complex (CPC): From Easy Rider to the Godfather of Mitosis. *Nat Rev Mol Cell Biol,* 13**,** 789-803.

Chan, J. Y. (2011). A Clinical Overview of Centrosome Amplification in Human Cancers. *Int J Biol Sci,* 7**,** 1122-44.

Chang, A. E., Karnell, L. H. & Menck, H. R. (1998). The National Cancer Data Base Report on Cutaneous and Noncutaneous Melanoma: A Summary Of 84,836 Cases from the Past Decade. The American College of Surgeons Commission on Cancer and the American Cancer Society. *Cancer,* 83**,** 1664-78.

Chavali, P. L., Chandrasekaran, G., Barr, A. R., Tatrai, P., Taylor, C., Papachristou, E. K., Woods, C. G., Chavali, S. & Gergely, F. (2016). A Cep215-HSET Complex Links Centrosomes with Spindle Poles and Drives Centrosome Clustering in Cancer. *Nat Commun,* 7**,** 11005.

Chen, J., Jin, S., Tahir, S. K., Zhang, H., Liu, X., Sarthy, A. V., Mcgonigal, T. P., Liu, Z., Rosenberg, S. H. & Ng, S. C. (2003). Survivin Enhances Aurora-B Kinase Activity and Localizes Aurora-B in Human Cells. *J Biol Chem,* 278**,** 486-90.

Chen, J., Li, S., Zhou, S., Cao, S., Lou, Y., Shen, H., Yin, J. & Li, G. (2017). Kinesin Superfamily Protein Expression and Its Association with Progression and Prognosis in Hepatocellular Carcinoma. *J Cancer Res Ther,* 13**,** 651-659.

Chung, E. & Chen, R. H. (2002). Spindle Checkpoint Requires Mad1-Bound and Mad1-Free Mad2. *Mol Biol Cell,* 13**,** 1501-11.

De Almeida, B. P., Vieira, A. F., Paredes, J., Bettencourt-Dias, M. & Barbosa-Morais, N. L. (2019). Pan-Cancer Association of a Centrosome Amplification Gene Expression Signature with Genomic Alterations and Clinical Outcome. *PLoS Comput Biol,* 15**,** E1006832.

De, S., Cipriano, R., Jackson, M. W. & Stark, G. R. (2009). Overexpression of Kinesins Mediates Docetaxel Resistance in Breast Cancer Cells. *Cancer Res,* 69**,** 8035-42.

Denu, R. A., Shabbir, M., Nihal, M., Singh, C. K., Longley, B. J., Burkard, M. E. & Ahmad, N. (2018). Centriole Overduplication Is the Predominant Mechanism Leading to Centrosome Amplification in Melanoma. *Mol Cancer Res,* 16**,** 517-527.

Denu, R. A., Zasadil, L. M., Kanugh, C., Laffin, J., Weaver, B. A. & Burkard, M. E. (2016). Centrosome Amplification Induces High Grade Features and is Prognostic of Worse Outcomes in Breast Cancer. *BMC Cancer,* 16**,** 47.

Elia, A. E., Boardman, A. P., Wang, D. C., Huttlin, E. L., Everley, R. A., Dephoure, N., Zhou, C., Koren, I., Gygi, S. P. & Elledge, S. J. (2015). Quantitative Proteomic Atlas of Ubiquitination and Acetylation in the DNA Damage Response. *Mol Cell,* 59**,** 867-81.

Erpapazoglou, Z., Walker, O. & Haguenauer-Tsapis, R. (2014). Versatile Roles of K63-Linked Ubiquitin Chains in Trafficking. *Cells,* 3**,** 1027-88.

Faccion, R. S., Bernardo, P. S., De Lopes, G. P. F., Bastos, L. S., Teixeira, C. L., De Oliveira, J. A., Fernandes, P. V., Dubois, L. G., Chimelli, L. & Maia, R. C. (2018). p53 Expression and

Subcellular Survivin Localization Improve the Diagnosis and Prognosis of Patients with Diffuse Astrocytic Tumors. *Cell Oncol (Dordr),* 41**,** 141-157.

Fei, C., Li, Z., Li, C., Chen, Y., Chen, Z., He, X., Mao, L., Wang, X., Zeng, R. & Li, L. (2013). Smurf1-Mediated Lys29-Linked Nonproteolytic Polyubiquitination Of Axin Negatively Regulates Wnt/Beta-Catenin Signaling. *Mol Cell Biol,* 33**,** 4095-105.

Feng, X., Degese, M. S., Iglesias-Bartolome, R., Vaque, J. P., Molinolo, A. A., Rodrigues, M., Zaidi, M. R., Ksander, B. R., Merlino, G., Sodhi, A., Chen, Q. & Gutkind, J. S. (2014). Hippo-Independent Activation of YAP by the GNAQ Uveal Melanoma Oncogene Through a Trio-Regulated Rho GTPase Signaling Circuitry. *Cancer Cell,* 25**,** 831-45.

Fu, J., Chen, Y., Cao, J., Luo, T., Qian, Y. W., Yang, W., Ren, Y. B., Su, B., Cao, G. W., Yang, Y., Yan, Y. Q., Shen, F., Wu, M. C., Feng, G. S. & Wang, H. Y. (2011). p28GANK Overexpression Accelerates Hepatocellular Carcinoma Invasiveness and Metastasis Via Phosphoinositol 3-Kinase/AKT/Hypoxia-Inducible Factor-1alpha Pathways. *Hepatology,* 53**,** 181-92.

Fu, X., Zhu, Y., Zheng, B., Zou, Y., Wang, C., Wu, P., Wang, J., Chen, H., Du, P., Liang, B. & Fang, L. (2018). KIFC1, a Novel Potential Prognostic Factor and Therapeutic Target in Hepatocellular Carcinoma. *Int J Oncol,* 52**,** 1912-1922.

Furuta, K. & Toyoshima, Y. Y. (2008). Minus-End-Directed Motor Ncd Exhibits Processive Movement That Is Enhanced by Microtubule Bundling In Vitro. *Curr Biol,* 18**,** 152-7.

Ganem, N. J., Godinho, S. A. & Pellman, D. (2009). A Mechanism Linking Extra Centrosomes to Chromosomal Instability. *Nature,* 460**,** 278-82.

Gatti, M., Pinato, S., Maiolica, A., Rocchio, F., Prato, M. G., Aebersold, R. & Penengo, L. (2015). Rnf168 Promotes Noncanonical K27 Ubiquitination to Signal DNA Damage. *Cell Rep,* 10**,** 226-38.

Godinho, S. A., Kwon, M. & Pellman, D. (2009). Centrosomes and Cancer: How Cancer Cells Divide with Too Many Centrosomes. *Cancer Metastasis Rev,* 28**,** 85-98.

Godinho, S. A., Picone, R., Burute, M., Dagher, R., Su, Y., Leung, C. T., Polyak, K., Brugge, J. S., Thery, M. & Pellman, D. (2014). Oncogene-Like Induction of Cellular Invasion from Centrosome Amplification. *Nature,* 510**,** 167-71.

Goshima, G., Wollman, R., Stuurman, N., Scholey, J. M. & Vale, R. D. (2005). Length Control of the Metaphase Spindle. *Curr Biol,* 15**,** 1979-88.

Greenfield, N. J. (2006). Using Circular Dichroism Spectra to Estimate Protein Secondary Structure. *Nat Protoc,* 1**,** 2876-90.

Grinberg-Rashi, H., Ofek, E., Perelman, M., Skarda, J., Yaron, P., Hajduch, M., Jacob-Hirsch, J., Amariglio, N., Krupsky, M., Simansky, D. A., Ram, Z., Pfeffer, R., Galernter, I., Steinberg, D. M., Ben-Dov, I., Rechavi, G. & Izraeli, S. (2009). The Expression of Three Genes in Primary Non-Small Cell Lung Cancer Is Associated with Metastatic Spread to the Brain. *Clin Cancer Res,* 15**,** 1755-61.

Hallen, M. A., Liang, Z. Y. & Endow, S. A. (2011). Two-State Displacement by the Kinesin-14 Ncd Stalk. *Biophys Chem,* 154**,** 56-65.

Han, J., Wang, F., Lan, Y., Wang, J., Nie, C., Liang, Y., Song, R., Zheng, T., Pan, S., Pei, T., Xie, C.,

Yang, G., Liu, X., Zhu, M., Wang, Y., Liu, Y., Meng, F., Cui, Y., Zhang, B., Liu, Y., Meng, X., Zhang, J. & Liu, L. (2019). KIFC1 Regulated by MiR-532-3p Promotes Epithelial-To-Mesenchymal Transition and Metastasis of Hepatocellular Carcinoma Via Gankyrin/AKT Signaling. *Oncogene,* 38**,** 406-420.

Harada, R., Vadnais, C., Sansregret, L., Leduy, L., Berube, G., Robert, F. & Nepveu, A. (2008). Genome-Wide Location Analysis and Expression Studies Reveal a Role for P110 CUX1 in the Activation of DNA Replication Genes. *Nucleic Acids Res,* 36**,** 189-202.

Harbour, J. W., Onken, M. D., Roberson, E. D., Duan, S., Cao, L., Worley, L. A., Council, M. L., Matatall, K. A., Helms, C. & Bowcock, A. M. (2010). Frequent Mutation of BAP1 in Metastasizing Uveal Melanomas. *Science,* 330**,** 1410-3.

Helgadottir, H. & Hoiom, V. (2016). The Genetics of Uveal Melanoma: Current Insights. *Appl Clin Genet,* 9**,** 147-55.

Hofmann, R. M. & Pickart, C. M. (1999). Noncanonical MMS2-Encoded Ubiquitin-Conjugating Enzyme Functions in Assembly of Novel Polyubiquitin Chains for DNA Repair. *Cell,* 96**,** 645-53.

Hong, P., Koza, S. & Bouvier, E. S. (2012). Size-Exclusion Chromatography for the Analysis of Protein Biotherapeutics and Their Aggregates. *J Liq Chromatogr Relat Technol,* 35**,** 2923-2950.

Huang, F., Zeng, X., Kim, W., Balasubramani, M., Fortian, A., Gygi, S. P., Yates, N. A. & Sorkin, A. (2013). Lysine 63-Linked Polyubiquitination Is Required for EGF Receptor Degradation. *Proc Natl Acad Sci U S A,* 110**,** 15722-7.

Husnjak, K. & Dikic, I. 2012. Ubiquitin-Binding Proteins: Decoders of Ubiquitin-Mediated Cellular Functions. *Annu Rev Biochem,* 81**,** 291-322.

Imai, T., Oue, N., Yamamoto, Y., Asai, R., Uraoka, N., Sentani, K., Yoshida, K. & Yasui, W. (2017). Overexpression of KIFC1 and Its Association with Spheroid Formation in Esophageal Squamous Cell Carcinoma. *Pathol Res Pract,* 213**,** 1388-1393.

Ismail, I. H., Davidson, R., Gagne, J. P., Xu, Z. Z., Poirier, G. G. & Hendzel, M. J. (2014). Germline Mutations in BAP1 Impair Its Function in DNA Double-Strand Break Repair. *Cancer Res,* 74**,** 4282-94.

Jager, M. J., Magner, J. A., Ksander, B. R. & Dubovy, S. R. (2016). Uveal Melanoma Cell Lines: Where Do They Come From? (An American Ophthalmological Society Thesis). *Trans Am Ophthalmol Soc,* 114**,** T5.

Jiang, Y., Saavedra, H. I., Holloway, M. P., Leone, G. & Altura, R. A. (2004). Aberrant Regulation of Survivin by the Rb/E2F Family of Proteins. *J Biol Chem,* 279**,** 40511-20.

Jungwirth, G., Yu, T., Moustafa, M., Rapp, C., Warta, R., Jungk, C., Sahm, F., Dettling, S., Zweckberger, K., Lamszus, K., Senft, C., Loehr, M., Kessler, A. F., Ketter, R., Westphal, M., Debus, J., Von Deimling, A., Simon, M., Unterberg, A., Abdollahi, A. & Herold-Mende, C. (2019). Identification of KIF11 As a Novel Target in Meningioma. *Cancers (Basel),* 11.

Kalab, P. & Heald, R. (2008). The RanGTP Gradient - A GPS For the Mitotic Spindle. *J Cell Sci,* 121**,** 1577-86.

Kent, L. N. & Leone, G. (2019). The Broken Cycle: E2F Dysfunction in Cancer. *Nat Rev Cancer,* 19**,** 326-338.

Khan, M. A., Chen, H. C., Zhang, D. & Fu, J. (2013). TWIST: A Molecular Target in Cancer Therapeutics. *Tumour Biol,* 34**,** 2497-506.

Khodjakov, A., Rieder, C. L., Sluder, G., Cassels, G., Sibon, O. & Wang, C. L. (2002). De Novo Formation of Centrosomes in Vertebrate Cells Arrested During S Phase. *J Cell Biol,* 158**,** 1171-81.

Kim, N. & Song, K. (2013). KIFC1 Is Essential for Bipolar Spindle Formation and Genomic Stability in the Primary Human Fibroblast IMR-90 Cell. *Cell Struct Funct,* 38**,** 21-30.

Kim, W., Bennett, E. J., Huttlin, E. L., Guo, A., Li, J., Possemato, A., Sowa, M. E., Rad, R., Rush, J., Comb, M. J., Harper, J. W. & Gygi, S. P. (2011). Systematic and Quantitative Assessment of the Ubiquitin-Modified Proteome. *Mol Cell,* 44**,** 325-40.

Kim, Y. J., Ketter, R., Steudel, W. I. & Feiden, W. (2007). Prognostic Significance of the Mitotic Index Using the Mitosis Marker Anti-Phosphohistone H3 in Meningiomas. *Am J Clin Pathol,* 128**,** 118-25.

Kleylein-Sohn, J., Pollinger, B., Ohmer, M., Hofmann, F., Nigg, E. A., Hemmings, B. A. & Wartmann, M. (2012). Acentrosomal Spindle Organization Renders Cancer Cells Dependent on the Kinesin HSET. *J Cell Sci,* 125**,** 5391-402.

Kramer, A., Maier, B. & Bartek, J. (2011). Centrosome Clustering and Chromosomal (In)Stability: A Matter of Life and Death. *Mol Oncol,* 5**,** 324-35.

Krantz, B. A., Dave, N., Komatsubara, K. M., Marr, B. P. & Carvajal, R. D. (2017). Uveal Melanoma: Epidemiology, Etiology, and Treatment of Primary Disease. *Clin Ophthalmol,* 11**,** 279-289.

Krauthammer, M., Kong, Y., Ha, B. H., Evans, P., Bacchiocchi, A., Mccusker, J. P., Cheng, E., Davis, M. J., Goh, G., Choi, M., Ariyan, S., Narayan, D., Dutton-Regester, K., Capatana, A., Holman, E. C., Bosenberg, M., Sznol, M., Kluger, H. M., Brash, D. E., Stern, D. F., Materin, M. A., Lo, R. S., Mane, S., Ma, S., Kidd, K. K., Hayward, N. K., Lifton, R. P., Schlessinger, J., Boggon, T. J. & Halaban, R. (2012). Exome Sequencing Identifies Recurrent Somatic RAC1 Mutations in Melanoma. *Nat Genet,* 44**,** 1006-14.

Kriegsmann, M. & Warth, A. (2016). Ki-67 Expression in Pulmonary Tumors-Reply. *Transl Lung Cancer Res,* 5**,** 552-553.

Kwon, M., Godinho, S. A., Chandhok, N. S., Ganem, N. J., Azioune, A., Thery, M. & Pellman, D. (2008). Mechanisms to Suppress Multipolar Divisions in Cancer Cells with Extra Centrosomes. *Genes Dev,* 22**,** 2189-203.

Lebendiker, M. & Danieli, T. (2014). Production of Prone-To-Aggregate Proteins. *FEBS Lett,* 588**,** 236-46.

Levine, M. S., Bakker, B., Boeckx, B., Moyett, J., Lu, J., Vitre, B., Spierings, D. C., Lansdorp, P. M., Cleveland, D. W., Lambrechts, D., Foijer, F. & Holland, A. J. (2017). Centrosome Amplification Is Sufficient to Promote Spontaneous Tumorigenesis in Mammals. *Dev Cell,* 40**,** 313-322 E5.

Li, G., Chong, T., Yang, J., Li, H. & Chen, H. (2018). Kinesin Motor Protein KIFC1 is a Target

Protein of MiR-338-3p and Is Associated with Poor Prognosis and Progression of Renal Cell Carcinoma. *Oncol Res,* 27**,** 125-137.

Li, H., Niederkorn, J. Y., Neelam, S. & Alizadeh, H. (2006). Downregulation of Survivin Expression Enhances Sensitivity of Cultured Uveal Melanoma Cells to Cisplatin Treatment. *Exp Eye Res,* 83**,** 176-82.

Li, Y., Lu, W., Chen, D., Boohaker, R. J., Zhai, L., Padmalayam, I., Wennerberg, K., Xu, B. & Zhang, W. (2015). KIFC1 is a Novel Potential Therapeutic Target for Breast Cancer. *Cancer Biol Ther,* 16**,** 1316-22.

Licchesi, J. D., Mieszczanek, J., Mevissen, T. E., Rutherford, T. J., Akutsu, M., Virdee, S., El Oualid, F., Chin, J. W., Ovaa, H., Bienz, M. & Komander, D. (2011). An Ankyrin-Repeat Ubiquitin-Binding Domain Determines TRABID's Specificity for Atypical Ubiquitin Chains. *Nat Struct Mol Biol,* 19**,** 62-71.

Lin, J. J., Lehmann, L. W., Bonora, G., Sridharan, R., Vashisht, A. A., Tran, N., Plath, K., Wohlschlegel, J. A. & Carey, M. (2011). Mediator Coordinates PIC Assembly with Recruitment of CHD1. *Genes Dev,* 25**,** 2198-209.

Lingle, W. L., Barrett, S. L., Negron, V. C., D'assoro, A. B., Boeneman, K., Liu, W., Whitehead, C. M., Reynolds, C. & Salisbury, J. L. (2002). Centrosome Amplification Drives Chromosomal Instability in Breast Tumor Development. *Proc Natl Acad Sci U S A,* 99**,** 1978-83.

Liu, Y., Peterson, D. A., Kimura, H. & Schubert, D. (1997). Mechanism of Cellular 3-(4,5-Dimethylthiazol-2-Yl)-2,5-Diphenyltetrazolium Bromide (MTT) Reduction. *J Neurochem,* 69**,** 581-93.

Liu, Y., Zhan, P., Zhou, Z., Xing, Z., Zhu, S., Ma, C., Li, Q., Zhu, Q., Miao, Y., Zhang, J., Lv, T. & Song, Y. (2016). The Overexpression of KIFC1 Was Associated with the Proliferation and Prognosis of Non-Small Cell Lung Cancer. *J Thorac Dis,* 8**,** 2911-2923.

Lopes, C. A. M., Mesquita, M., Cunha, A. I., Cardoso, J., Carapeta, S., Laranjeira, C., Pinto, A. E., Pereira-Leal, J. B., Dias-Pereira, A., Bettencourt-Dias, M. & Chaves, P. (2018). Centrosome Amplification Arises Before Neoplasia and Increases Upon p53 Loss in Tumorigenesis. *J Cell Biol,* 217**,** 2353-2363.

Marteil, G., Guerrero, A., Vieira, A. F., De Almeida, B. P., Machado, P., Mendonca, S., Mesquita, M., Villarreal, B., Fonseca, I., Francia, M. E., Dores, K., Martins, N. P., Jana, S. C., Tranfield, E. M., Barbosa-Morais, N. L., Paredes, J., Pellman, D., Godinho, S. A. & Bettencourt-Dias, M. (2018). Over-Elongation of Centrioles in Cancer Promotes Centriole Amplification and Chromosome Missegregation. *Nat Commun,* 9**,** 1258.

Marthiens, V., Rujano, M. A., Pennetier, C., Tessier, S., Paul-Gilloteaux, P. & Basto, R. (2013). Centrosome Amplification Causes Microcephaly. *Nat Cell Biol,* 15**,** 731-40.

Martin, M., Masshofer, L., Temming, P., Rahmann, S., Metz, C., Bornfeld, N., Van De Nes, J., Klein-Hitpass, L., Hinnebusch, A. G., Horsthemke, B., Lohmann, D. R. & Zeschnigk, M. (2013). Exome Sequencing Identifies Recurrent Somatic Mutations in EIF1AX And SF3B1 In Uveal Melanoma with Disomy 3. *Nat Genet,* 45**,** 933-6.

Mcilwain, D. R., Berger, T. & Mak, T. W. (2013). Caspase Functions in Cell Death and Disease.

Cold Spring Harb Perspect Biol, 5**,** A008656.

Min, M., Mayor, U., Dittmar, G. & Lindon, C. (2014). Using In Vivo Biotinylated Ubiquitin to Describe a Mitotic Exit Ubiquitome From Human Cells. *Mol Cell Proteomics,* 13**,** 2411-25.

Mittal, K., Choi, D. H., Klimov, S., Pawar, S., Kaur, R., Mitra, A. K., Gupta, M. V., Sams, R., Cantuaria, G., Rida, P. C. G. & Aneja, R. (2016). A Centrosome Clustering Protein, KIFC1, Predicts Aggressive Disease Course in Serous Ovarian Adenocarcinomas. *J Ovarian Res,* 9**,** 17.

Morris, J. R. & Solomon, E. (2004). BRCA1 : BARD1 Induces the Formation of Conjugated Ubiquitin Structures, Dependent on K6 Of Ubiquitin, in Cells During DNA Replication and Repair. *Hum Mol Genet,* 13**,** 807-17.

Mountain, V., Simerly, C., Howard, L., Ando, A., Schatten, G. & Compton, D. A. 1999. The Kinesin-Related Protein, HSET, Opposes the Activity of Eg5 and Cross-Links Microtubules in the Mammalian Mitotic Spindle. *J Cell Biol,* 147**,** 351-66.

Nigg, E. A. (2002). Centrosome Aberrations: Cause or Consequence of Cancer Progression? *Nat Rev Cancer,* 2**,** 815-25.

Nigg, E. A. & Raff, J. W. (2009). Centrioles, Centrosomes, and Cilia in Health and Disease. *Cell,* 139**,** 663-78.

Nishikawa, H., Wu, W., Koike, A., Kojima, R., Gomi, H., Fukuda, M. & Ohta, T. (2009). BRCA1-Associated Protein 1 Interferes with BRCA1/BARD1 Ring Heterodimer Activity. *Cancer Res,* 69**,** 111-9.

Ogden, A., Garlapati, C., Li, X. B., Turaga, R. C., Oprea-Ilies, G., Wright, N., Bhattarai, S., Mittal, K., Wetherilt, C. S., Krishnamurti, U., Reid, M. D., Jones, M., Gupta, M., Osan, R., Pattni, S., Riaz, A., Klimov, S., Rao, A., Cantuaria, G., Rida, P. C. & Aneja, R. (2017). Multi-Institutional Study of Nuclear KIFC1 as a Biomarker of Poor Prognosis in African American Women with Triple-Negative Breast Cancer. *Sci Rep,* 7**,** 42289.

Ogden, A., Rida, P. C. & Aneja, R. (2012). Let's Huddle to Prevent a Muddle: Centrosome Declustering as an Attractive Anticancer Strategy. *Cell Death Differ,* 19**,** 1255-67.

Ogden, A., Rida, P. C. & Aneja, R. (2013). Heading Off with the Herd: How Cancer Cells Might Maneuver Supernumerary Centrosomes for Directional Migration. *Cancer Metastasis Rev,* 32**,** 269-87.

Onken, M. D., Makepeace, C. M., Kaltenbronn, K. M., Kanai, S. M., Todd, T. D., Wang, S., Broekelmann, T. J., Rao, P. K., Cooper, J. A. & Blumer, K. J. (2018). Targeting Nucleotide Exchange to Inhibit Constitutively Active G Protein Alpha Subunits in Cancer Cells. *Sci Signal,* 11.

Ordureau, A., Heo, J. M., Duda, D. M., Paulo, J. A., Olszewski, J. L., Yanishevski, D., Rinehart, J., Schulman, B. A. & Harper, J. W. (2015). Defining Roles of Parkin and Ubiquitin Phosphorylation by PINK1 in Mitochondrial Quality Control Using A Ubiquitin Replacement Strategy. *Proc Natl Acad Sci U S A,* 112**,** 6637-42.

Ordureau, A., Sarraf, S. A., Duda, D. M., Heo, J. M., Jedrychowski, M. P., Sviderskiy, V. O., Olszewski, J. L., Koerber, J. T., Xie, T., Beausoleil, S. A., Wells, J. A., Gygi, S. P., Schulman,

B. A. & Harper, J. W. (2014). Quantitative Proteomics Reveal A Feedforward Mechanism for Mitochondrial Parkin Translocation and Ubiquitin Chain Synthesis. *Mol Cell,* 56**,** 360-75.

Oue, N., Mukai, S., Imai, T., Pham, T. T., Oshima, T., Sentani, K., Sakamoto, N., Yoshida, K. & Yasui, W. (2016). Induction of KIFC1 Expression in Gastric Cancer Spheroids. *Oncol Rep,* 36**,** 349-55.

Page, R., Peti, W., Wilson, I. A., Stevens, R. C. & Wuthrich, K. (2005). NMR Screening and Crystal Quality of Bacterially Expressed Prokaryotic and Eukaryotic Proteins in a Structural Genomics Pipeline. *Proc Natl Acad Sci U S A,* 102**,** 1901-5.

Pannu, V., Mittal, K., Cantuaria, G., Reid, M. D., Li, X., Donthamsetty, S., Mcbride, M., Klimov, S., Osan, R., Gupta, M. V., Rida, P. C. & Aneja, R. (2015). Rampant Centrosome Amplification Underlies More Aggressive Disease Course of Triple Negative Breast Cancers. *Oncotarget,* 6**,** 10487-97.

Pannu, V., Rida, P. C., Ogden, A., Turaga, R. C., Donthamsetty, S., Bowen, N. J., Rudd, K., Gupta, M. V., Reid, M. D., Cantuaria, G., Walczak, C. E. & Aneja, R. (2015). HSET Overexpression Fuels Tumor Progression Via Centrosome Clustering-Independent Mechanisms in Breast Cancer Patients. *Oncotarget,* 6**,** 6076-91.

Patel, N., Weekes, D., Drosopoulos, K., Gazinska, P., Noel, E., Rashid, M., Mirza, H., Quist, J., Braso-Maristany, F., Mathew, S., Ferro, R., Pereira, A. M., Prince, C., Noor, F., Francesch-Domenech, E., Marlow, R., De Rinaldis, E., Grigoriadis, A., Linardopoulos, S., Marra, P. & Tutt, A. N. J. (2018). Integrated Genomics and Functional Validation Identifies Malignant Cell Specific Dependencies in Triple Negative Breast Cancer. *Nat Commun,* 9**,** 1044.

Pawar, S., Donthamsetty, S., Pannu, V., Rida, P., Ogden, A., Bowen, N., Osan, R., Cantuaria, G. & Aneja, R. (2014). KIFC1, A Novel Putative Prognostic Biomarker for Ovarian Adenocarcinomas: Delineating Protein Interaction Networks and Signaling Circuitries. *J Ovarian Res,* 7**,** 53.

Quintyne, N. J., Reing, J. E., Hoffelder, D. R., Gollin, S. M. & Saunders, W. S. (2005). Spindle Multipolarity Is Prevented by Centrosomal Clustering. *Science,* 307**,** 127-9.

Rimoldi, D., Salvi, S., Lienard, D., Lejeune, F. J., Speiser, D., Zografos, L. & Cerottini, J. C. (2003). Lack of BRAF Mutations in Uveal Melanoma. *Cancer Res,* 63**,** 5712-5.

Robertson, A. G., Shih, J., Yau, C., Gibb, E. A., Oba, J., Mungall, K. L., Hess, J. M., Uzunangelov, V., Walter, V., Danilova, L., Lichtenberg, T. M., Kucherlapati, M., Kimes, P. K., Tang, M., Penson, A., Babur, O., Akbani, R., Bristow, C. A., Hoadley, K. A., Iype, L., Chang, M. T., Network, T. R., Cherniack, A. D., Benz, C., Mills, G. B., Verhaak, R. G. W., Griewank, K. G., Felau, I., Zenklusen, J. C., Gershenwald, J. E., Schoenfield, L., Lazar, A. J., Abdel-Rahman, M. H., Roman-Roman, S., Stern, M. H., Cebulla, C. M., Williams, M. D., Jager, M. J., Coupland, S. E., Esmaeli, B., Kandoth, C. & Woodman, S. E. (2017). Integrative Analysis Identifies Four Molecular and Clinical Subsets in Uveal Melanoma. *Cancer Cell,* 32**,** 204-220 E15.

Sabino, D., Gogendeau, D., Gambarotto, D., Nano, M., Pennetier, C., Dingli, F., Arras, G.,

Loew, D. & Basto, R. (2015). Moesin Is A Major Regulator of Centrosome Behavior In Epithelial Cells with Extra Centrosomes. *Curr Biol,* 25**,** 879-89.

Sansregret, L., Vadnais, C., Livingstone, J., Kwiatkowski, N., Awan, A., Cadieux, C., Leduy, L., Hallett, M. T. & Nepveu, A. (2011). Cut Homeobox 1 Causes Chromosomal Instability by Promoting Bipolar Division After Cytokinesis Failure. *Proc Natl Acad Sci U S A,* 108**,** 1949-54.

Schneekloth, A. R., Pucheault, M., Tae, H. S. & Crews, C. M. (2008). Targeted Intracellular Protein Degradation Induced by A Small Molecule: En Route To Chemical Proteomics. *Bioorg Med Chem Lett,* 18**,** 5904-8.

Schuh, M. & Ellenberg, J. (2007). Self-Organization of MTOCs Replaces Centrosome Function During Acentrosomal Spindle Assembly in Live Mouse Oocytes. *Cell,* 130**,** 484-98.

Schuster, R., Bechrakis, N. E., Stroux, A., Busse, A., Schmittel, A., Scheibenbogen, C., Thiel, E., Foerster, M. H. & Keilholz, U. (2007). Circulating Tumor Cells as Prognostic Factor for Distant Metastases and Survival in Patients with Primary Uveal Melanoma. *Clin Cancer Res,* 13**,** 1171-8.

Schuyler, S. C., Wu, Y. F. & Kuan, V. J. (2012). The Mad1-Mad2 Balancing Act--A Damaged Spindle Checkpoint in Chromosome Instability and Cancer. *J Cell Sci,* 125**,** 4197-206.

Sekino, Y., Oue, N., Koike, Y., Shigematsu, Y., Sakamoto, N., Sentani, K., Teishima, J., Shiota, M., Matsubara, A. & Yasui, W. (2019). KIFC1 Inhibitor CW069 Induces Apoptosis and Reverses Resistance to Docetaxel in Prostate Cancer. *J Clin Med,* 8.

Sekino, Y., Oue, N., Shigematsu, Y., Ishikawa, A., Sakamoto, N., Sentani, K., Teishima, J., Matsubara, A. & Yasui, W. (2017). KIFC1 Induces Resistance to Docetaxel and Is Associated with Survival of Patients with Prostate Cancer. *Urol Oncol,* 35**,** 31 E13-31 E20.

She, Z. Y. & Yang, W. X. (2017). Molecular Mechanisms of Kinesin-14 Motors in Spindle Assembly and Chromosome Segregation. *J Cell Sci,* 130**,** 2097-2110.

Shi, B., Zhang, X., Chao, L., Zheng, Y., Tan, Y., Wang, L. & Zhang, W. (2018). Comprehensive Analysis of Key Genes, MicroRNAs and Long Non-Coding RNAs in Hepatocellular Carcinoma. *Febs Open Bio,* 8**,** 1424-1436.

Silkworth, W. T., Nardi, I. K., Scholl, L. M. & Cimini, D. (2009). Multipolar Spindle Pole Coalescence Is A Major Source of Kinetochore Mis-Attachment and Chromosome Mis-Segregation in Cancer Cells. *PLoS One,* 4**,** E6564.

Simeonov, D. R., Kenny, K., Seo, L., Moyer, A., Allen, J. & Paluh, J. L. (2009). Distinct Kinesin-14 Mitotic Mechanisms in Spindle Bipolarity. *Cell Cycle,* 8**,** 3571-83.

Singh, A. D., Turell, M. E. & Topham, A. K. (2011). Uveal Melanoma: Trends in Incidence, Treatment, and Survival. *Ophthalmology,* 118**,** 1881-5.

Singh, S. A., Winter, D., Kirchner, M., Chauhan, R., Ahmed, S., Ozlu, N., Tzur, A., Steen, J. A. & Steen, H. (2014). Co-Regulation Proteomics Reveals Substrates and Mechanisms Of APC/C-Dependent Degradation. *Embo J,* 33**,** 385-99.

Swatek, K. N. & Komander, D. 2016. Ubiquitin Modifications. *Cell Res,* 26**,** 399-422.

Tamm, I., Wang, Y., Sausville, E., Scudiero, D. A., Vigna, N., Oltersdorf, T. & Reed, J. C. (1998).

IAP-Family Protein Survivin Inhibits Caspase Activity and Apoptosis Induced by Fas (CD95), Bax, Caspases, and Anticancer Drugs. *Cancer Res,* 58**,** 5315-20.

Tauriello, D. V. & Maurice, M. M. (2010). The Various Roles of Ubiquitin in Wnt Pathway Regulation. *Cell Cycle,* 9**,** 3700-9.

Teng, K., Wei, S., Zhang, C., Chen, J., Chen, J., Xiao, K., Liu, J., Dai, M., Guan, X., Yun, J. & Xie, D. (2019). KIFC1 Is Activated by TCF-4 and Promotes Hepatocellular Carcinoma Pathogenesis by Regulating HMGA1 Transcriptional Activity. *J Exp Clin Cancer Res,* 38**,** 329.

Thompson, S. L. & Compton, D. A. (2008). Examining the Link Between Chromosomal Instability and Aneuploidy in Human Cells. *J Cell Biol,* 180**,** 665-72.

Troxell, C. L., Sweezy, M. A., West, R. R., Reed, K. D., Carson, B. D., Pidoux, A. L., Cande, W. Z. & Mcintosh, J. R. (2001). Pkl1(+) and Klp2(+): Two Kinesins of the Kar3 Subfamily in Fission Yeast Perform Different Functions in Both Mitosis and Meiosis. *Mol Biol Cell,* 12**,** 3476-88.

Truscott, M., Harada, R., Vadnais, C., Robert, F. & Nepveu, A. (2008). P110 CUX1 Cooperates with E2F Transcription Factors in the Transcriptional Activation of Cell Cycle-Regulated Genes. *Mol Cell Biol,* 28**,** 3127-38.

Van Allen, E. M., Miao, D., Schilling, B., Shukla, S. A., Blank, C., Zimmer, L., Sucker, A., Hillen, U., Foppen, M. H. G., Goldinger, S. M., Utikal, J., Hassel, J. C., Weide, B., Kaehler, K. C., Loquai, C., Mohr, P., Gutzmer, R., Dummer, R., Gabriel, S., Wu, C. J., Schadendorf, D. & Garraway, L. A. (2015). Genomic Correlates of Response to CTLA-4 Blockade in Metastatic Melanoma. *Science,* 350**,** 207-211.

Van Raamsdonk, C. D., Griewank, K. G., Crosby, M. B., Garrido, M. C., Vemula, S., Wiesner, T., Obenauf, A. C., Wackernagel, W., Green, G., Bouvier, N., Sozen, M. M., Baimukanova, G., Roy, R., Heguy, A., Dolgalev, I., Khanin, R., Busam, K., Speicher, M. R., O'brien, J. & Bastian, B. C. (2010). Mutations in GNA11 in Uveal Melanoma. *N Engl J Med,* 363**,** 2191-9.

Violanti, S. S., Bononi, I., Gallenga, C. E., Martini, F., Tognon, M. & Perri, P. (2019). New Insights into Molecular Oncogenesis and Therapy of Uveal Melanoma. *Cancers (Basel),* 11.

Virgili, G., Gatta, G., Ciccolallo, L., Capocaccia, R., Biggeri, A., Crocetti, E., Lutz, J. M., Paci, E. & Group, E. W. (2007). Incidence of Uveal Melanoma in Europe. *Ophthalmology,* 114**,** 2309-15.

Vitre, B., Holland, A. J., Kulukian, A., Shoshani, O., Hirai, M., Wang, Y., Maldonado, M., Cho, T., Boubaker, J., Swing, D. A., Tessarollo, L., Evans, S. M., Fuchs, E. & Cleveland, D. W. (2015). Chronic Centrosome Amplification Without Tumorigenesis. *Proc Natl Acad Sci U S A,* 112**,** E6321-30.

Wang, H., Vo, T., Hajar, A., Li, S., Chen, X., Parissenti, A. M., Brindley, D. N. & Wang, Z. (2014). Multiple Mechanisms Underlying Acquired Resistance to Taxanes in Selected Docetaxel-Resistant MCF-7 Breast Cancer Cells. *BMC Cancer,* 14**,** 37.

Wang, Y., Probin, V. & Zhou, D. (2006). Cancer Therapy-Induced Residual Bone Marrow

Injury-Mechanisms of Induction and Implication for Therapy. *Curr Cancer Ther Rev,* 2**,** 271-279.

Watts, C. A., Richards, F. M., Bender, A., Bond, P. J., Korb, O., Kern, O., Riddick, M., Owen, P., Myers, R. M., Raff, J., Gergely, F., Jodrell, D. I. & Ley, S. V. (2013). Design, Synthesis, and Biological Evaluation of An Allosteric Inhibitor of HSET that Targets Cancer Cells with Supernumerary Centrosomes. *Chem Biol,* 20**,** 1399-410.

Wei, Y. L. & Yang, W. X. (2019). Kinesin-14 Motor Protein KIFC1 Participates in DNA Synthesis and Chromatin Maintenance. *Cell Death Dis,* 10**,** 402.

Weis, E., Shah, C. P., Lajous, M., Shields, J. A. & Shields, C. L. (2006). The Association Between Host Susceptibility Factors and Uveal Melanoma: A Meta-Analysis. *Arch Ophthalmol,* 124**,** 54-60.

Wickliffe, K. E., Williamson, A., Meyer, H. J., Kelly, A. & Rape, M. (2011). K11-Linked Ubiquitin Chains as Novel Regulators of Cell Division. *Trends Cell Biol,* 21**,** 656-63.

Wu, J., Mikule, K., Wang, W., Su, N., Petteruti, P., Gharahdaghi, F., Code, E., Zhu, X., Jacques, K., Lai, Z., Yang, B., Lamb, M. L., Chuaqui, C., Keen, N. & Chen, H. (2013). Discovery and Mechanistic Study of a Small Molecule Inhibitor for Motor Protein KIFC1. *ACS Chem Biol,* 8**,** 2201-8.

Wu, X. Y., Fu, Z. X. & Wang, X. H. (2010). Effect of Hypoxia-Inducible Factor 1-Alpha on Survivin in Colorectal Cancer. *Mol Med Rep,* 3**,** 409-15.

Xiao, Y. X., Shen, H. Q., She, Z. Y., Sheng, L., Chen, Q. Q., Chu, Y. L., Tan, F. Q. & Yang, W. X. (2017). C-Terminal Kinesin Motor KIFC1 Participates in Facilitating Proper Cell Division of Human Seminoma. *Oncotarget,* 8**,** 61373-61384.

Xiao, Y. X. & Yang, W. X. (2016). KIFC1: A Promising Chemotherapy Target for Cancer Treatment? *Oncotarget,* 7**,** 48656-48670.

Yam, C. H., Fung, T. K. & Poon, R. Y. (2002). Cyclin A in Cell Cycle Control and Cancer. *Cell Mol Life Sci,* 59**,** 1317-26.

Yang, J., Manson, D. K., Marr, B. P. & Carvajal, R. D. 2018. Treatment of Uveal Melanoma: Where Are We Now? *Ther Adv Med Oncol,* 10**,** 1758834018757175.

Yang, M. H. & Wu, K. J. (2008). TWIST Activation by Hypoxia Inducible Factor-1 (HIF-1): Implications in Metastasis and Development. *Cell Cycle,* 7**,** 2090-6.

Yavuzyigitoglu, S., Kilic, E., Vaarwater, J., De Klein, A., Paridaens, D., Verdijk, R. M. & Rotterdam Ocular Melanoma Study, G. (2016). Lipomatous Change in Uveal Melanoma: Histopathological, Immunohistochemical and Cytogenetic Analysis. *Ocul Oncol Pathol,* 2**,** 133-5.

Yuan, W. C., Lee, Y. R., Lin, S. Y., Chang, L. Y., Tan, Y. P., Hung, C. C., Kuo, J. C., Liu, C. H., Lin, M. Y., Xu, M., Chen, Z. J. & Chen, R. H. (2014). K33-Linked Polyubiquitination of Coronin 7 by Cul3-KLHL20 Ubiquitin E3 Ligase Regulates Protein Trafficking. *Mol Cell,* 54**,** 586-600.

Yukawa, M., Yamauchi, T., Kurisawa, N., Ahmed, S., Kimura, K. I. & Toda, T. (2018). Fission Yeast Cells Overproducing HSET/KIFC1 Provides a Useful Tool for Identification and Evaluation of Human Kinesin-14 Inhibitors. *Fungal Genet Biol,* 116**,** 33-41.

Zhang, C., Chen, X., Chen, X., Wang, X., Ji, A., Jiang, L., Sang, F. & Li, F. (2016). MiR-135a Acts as a Tumor Suppressor in Gastric Cancer in Part by Targeting KIFC1. *Onco Targets Ther,* 9**,** 3555-63.

Zhang, W., Zhai, L., Wang, Y., Boohaker, R. J., Lu, W., Gupta, V. V., Padmalayam, I., Bostwick, R. J., White, E. L., Ross, L. J., Maddry, J., Ananthan, S., Augelli-Szafran, C. E., Suto, M. J., Xu, B., Li, R. & Li, Y. (2016). Discovery of a Novel Inhibitor of Kinesin-Like Protein KIFC1. *Biochem J,* 473**,** 1027-35.

Zhang, Y. & Sperry, A. O. (2004). Comparative Analysis of Two C-Terminal Kinesin Motor Proteins: KIFC1 and KIFC5a. *Cell Motil Cytoskeleton,* 58**,** 213-30.

Zhao, J., Tenev, T., Martins, L. M., Downward, J. & Lemoine, N. R. (2000). The Ubiquitin-Proteasome Pathway Regulates Survivin Degradation in a Cell Cycle-Dependent Manner. *J Cell Sci,* 113 Pt 23**,** 4363-71.

Zou, J. X., Duan, Z., Wang, J., Sokolov, A., Xu, J., Chen, C. Z., Li, J. J. & Chen, H. W. (2014). Kinesin Family Deregulation Coordinated by Bromodomain Protein ANCCA and Histone Methyltransferase MLL for Breast Cancer Cell Growth, Survival, and Tamoxifen Resistance. *Mol Cancer Res,* 12**,** 539-49.

7. Appendices

Appendix 1. NMR Spectrum of Compound **1**, Product of Reaction **a**, a Boc Protection

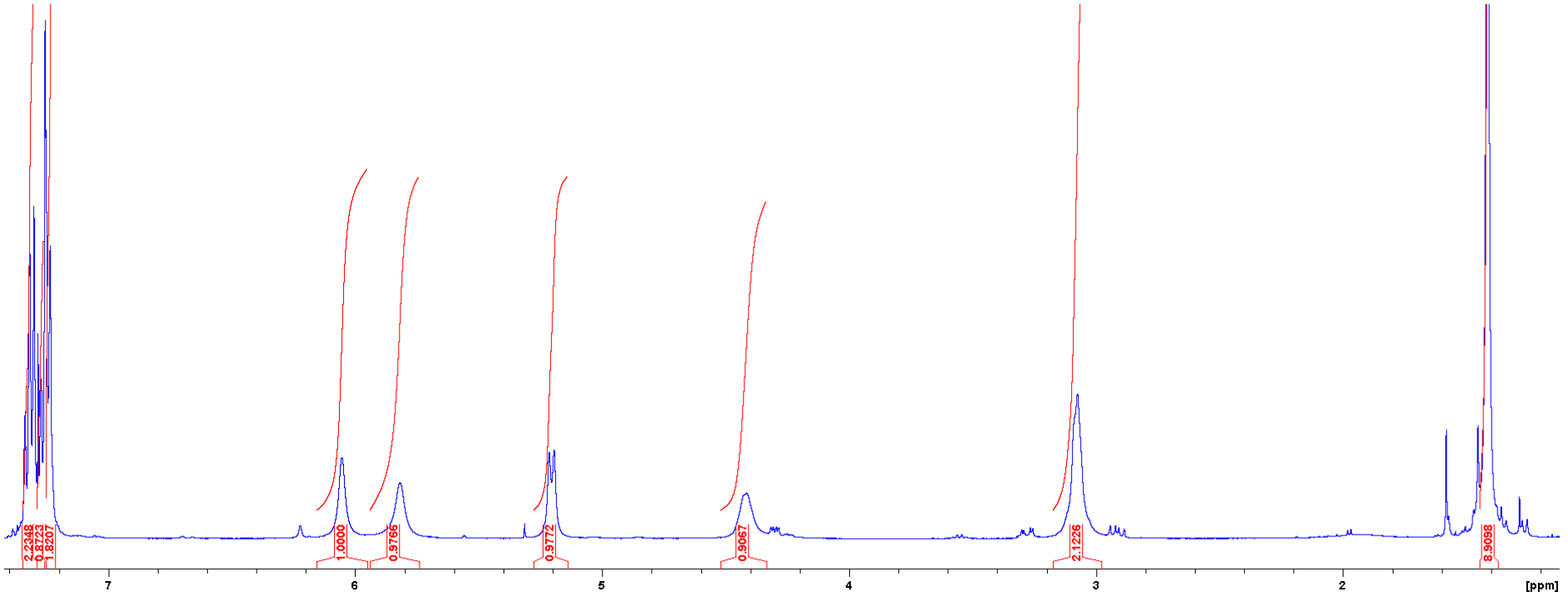

Appendix 2. NMR Spectrum of Compound **2**, Product of Reaction **b**, a Buchwald-Hartwig Coupling Reaction

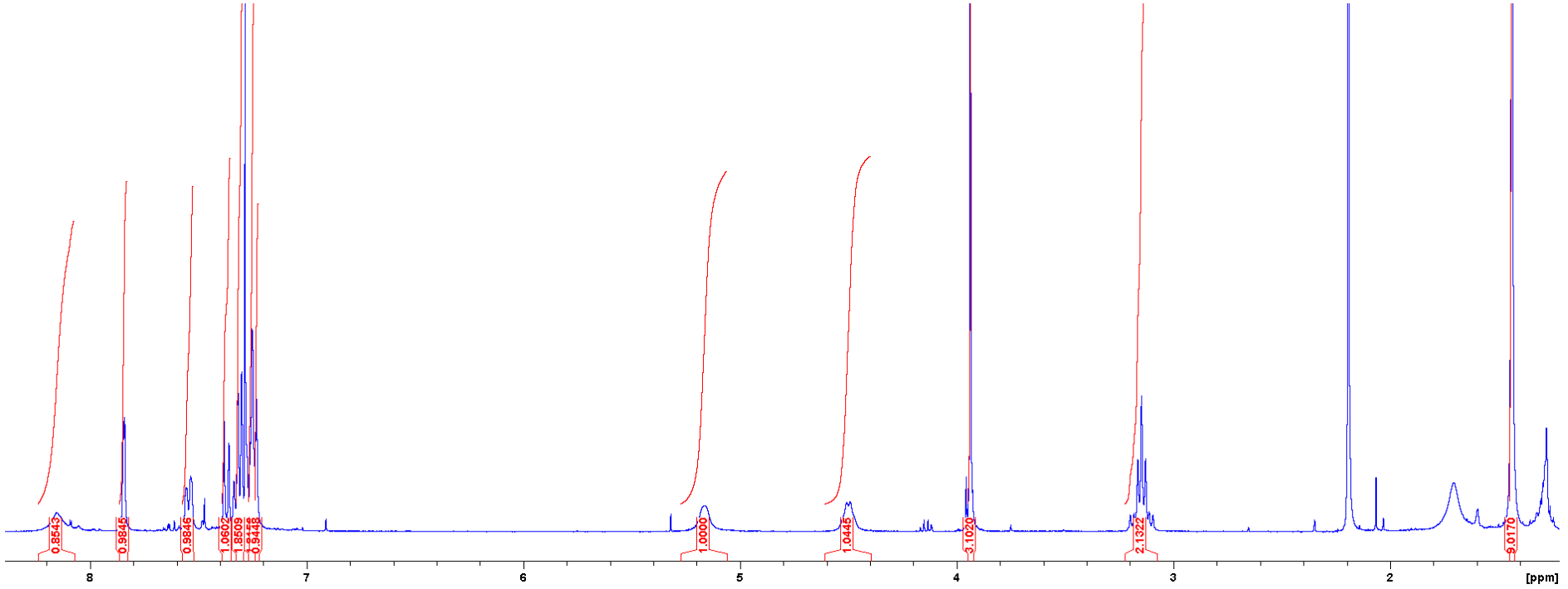

Appendix 3. NMR Spectrum of Compound **3**, Product of Reaction **c**, a TFA Cleavage Reaction

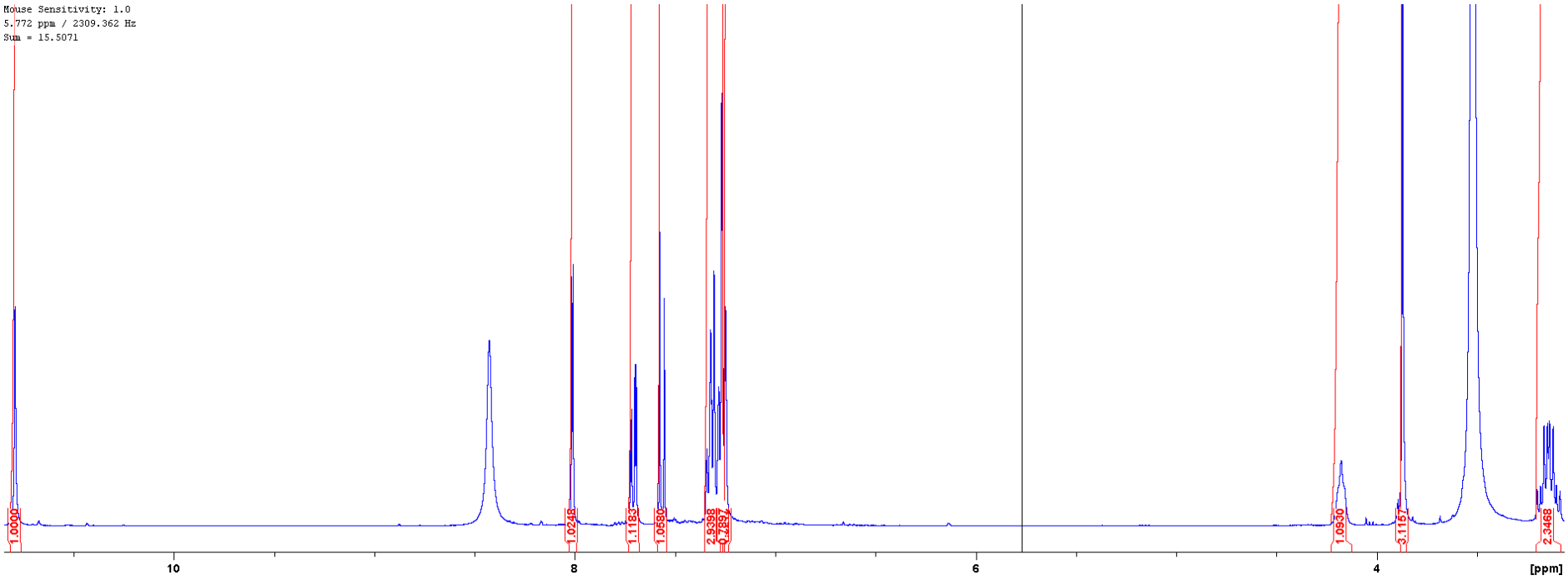

Appendix 4. NMR Spectrum of the Basified, Free Amine of Compound **3**, a TFA Cleavage Reaction

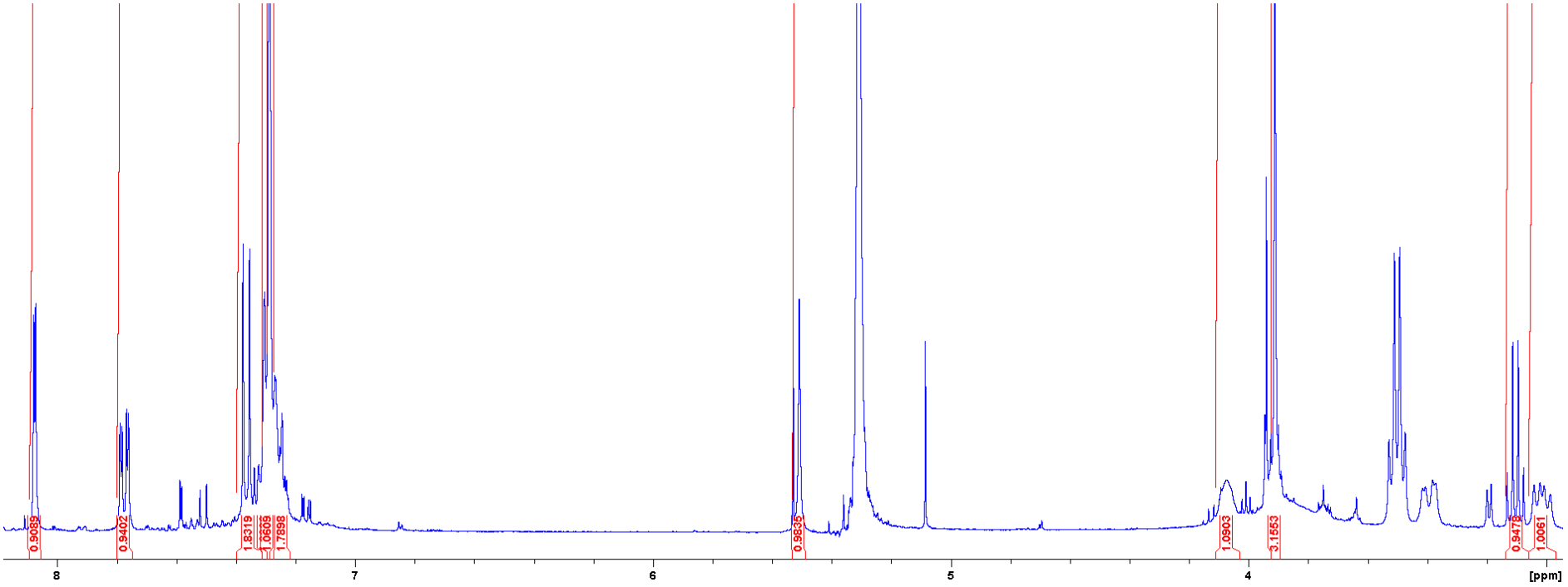

Appendix 5. NMR Spectrum of Compound **4**, Product of a Phthalimide Protection Reaction

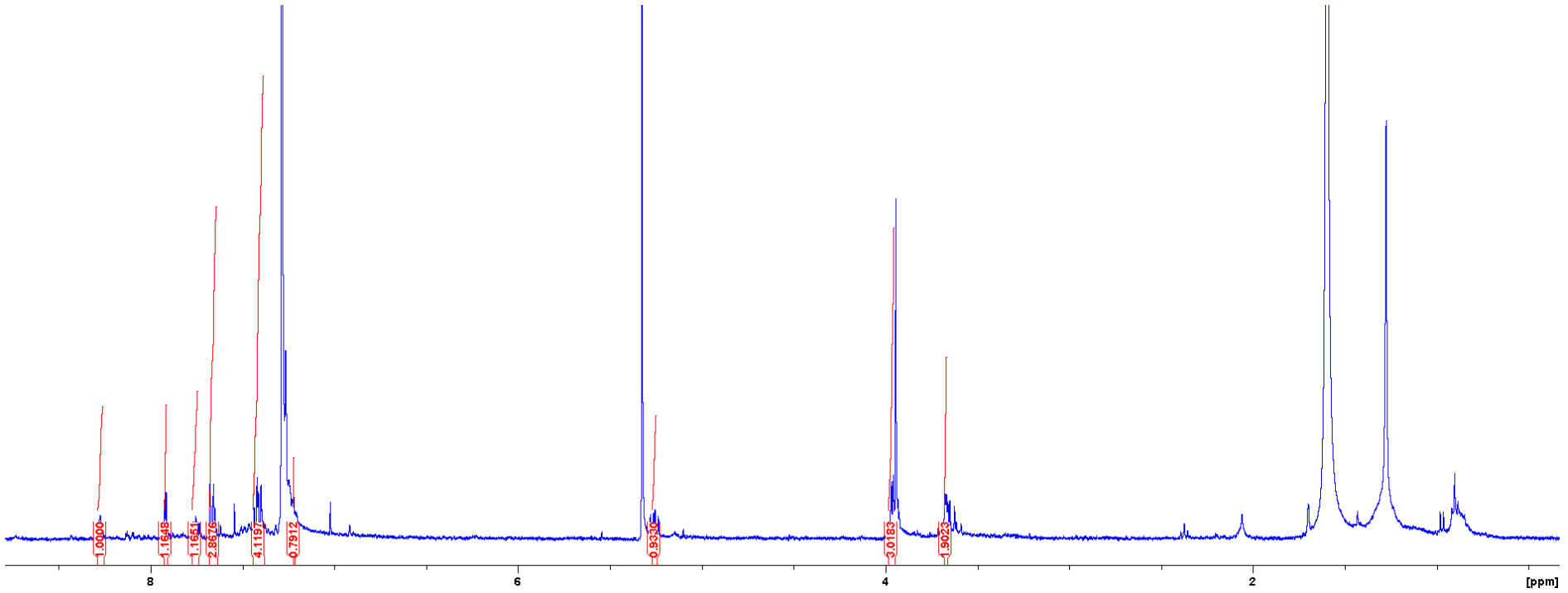

Appendix 6. NMR Spectrum of Compound **5**, Product of a Nucleophilic Addition-Elimination Reaction

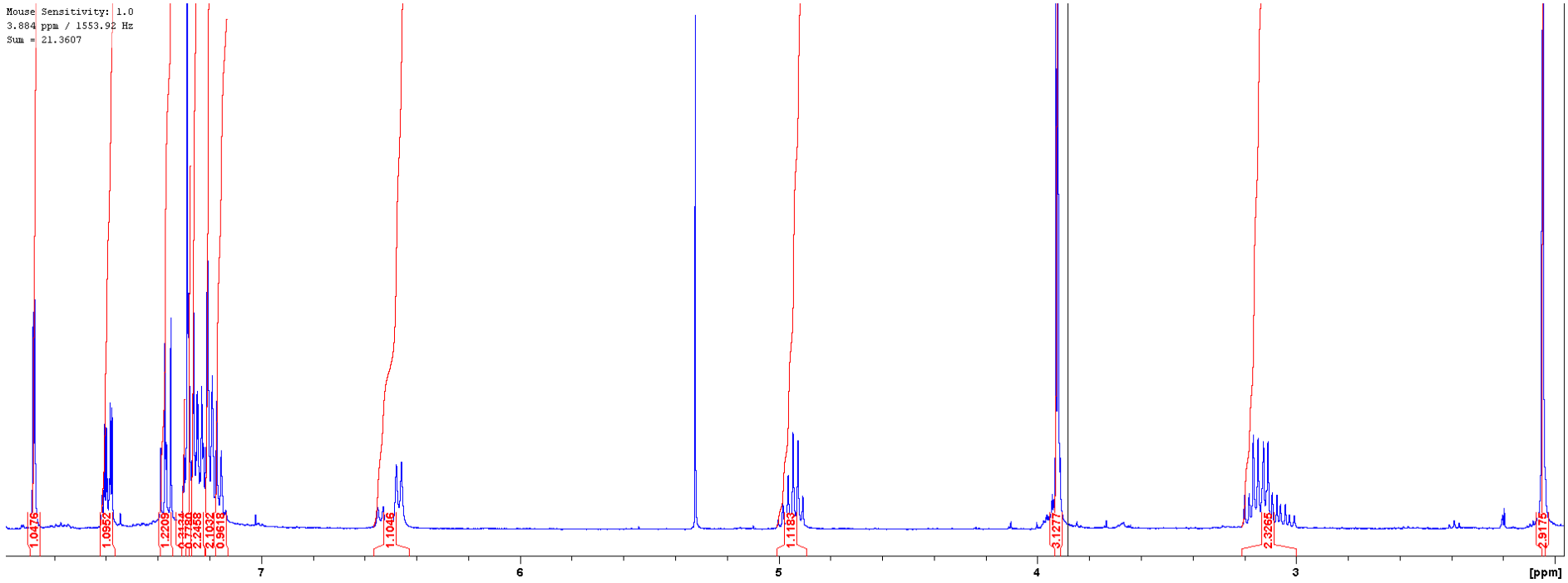

Appendix 7. NMR Spectrum of Compound **6**, Product of a Nucleophilic Addition-Elimination Reaction